ERDC/CHL TR-16-17

US Army Corps
of Engineers®
Engineer Research and
Development Center

ERDC
INNOVATIVE SOLUTIONS
for a safer, better world

Coastal Inlets Research Program

Hydrodynamic Modeling for Channel and Shoreline Stabilization at Rhodes Point, Smith Island, Maryland

Zeki Demirbilek, Lihwa Lin, Thomas D. Laczo,
and Anthony A. Clark

November 2016

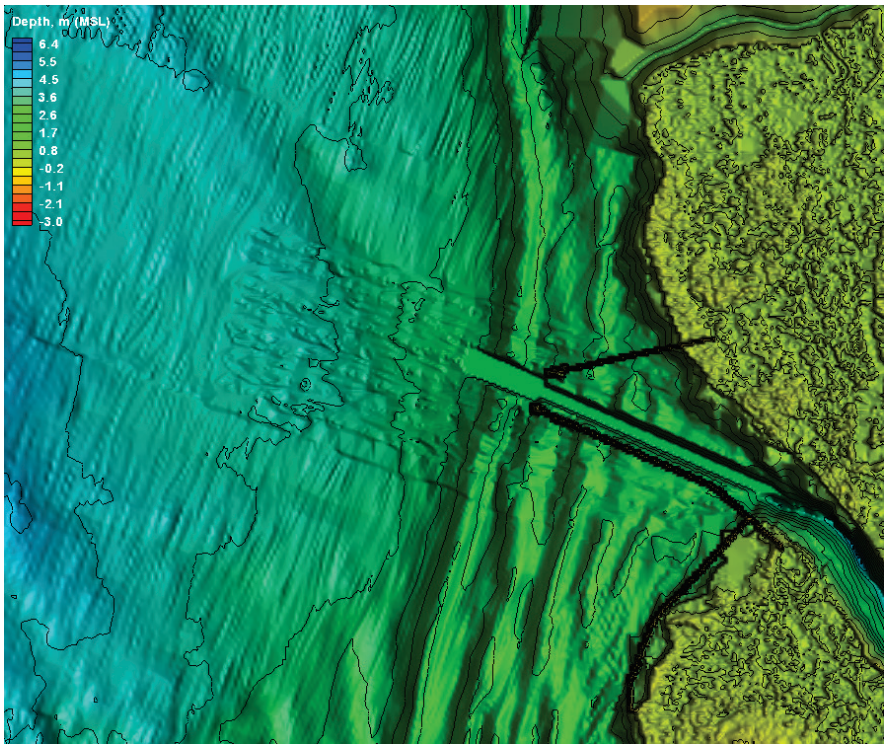

Coastal and Hydraulics Laboratory

The U.S. Army Engineer Research and Development Center (ERDC) solves the nation's toughest engineering and environmental challenges. ERDC develops innovative solutions in civil and military engineering, geospatial sciences, water resources, and environmental sciences for the Army, the Department of Defense, civilian agencies, and our nation's public good. Find out more at www.erdc.usace.army.mil.

To search for other technical reports published by ERDC, visit the ERDC online library at http://acwc.sdp.sirsi.net/client/default.

ERDC/CHL TR-16-17
November 2016

Hydrodynamic Modeling for Channel and Shoreline Stabilization at Rhodes Point, Smith Island, Maryland

Zeki Demirbilek and Lihwa Lin

Coastal and Hydraulics Laboratory
U.S. Army Engineer Research and Development Center
3909 Halls Ferry Road
Vicksburg, MS 39180-6199

Thomas D. Laczo and Anthony A. Clark

U.S. Army Engineer District, Baltimore
10 South Howard Street
Baltimore, MD 21201

Final report

Prepared for U.S. Army Engineer District, Baltimore
10 South Howard Street, MD 21201

Under Project No. 113464, “Rhodes Point, MD”

Abstract

This report documents numerical wave and flow modeling for stabilizing a shallow-draft navigation channel and adjacent shorelines at Rhodes Point, located on Smith Island, MD, in the Chesapeake Bay. The U.S. Army Engineer District, Baltimore (NAB), is considering structures to protect the western entrance of the channel and reduce erosion of shorelines by stabilizing the channel. The U.S. Army Engineer Research and Development Center (ERDC), Coastal and Hydraulics Laboratory (CHL), performed a numerical study to develop preliminary designs for the optimal location of structures and to determine effects of waves and hydrodynamics on the structures.

The Coastal Modeling System (CMS)-Wave and CMS-Flow models were used for wave and flow modeling in the Chesapeake Bay. Numerical results indicated Alternative 1, with a shore-connected north jetty nearly normal to the north shoreline at the channel entrance and a south jetty parallel to the channel with revetment structures protecting the south shorelines, offered a cost-effective solution by reducing wave energy inside the channel and along the shores. Alternative 2 with two parallel jetties provided similar wave energy reduction in the channel and along the shorelines but showed higher currents and erosional pockets developing in the channel, which could undermine the stability of the jetties.

Contents

Figures and Tables

Figures

Tables

Preface

This study was conducted for the U.S. Army Engineer District, Baltimore (NAB), under the Baltimore District, Planning Division, Civil Project Development Branch; Project No. 113464, "Rhodes Point Project, Maryland." The technical monitor was Thomas D. Laczo (CENAB-ENC-W).

This study was partially funded by the USACE Coastal Inlets Research Program (CIRP), Headquarters, U.S. Army Corps of Engineers (HQUSACE), Washington D.C. (Project Element No. 060000, Project No. 454634, Task No. A1100, Work Unit No. 58F268). The USACE CIRP Program Manager was Dr. Julie D. Rosati, CEERD-HF-CI. Jeffrey A. McKee was the HQUSACE Navigation Business Line Manager overseeing the CIRP Program.

At the time of publication, James D. Gutshall was Chief, CEERD-HN-H; Tanya M. Beck was Chief, CEERD-HN-C; Dr. Jackie S. Pettway was Chief, CEERD-HN; and W. Jeff Lillycrop (ERDC-CHL) was the ERDC Technical Director for Civil Works and Navigation Research, Development, and Technology Transfer (RD&T) portfolio. The Director of ERDC-CHL was José E. Sánchez.

The Commander of ERDC was COL Bryan S. Green, and the Director was Dr. Jeffery P. Holland.

Unit Conversion Factors

Multiply	By	To Obtain
degrees (angle)	0.01745329	radians
feet	0.3048	meters
inches	0.0254	meters
feet^2	0.0929	meters^2
gallons (U.S. liquid)	0.003785412	cubic meters
gallons (U.S. liquid) per minute per foot	0.00020699	cubic meters per second per meter
pounds (mass)	453.59237	grams
pounds (force)	4.448222	Newtons

1 Study Needs and Plan

1.1 Background

Details of a numerical modeling study conducted for stabilization of the Rhodes Point west navigation channel, located on Smith Island, MD, in the Chesapeake Bay, are described in this report. Estimates of water level, wave, current, sediment transport, and morphologic change inside this narrow channel and along the eroding north and south shorelines of the west entrance channel were calculated with an integrated numerical wave, current, and morphology change model. The modeling area included the west entrance channel and the connecting short mid-section of the narrow boat canal. The study investigated the optimal geometry and size of structures (number of structures and their placement location, orientation, and length), assessment of the efficacy of proposed jetty alternatives, and development of water level, wave, and current estimates for follow-up structural design calculations. Impacts of environmental forcings (winds, water levels, waves, and currents) on areas of interest were examined with and without structures, using numerical models. Details of the numerical modeling study, tasks, results, and findings are provided in this report.

The study area of interest includes the west channel and navigation canal that passes through the Sheep Pen Gut on Smith Island, MD, that connect Rhodes Point to the Chesapeake Bay (Figures 1-1 and 1-2). Rhodes Point is located on the west side of Smith Island (37.980 N Latitude, 76.030 W Longitude). Smith Island, located between Tangier Sound to the east and Chesapeake Bay to the west, lies mostly in the Maryland portion of the Chesapeake Bay, straddling the Maryland and Virginia state line with only its southern tip on the Virginia side.

Smith Island is approximately 10 miles west of City of Crisfield, MD, and 95 miles south of Baltimore, and consists of several smaller islands separated by shallow tidal creeks or channels called “guts.” Smith Island is sparsely populated and has three small residential fishing communities. These are Rhodes Point, Ewell, and Tylerton, all located in Maryland and are accessible only by boat. The small upland regions are the residential portions of these three fishing towns. The land elevation in the study area is low, with several fine-grained sand ridges, marshlands, and numerous creeks. The island’s highest elevations are only 3 to 5 feet (ft) (1 to 1.5 meters [m]) above mean sea level (MSL) at the populated areas of the island.

Figure 1-1. Location of Smith Island in the Chesapeake Bay.

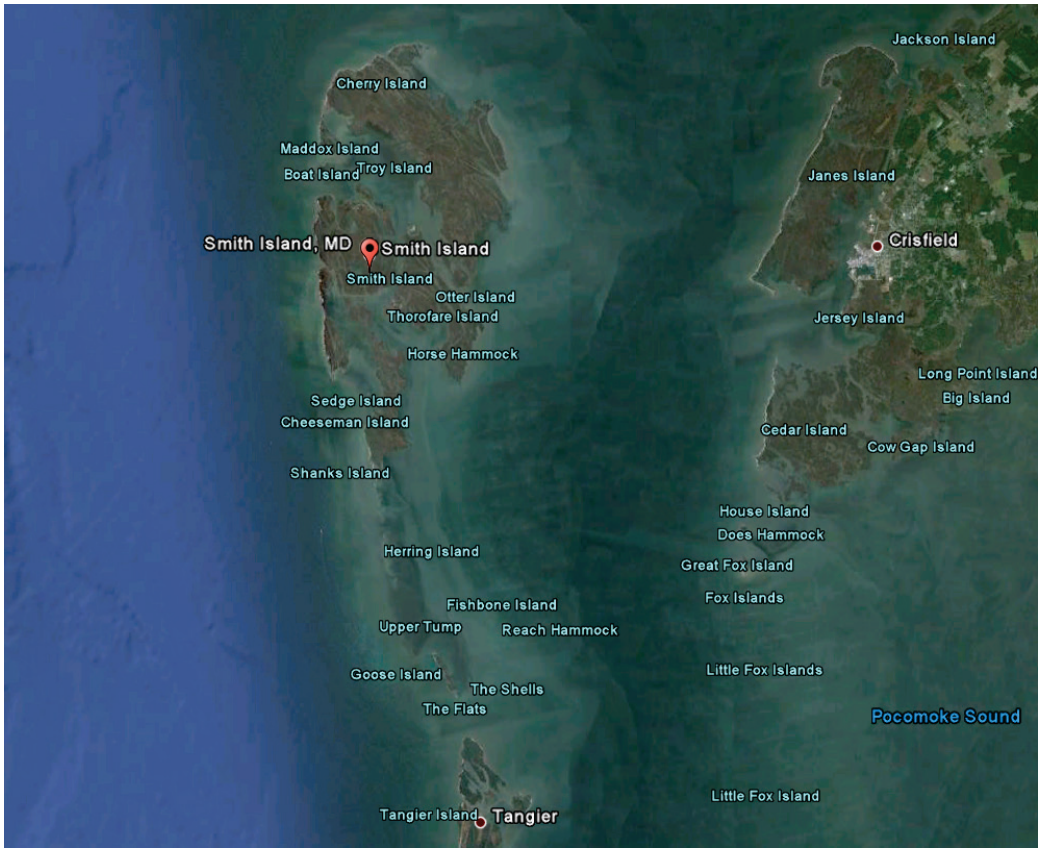

As shown in Figures 1-2 and 1-3, there is a 150 ft wide boat channel located at the midpoint of Smith Island that runs east-west across the island and passes through the Sheep Pen Gut and Rhodes Point. Technically termed a navigation channel, this narrow canal is maintained by U.S. Army Engineer District, Baltimore (NAB), for small-boat traffic. The average width and depth of this east-west linkage route are approximately 50 m and 3 m, respectively, which vary in different segments along the canal. The canal supports seafood and tourism needs of Smith Island, which are two sources of livelihood for the island residents. Fishermen have mooring docks and seafood-processing sheds and other infrastructure for the fishing fleet along the shorelines on both sides of the canal. Maintenance and improvement of this canal are critical to the economy of the island. Proposed improvements for the west entrance to Rhodes Point section of the canal include realignment of the channel, protecting it with two jetties, protection of north and south shorelines to prevent flanking, and establishing fill areas behind the shore protection. These modifications are expected to reduce the cost of channel dredging to improve the use of the channel by larger boats and reduce the erosion of shorelines caused by waves and currents.

Figure 1-2. Channels, creeks, guts, and three main towns of Smith Island.

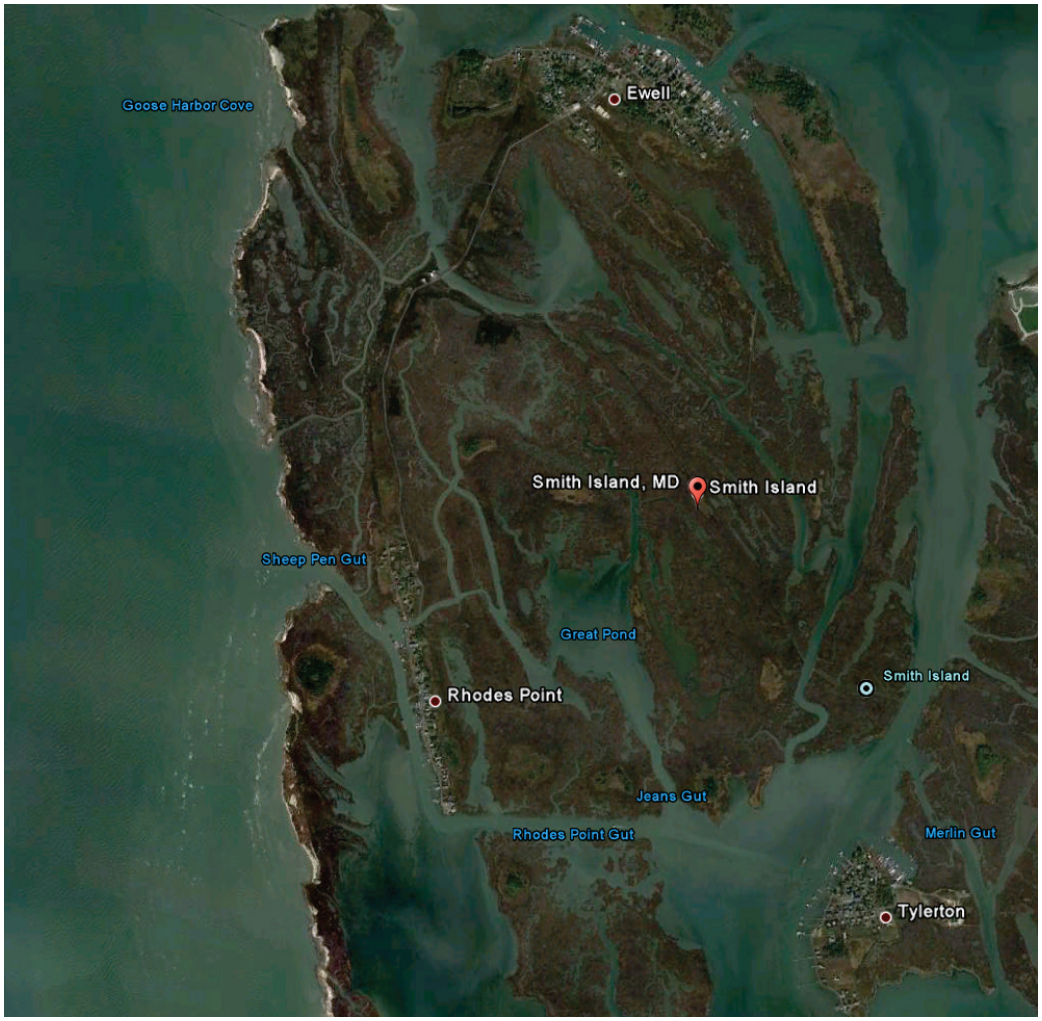

The east side of the island as shown in Figures 1-1 through 1-3 is well sheltered from the effects of storms, northeasters, and hurricanes. The short fetch distances from the Delmarva Peninsula do not provide sufficient distance for large wind waves to generate and grow. The longest fetch on the east side of Smith Island is along Tangier Sound. Wind-generated waves from the south can grow and propagate through Tangier Sound. These waves affect the east side of Smith Island and Janes Island (Figure 1-1) and may be the primary source of chronic flooding at the vulnerable town of Crisfield, MD. In contrast, the western side of Smith Island is connected to Chesapeake Bay and is exposed to large wind waves approaching the island from the northwest through southwest quadrants. Consequently, the west shoreline of Smith Island has long experienced progressive flooding and erosion. Based on prevailing wind patterns in the Chesapeake Bay, the longshore transport along the Smith Island west shoreline appears to be towards the south.

Figure 1-3. Existing western channel entrance at Sheep Pen Gut.

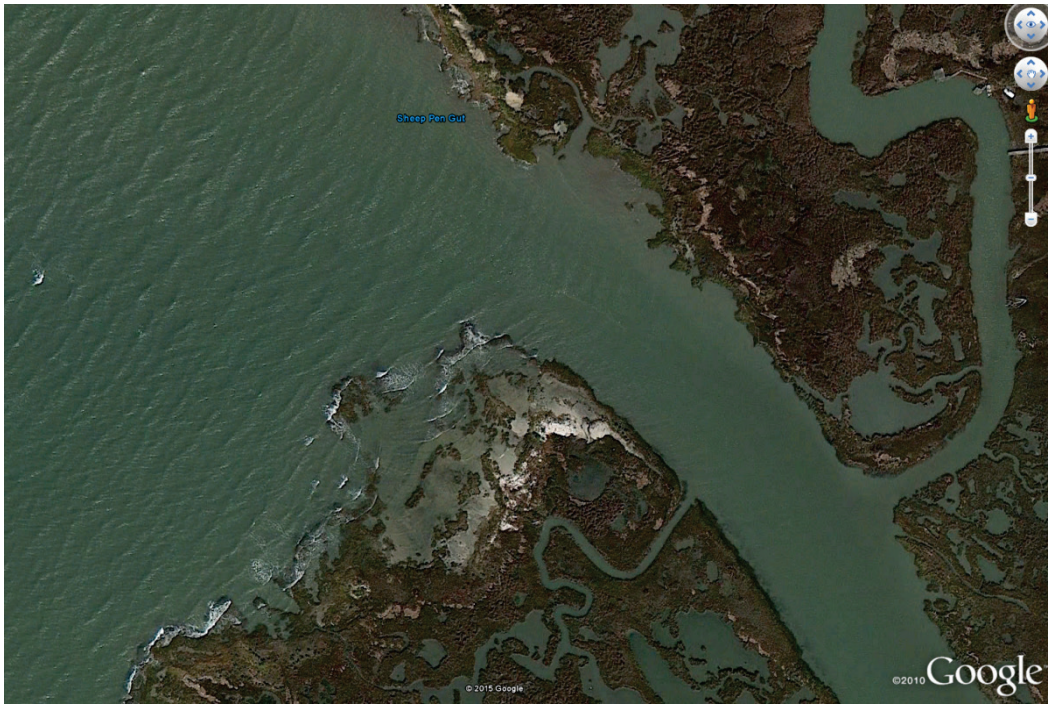

Figure 1-4. The dual-jetty system evaluated in the 2009 modeling study.

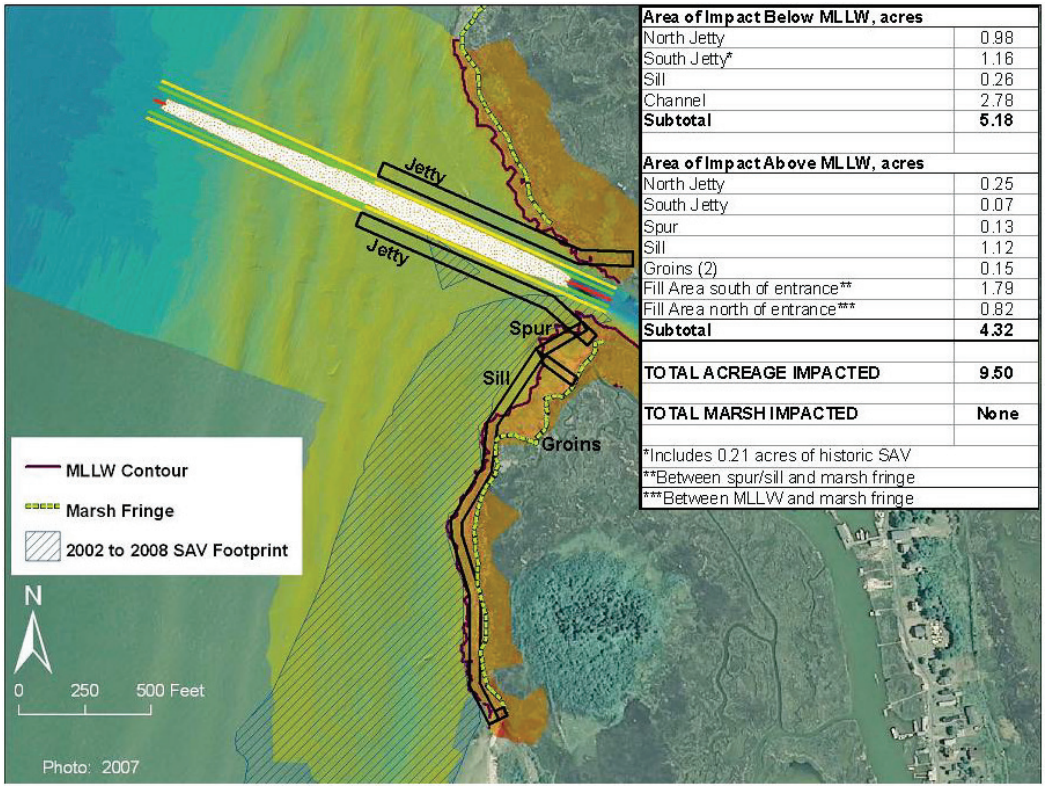

Area of Impact Below MLLW, acres	
North Jetty	0.98
South Jetty*	1.16
Sill	0.26
Channel	2.78
Subtotal	**5.18**
Area of Impact Above MLLW, acres	
North Jetty	0.25
South Jetty	0.07
Spur	0.13
Sill	1.12
Groins (2)	0.15
Fill Area south of entrance**	1.79
Fill Area north of entrance***	0.82
Subtotal	**4.32**
TOTAL ACREAGE IMPACTED	**9.50**
TOTAL MARSH IMPACTED	**None**
*Includes 0.21 acres of historic SAV	
**Between spur/sill and marsh fringe	
***Between MLLW and marsh fringe	

Figure 1-4 shows a proposed realigned channel with dual jetties that was investigated by NAB in a feasibility study in 2009 (Kraus 2009). This jetty configuration is Alternative 2 (Alt-2) in the present study that will be re-evaluated using the latest bathymetry and environmental forcing conditions (winds, waves, water levels, and currents). The extent of reduction of waves and currents along the channel and north and south shorelines, estimates of channel shoaling rates with/without jetties, and wave parameters for jetty structure design will be investigated in the present modeling study. The water level variations will include the effects of sea level rise (SLR).

1.2 Objectives

The objectives of this study were to perform a numerical modeling evaluation for the west entrance channel at Rhodes Point without jetties ("no-project," Alt-0) and one Alternative with jetties (Alt-1) to reduce wave energy in the western portion of the canal. Alt-2 from the 2009 study was re-evaluated. The present study shows comparison of hydrodynamic, wave, and sediment transport modeling results for Alt-0, Alt-1, and Alt-2 to determine effects of the proposed infrastructure modifications to the entrance channel. Engineering estimates of environmental forcings (winds, waves, currents, and water levels) at the west entrance channel are investigated for future design of a realigned channel with jetties. The impacts of jetties on wave energy reduction, changes on shoaling patterns of the entrance channel, and structural design estimates for jetties and south shore revetment are provided.

1.3 Modeling approach

The project team agreed on a modeling approach that was commensurate with the study schedule. Since no field data were available for winds, water levels, waves, and currents at Rhodes Point, the model-calculated estimates of waves, flow, and sediment transport were necessary. Because no field data were available, the modeling results could not be checked against site measurements, but the modeling results were required for qualitative evaluation of the Alternatives and recommended solutions.

The study site is exposed to open water in Chesapeake Bay. In the absence of field data, the study team considered using results from recent studies, including the Tangier Island project (Demirbilek et al. 2015), the North Atlantic Coast Comprehensive Study (NACCS) post-Sandy study (Cialone

et al. 2015), and the preliminary 2009 numerical modeling study for Rhodes Point (Kraus 2009). These three studies were evaluated, as well as other prior and ongoing studies by the USACE, other government agencies, and academic institutes of the Chesapeake Bay for available metocean sources of day-to-day conditions and storms data applicable to the Rhodes Point study. For its primary mission of regional-scale project performance evaluation, the NACCS used a large domain study to model the east coast region from Maine to Virginia. A detailed resolution of project-specific areas within Chesapeake Bay would require developing finer resolution grids and re-running the Bay-scale models, analyzing and preparing wind, water level, wave, and current predictions for any local study in the Bay.

The metocean forcing developed for Tangier Island (Demirbilek et al. 2015) located south of this project site had considered different storms and time periods and therefore could not be used for Rhodes Point. The 2009 feasibility modeling study for Rhodes Point (Kraus 2009) had used older bathymetry data. The difference between bathymetries used in the 2009 grid and 2015 survey data are highlighted in Figure 1-5. On the Bay side where surveys overlap in the west entrance, and areas along north and south shorelines, there is considerable bathymetric difference between 2009 and 2015 bathymetry data. Because of these issues, including the resolution of model grids and differences in bathymetry, the 2009 study forcing and results could not be used in the present modeling. Consequently, the modeling for this project could not be leveraged with recently completed studies.

Both the existing channel condition (no-project) and proposed channel realignment with jetties (with project) were investigated in the present study. Two structure Alternatives (Alt-1 and Alt-2) were evaluated relative to Alt-0 (no-project) in terms of effects of structures on waves, currents, and channel sedimentation (shoaling). Sketches of two geometries, Alt-1 and Alt-2, are shown in Figures 1-6 and 1-7, respectively. Details of these Alternatives are described in Chapter 2.

The Coastal Modeling System (CMS) was used to calculate waves, hydrodynamics, sediment transport, and morphology change (Demirbilek and Rosati 2011; Lin and Demirbilek 2005; Lin and Demirbilek 2011a,b). Wave modeling results (wave height, period, direction, and water depth) along the proposed structure footprints were used for the preliminary

structure design calculations, as discussed in Chapter 3. The structure calculations include armor stability, wave runup, and wave transmission through and overtopping the structures. The bathymetric, shoreline, and land data provided by the NAB were used to generate the numerical model grids in the present study. The bathymetry data included a 2012 lidar and a 2015 survey. Figure 1-8 shows the coverage area for the two data sets. Figures 1-9 and 1-10 show the extent of water and land coverages from these data sets at the project site.

Figure 1-5. Bathymetry difference between 2009 grid and 2015 surveys.

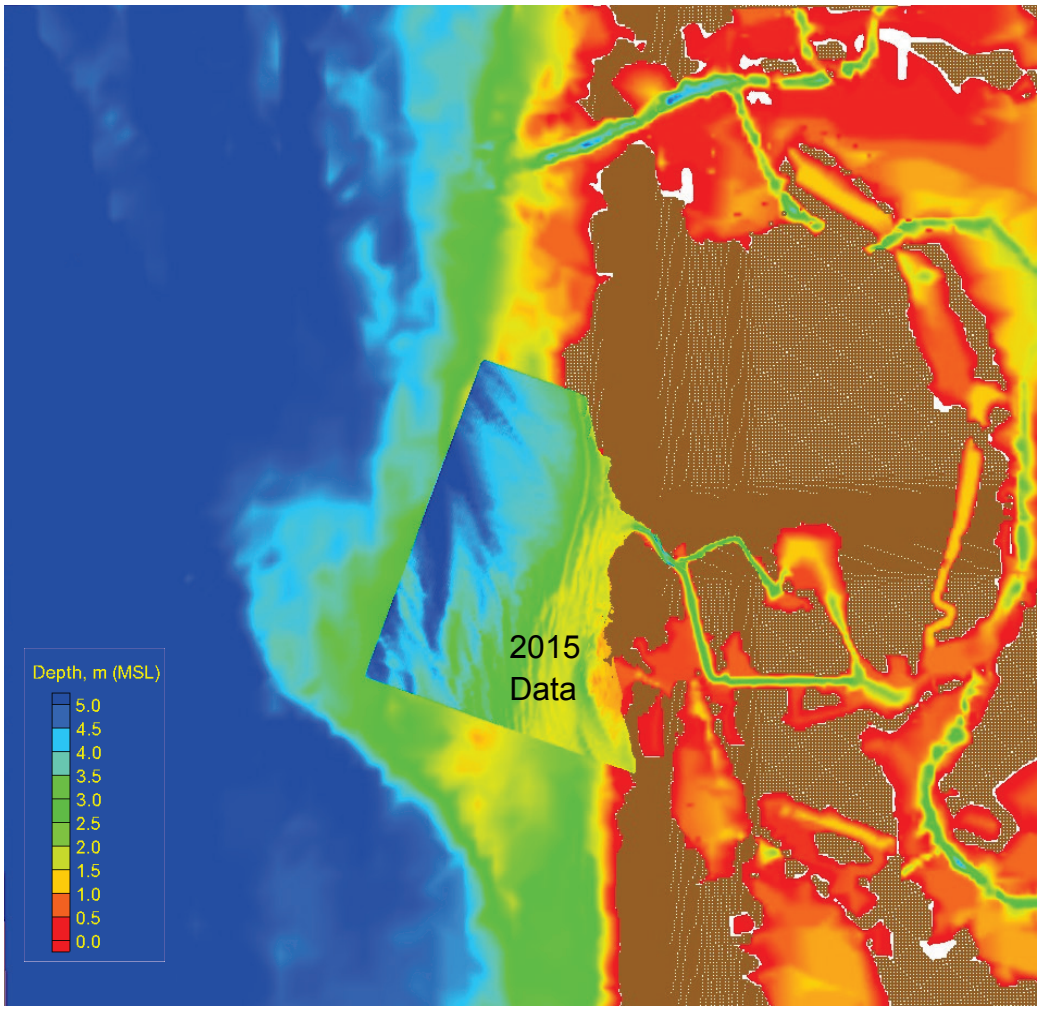

Figure 1-6. Shore-normal north jetty at Rhodes Point (Alt-1).

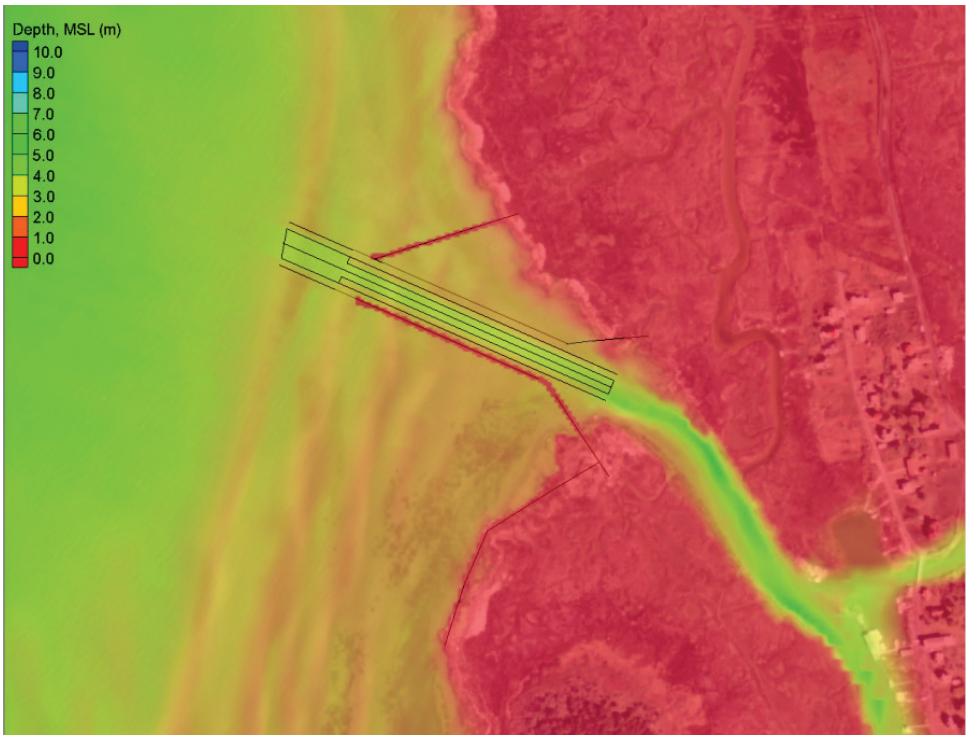

Figure 1-7. Parallel jetties at the Rhodes Point (Alt-2).

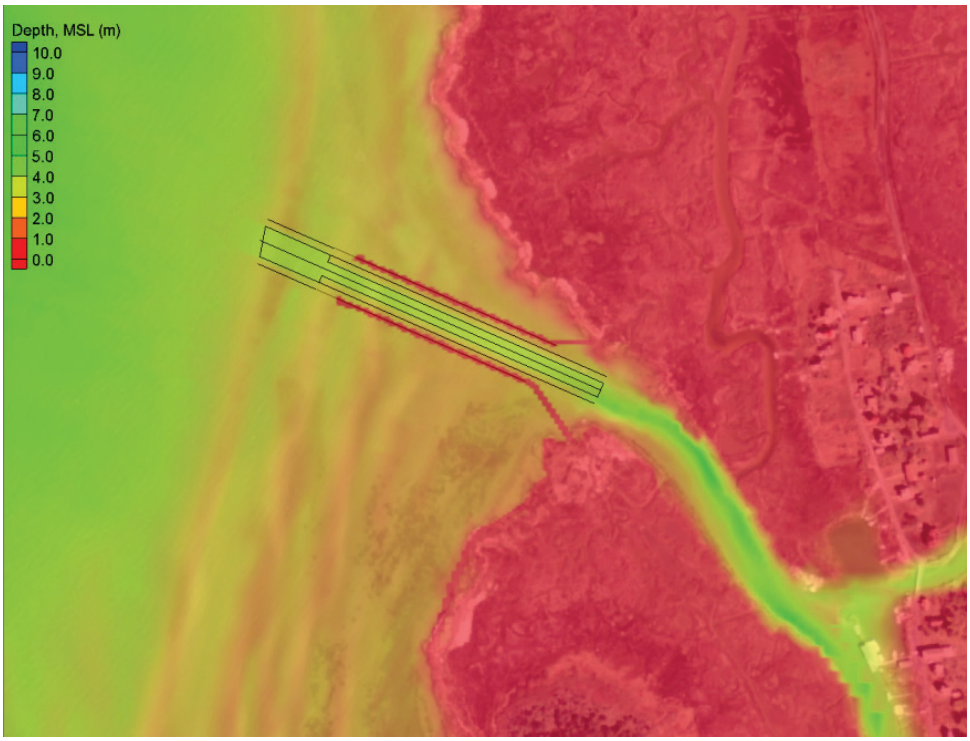

Figure 1-8. 2012 lidar survey land coverage of Smith Island and Rhodes Point.

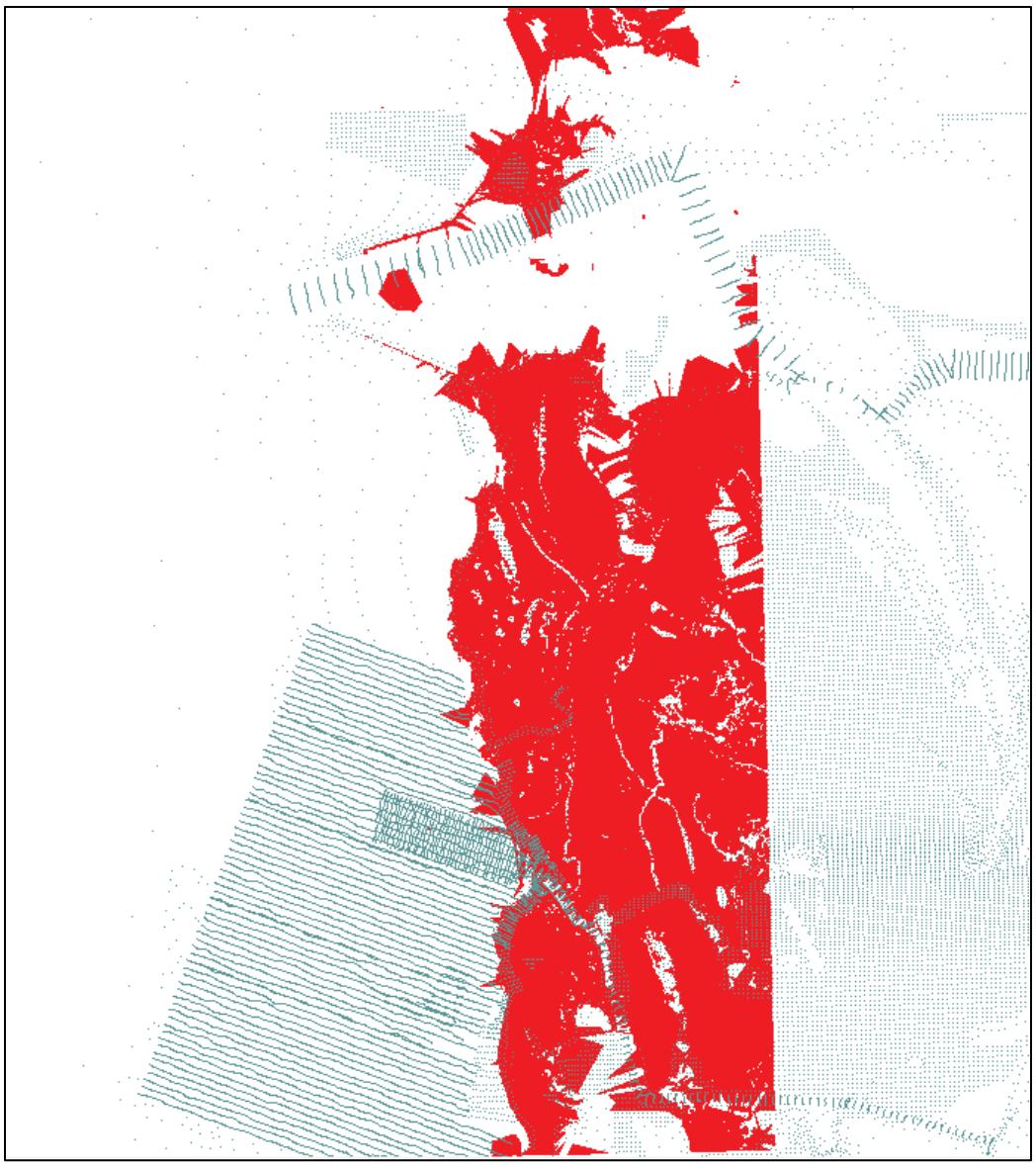

Figure 1-9. The 2012 lidar data coverage at the project site.

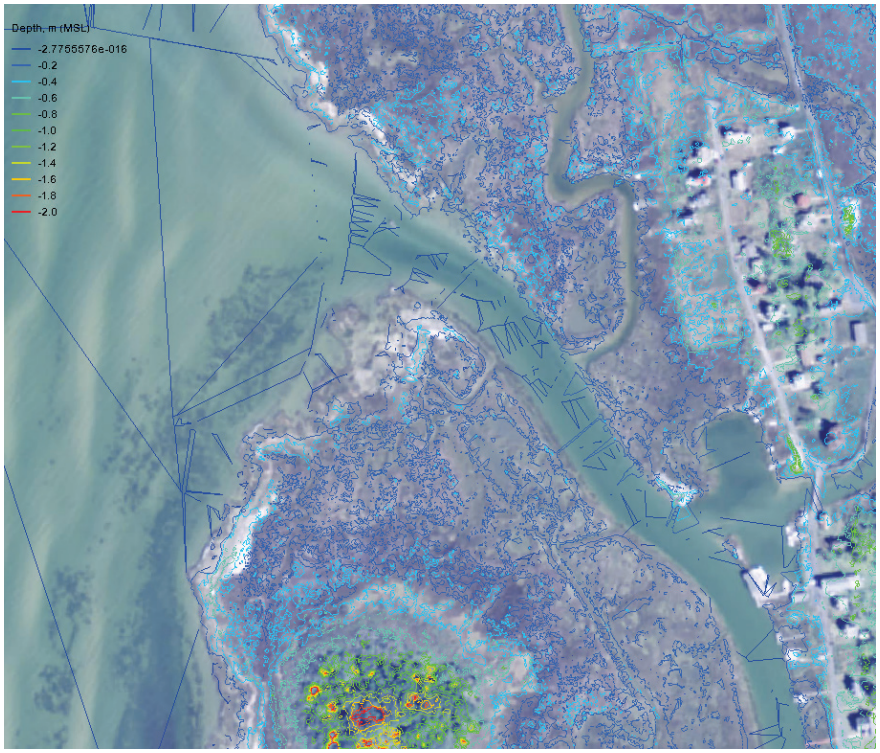

Figure 1-10. The 2015 survey coverage at the project site.

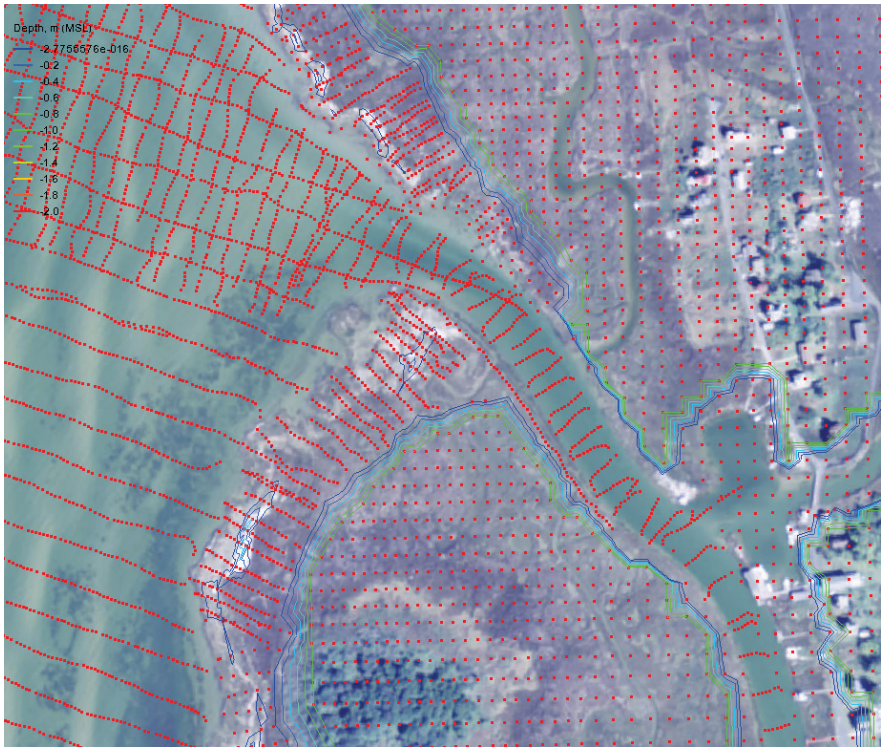

Forcing conditions for the numerical models were obtained from the meteorological and oceanographic (metocean) data sources. The metocean data (winds, waves, and water levels) available from various data sources and previous studies were assembled for nonstorm and storm conditions. Hurricane Sandy was selected as the design storm to represent a 50-year storm return period. Numerical models were set up with these data and conditions. Details of simulations performed for the existing (Alt-0) and with project Alternatives (Alts 1 and 2) are described in Chapter 2.

1.4 Tasks

Five primary activities of this numerical modeling study were (a) collect and format the input data required for numerical modeling for winds, tides, storms, bathymetry, sediments, and ancillary data; (b) set up and run wave, flow, and sediment transport models for both "as is" and "with project" scenarios; (c) document the reduction of waves and currents in the entrance area "with project" scenario, including changes in wave, flow, and sediment transport in the vicinity of proposed jetty and revetment structures, along the channel, and north and south shorelines on both sides of channel; (d) develop estimates of forcing parameters (water levels, waves, and currents) for jetty structural calculations from the modeling study results, and (e) discuss progress and issues with NAB on a regular basis as needed. The project-specific tasks are described next.

Task 1. Metocean forcing (winds, waves, tides, currents, water levels). Task 1 included preparing metocean forcing data required for numerical models. The local wave climate affecting the west side of Smith Island at Rhodes Point was generated within the Chesapeake Bay. Waves were estimated in the Bay by using wind input to a wave generation and propagation model. Available sources of day-to-day wind data applicable to Rhodes Point were obtained from local airports in the Chesapeake Bay region. The Hurricane Sandy wind fields were assembled for the Bay-scale simulations and for finer resolution modeling at Rhodes Point.

Task 2. Modeling of Alternative (Alt-1) and "as is" (Alt-0) geometries using post-Sandy bathymetry. The parallel-jetty Alternative considered in the 2009 feasibility study was remodeled in this study because of significant improvements to the CMS after completion of that study. New grids with proper resolution and updated bathymetry were generated using Task 1 data for Alt-0 (without), and Alt-1 and Alt-2 (with) project geometries.

The recommended locations of the realigned channel and parallel jetties from the 2009 study, and length and width of structures, were represented in the new grids. Coupled wave and flow models were used to evaluate changes to the location, size, and geometry of the jetty structures. Refined grids were used for accuracy of wave predictions at the inlet for representing wave diffraction, reflection, and transmission around the jetty structures.

Task 3. Channel sedimentation and morphology change modeling. Because the boat channel is a federally maintained, shallow-draft waterway regularly dredged by NAB, the proposed jetty structures should not exacerbate shoaling problems in the channel. Sediment grain size data were utilized from grab samples obtained by NAB that consisted of a mixture of sands and fine-grained material and were used in sediment transport modeling.

The CMS simulations with and without jetty structures were performed to determine the expected depositional and erosional areas in the west channel and along the north and south shorelines of Sheep Pen Gut to identify potential impacts of the proposed jetties on these most likely impacted areas.

Task 4. Wave parameters for structural design. Task 4 simulated storm wave conditions using CMS-Wave and local wind data. Wave estimates were developed along the realigned channel, seaward face of an equal length dual jetty system and a shore-normal north jetty system. Finally, model results were extracted along the perimeter of jetties, and wave heights, wave period, and water level were used in structural design to estimate structures (jetties and south shore revetment), crest elevation, crest width, side slopes, and stone size.

Task 5. Technical report. The last task summarized details of the modeling study to NAB in a report (this present technical report).

1.5 Report layout

Chapter 2 describes details of the numerical modeling study, including model domain, bathymetry, grids, forcing types, structural alternatives, save stations, conditions simulated, a comparison of Alternatives, and study findings and recommendations. Chapter 3 describes the structural design calculations, including determination of jetty structure stone size on front and leeside of the jetties, and transmitted wave heights for jetty

structure crest elevation of 5 ft (1.52 m) above the mean lower low water (MLLW) and 8 ft (2.4 m) crest width for three structural side slopes (V:H = 1:1.5, 1:2, and 1:2.5). The design estimate for the south shore revetment is based on a recent study at Tangier Island. The effects of SLR and general subsidence of the Bay were considered in the calculations. The study conclusions are summarized in Chapter 4.

2 Numerical Modeling of Waves, Currents, and Sediment Transport

2.1 Purpose

This numerical modeling study investigated waves and hydrodynamics at the western channel of Rhodes Point and developed wave, current, water-level, and sediment transport estimates with proposed jetties to reduce wave energy in the navigation channel. The geometries of the proposed structural Alternatives were investigated relative to the existing channel without jetty structure or south shore revetment. The effects of jetty structures on waves, currents, and sedimentation in the channel are described in this chapter.

2.2 Numerical models

The CMS was used to simulate waves, currents, sediment transport, and morphology change. The CMS includes wave, flow, and sediment transport modeling tools for coastal inlets and navigation projects (Demirbilek and Rosati 2011). Development and enhancement of CMS capabilities and tools have continued over the last 10 years. The version of the CMS model used in the present study has significant advancements included as compared to the version used in the 2009 feasibility study.

The CMS is an integrated modeling system that consists of a spectral wave model (CMS-Wave) and a two-dimensional (2D) circulation model (CMS-Flow) which includes sediment transport and morphology change capabilities. CMS-Wave is a steady-state, 2D spectral wave model (Lin et al. 2008; Lin et al. 2011a,b and 2005) capable of simulating coastal wave processes with ambient currents at open coast, bays and ports, and estuaries that include navigation channels and inlets.

CMS-Flow is a 2D hydrodynamic and sediment transport model capable of simulating depth-averaged circulation, salinity, and sediment transport forced by tides, wind, atmospheric pressure gradient, river inflow, and waves (Buttolph et al. 2006; Sanchez et al. 2011a,b). It solves the fluid mass and momentum conservation based on the continuity and momentum equations including terms for the Coriolis force, wind stress, wave stress, bottom stress, and turbulent diffusion.

The CMS uses the Surface-water Modeling System (SMS) (Zundel 2006) interface for grid generation, model setup, analysis of model results, plotting, and post-processing. Both CMS-Wave and CMS-Flow have been validated in many coastal/lake/bay projects and studies, and a comprehensive collection of CMS validation and verification cases is provided by Demirbilek and Rosati (2011), Lin et al. (2011a,b), and Sanchez et al. (2011a,b). Appendix A describes and summarizes additional information about the CMS and its capabilities.

The development of advances to CMS-Wave to address the project's specific needs was funded by the U.S. Army Corps of Engineers (USACE) Coastal Inlets Research Program (CIRP), a research and development program in the USACE Navigation Business Line. Three features of CMS-Wave required additional changes to model coding and improvement of wind inputs for storms. The revised model required considerable additional testing. The first set of coding changes involved modifications and testing of the full-plane and parent-child capabilities of the model for hurricanes and northeasters in the Chesapeake Bay estuary. The second set of changes included development of pre- and post-processing analysis codes for model setup. The third set of changes involved development of tools for structural design calculations.

Because no field data were available at Rhodes Point, the model was calibrated and validated with water level and current gauges in the vicinity of the project site. For additional information about the verification and validation (V&V) of CMS, interested readers should see a series of four reports published on V&V of CMS. These include Demirbilek and Rosati (2011) for a summary of approximately 30 test cases. Grays Harbor, WA, and Matagorda Bay, TX, were among the calibration and validation cases for field testing at bays and estuaries.

The project Alternatives were compared to without project condition based on a quantitative estimate of waves, currents, and sediment transport. Due to the absence of field data, the magnitudes of waves, flow, and sediment transport were not used in the selection of a recommended solution, so only a relative comparison of Alternatives is discussed. Thus, the wave, flow, and morphology changes in the channel are described by a relative comparison of Alternatives. Estimates for preliminary structural design calculations are provided. Details of the modeling, study findings, and structures (jetties and south shore revetment) design calculations are described next.

2.3 Model domain and bathymetry

The modeling area in this study was the west side of Smith Island where the existing western channel entrance at Sheep Pen Gut connects to Rhodes Point and a boat canal (Figure 2-1). Outside of the entrance, the channel turns southward and then to the southwest on the Chesapeake Bay side (Kraus 2009). At the entrance, the channel connects to a much narrower canal that is oriented to the southeast. This narrow and shallow canal cuts through the middle of Smith Island, connecting the east and west sides of Smith Island at Sheep Pen Gut. Width of the boat canal varies, with an average width of approximately 100 ft (30 m).

Figure 2-1. Existing western channel entrance at Rhodes Point.

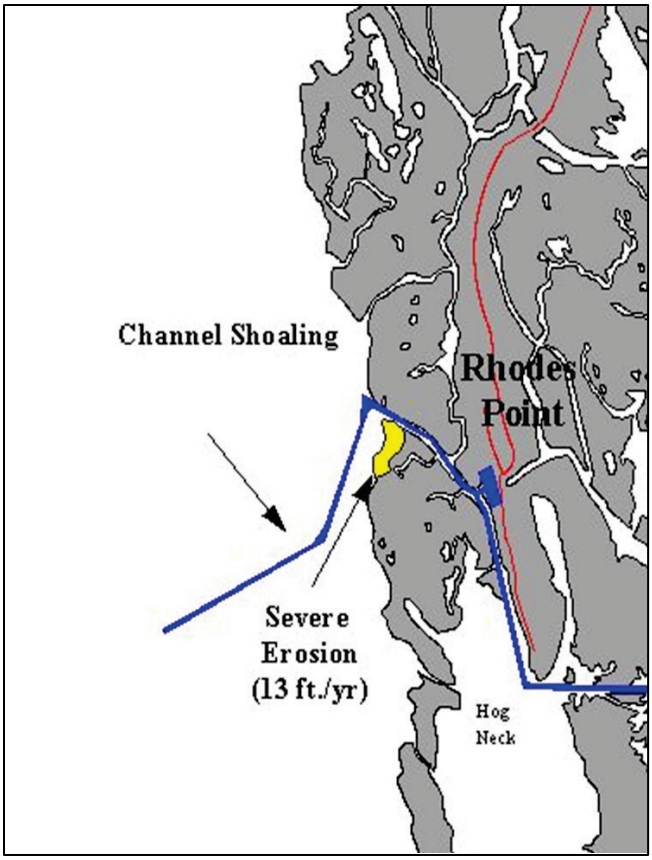

Recent surveys indicated this nearshore region of Smith Island west of the Rhodes Point entrance has experienced severe storm-induced shoaling with erosion along the shorelines. NAB has proposed a realigned channel protected by jetties. The realigned new channel would be oriented west-northwest and have a depth of 8 ft (2.4 m) MLLW.

In the 2009 feasibility study (Kraus 2009), a dual parallel jetty system with a realigned channel was proposed, and is Alt-2 in the present study. The crest elevation, crest width, and base width of the proposed jetties are +5 ft (1.52 m) above MLLW, 8 ft (2.4 m), and 65 ft (20 m), respectively. Figure 2-2 shows approximate dimensions and cross sections of the channel and jetties. The tie-ins (or spurs) connecting the two east ends of both jetties to the land are 200 ft long (61 m) and have crest elevations of +5 ft (1.52 m) MLLW. The District is considering disposal areas between the tie-ins and sills and fringe of the marsh vegetation north and south of the entrance shorelines.

Figure 2-2. Channel and jetty dimensions and cross sections.

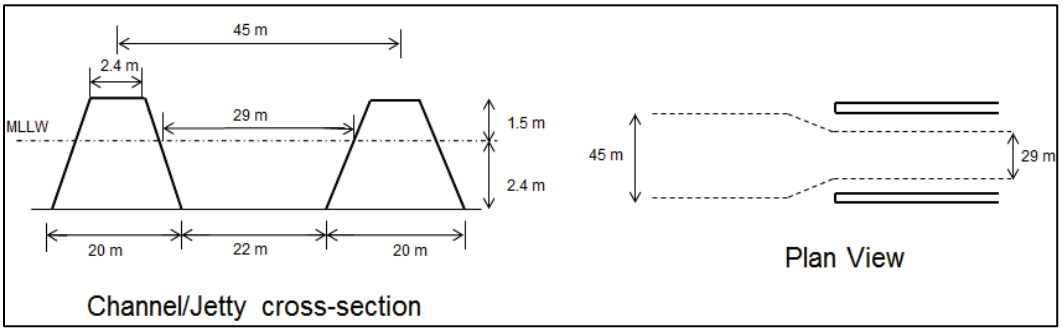

NAB provided survey data covering parts of the west channel, canal, and adjacent land areas. These survey data were augmented with data from other sources, including U.S. Geological Survey (USGS) coastal shoreline data and National Oceanic and Atmospheric Administration (NOAA) digital elevation model (DEM) data. The combined data set was necessary to properly resolve the details of the channel geometry and bathymetry, irregularly shaped shorelines, and elevations of the joining land areas for numerical modeling purposes. The extent of available bathymetry data and surveys are shown in Figures 2-3 and 2-4. The NAB 2015 survey had detailed coverage of the channel bathymetry and areas between the channel and north and south shorelines. The 2015 survey included land elevations for limited land areas along the north and south shorelines. Recent aerial photos were used to define the land-water interface.

Figure 2-3 shows the DEM quad sheets covering the Chesapeake Bay area. Figure 2-4 shows the 2012 post-Sandy lidar data for the west channel entrance and vicinity area. Figure 2-5 shows the coverage area of the west channel entrance for the NAB 2015 survey. MSL was used as the vertical datum for merging the 2012 lidar and 2015 surveys.

Figure 2-3. DEM bathymetry quad sheets for Chesapeake Bay.

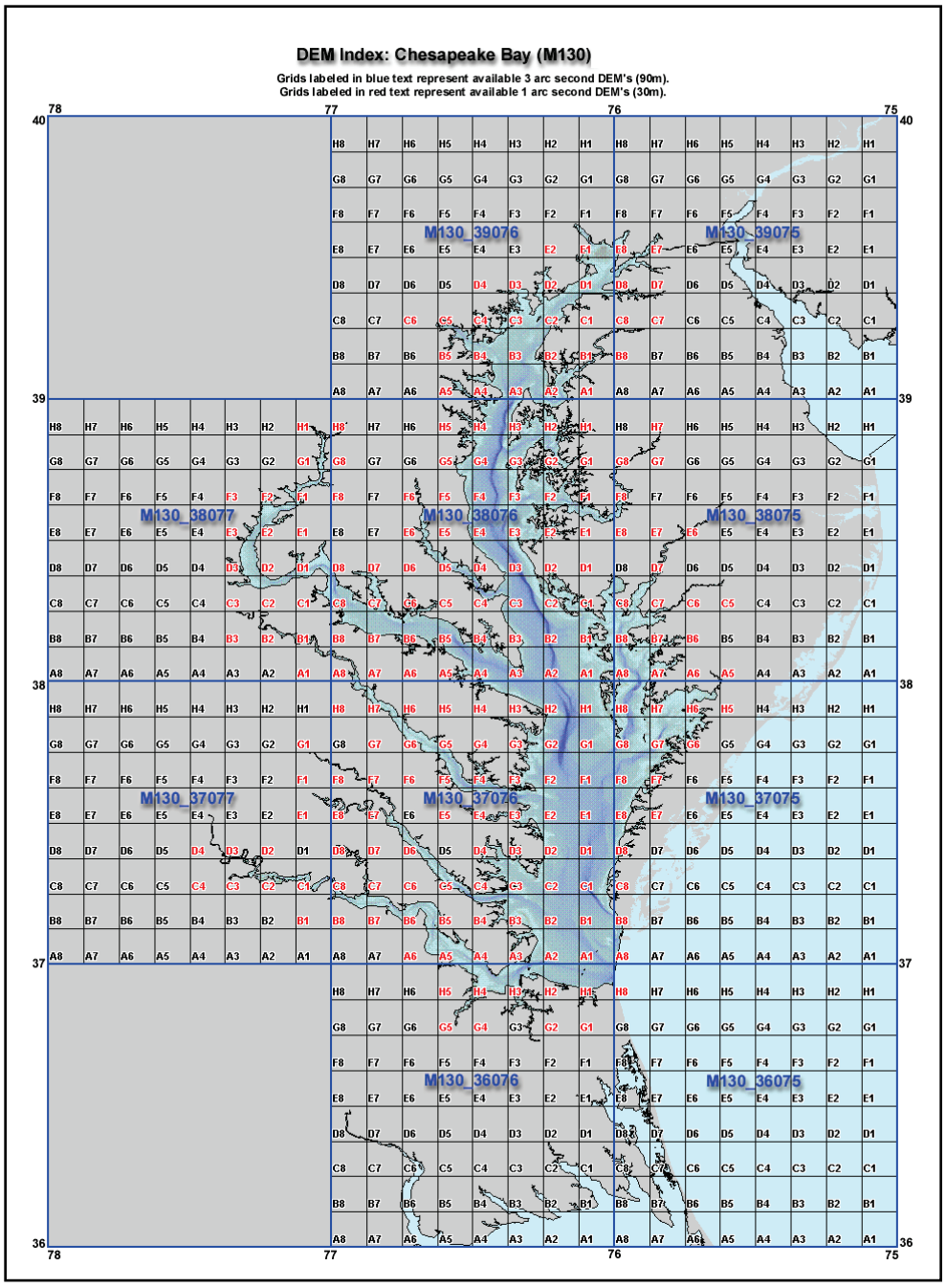

Figure 2-4. Post-Hurricane Sand lidar elevation contours for Smith Island.

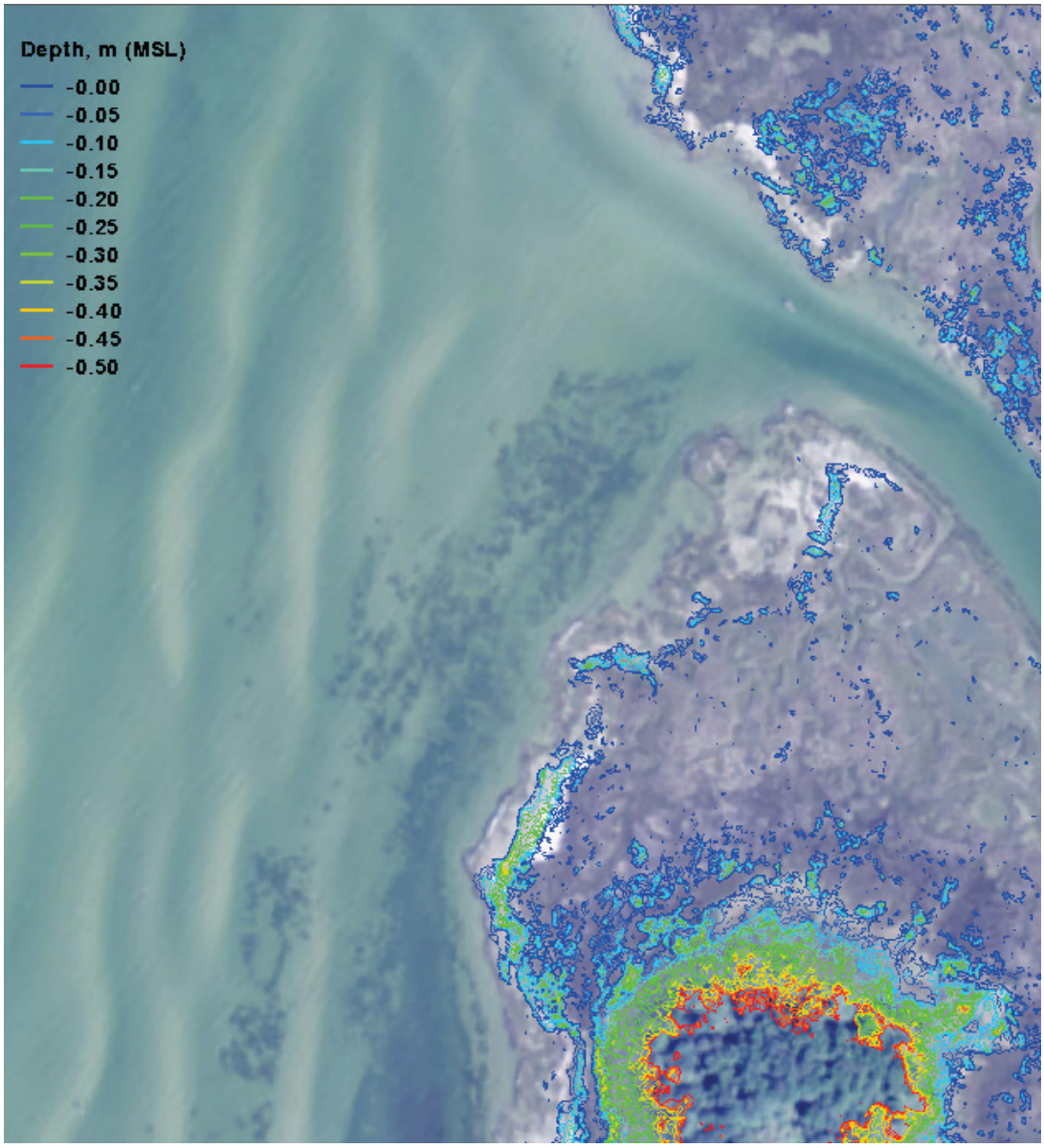

Figure 2-5. NAB 2015 survey data for west channel entrance (red points).

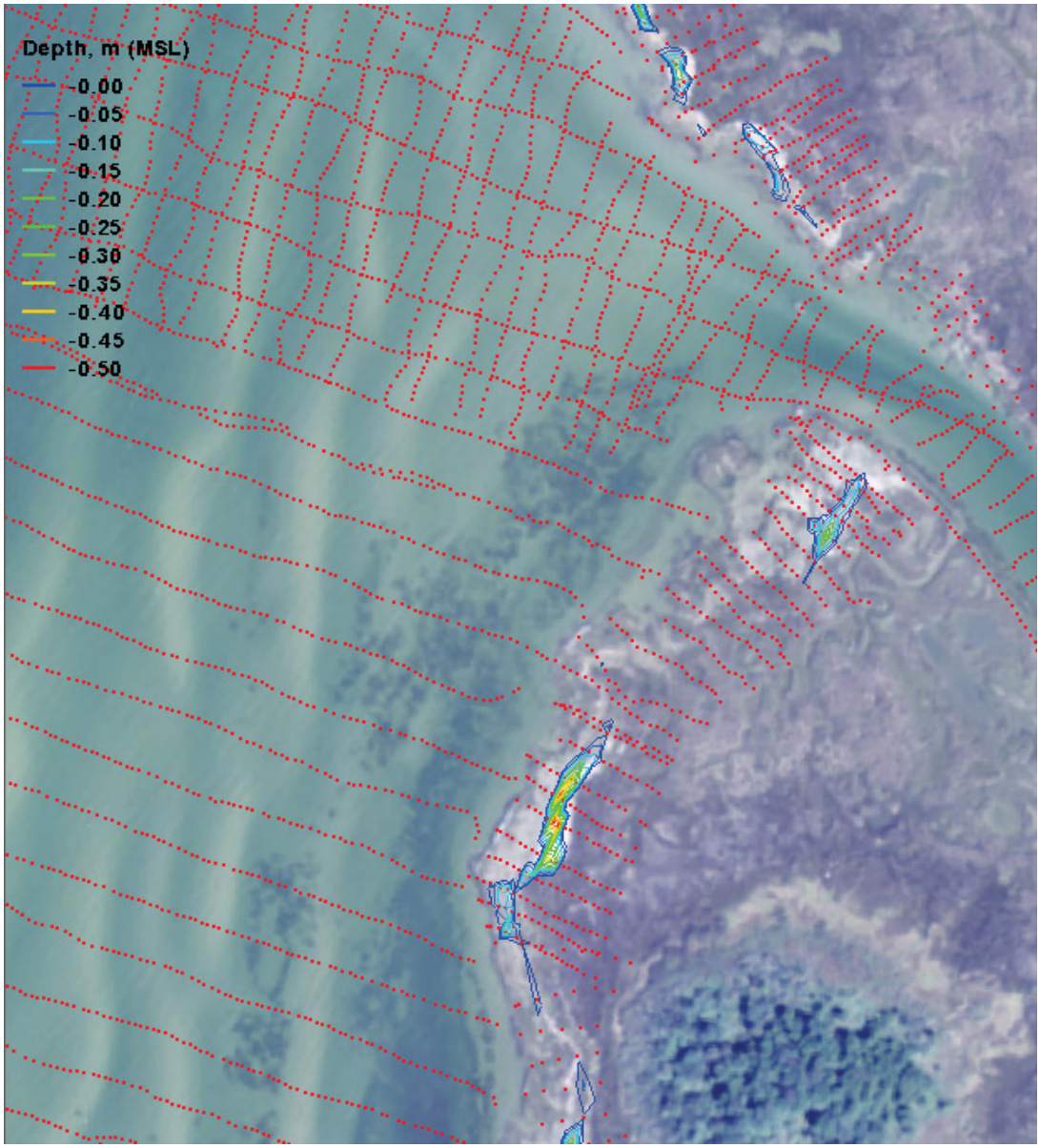

A dogleg north jetty (yellow line in Figure 2-6) was originally proposed to replace the long north jetty in Alt-2. This dogleg north jetty geometry was later modified to a simple shore-normal geometry (Figure 2-7) to reduce structural cost. In Figure 2-6, approximate shorelines (red lines) were extracted from aerial photos. Purple lines represent tentative locations of jetty and revetment structures that were considered initially. The final geometries of Alternatives (Alts 1 and 2) evaluated are described in Section 2.6.

Figure 2-6. North and south shorelines extracted from aerial photos (red lines).

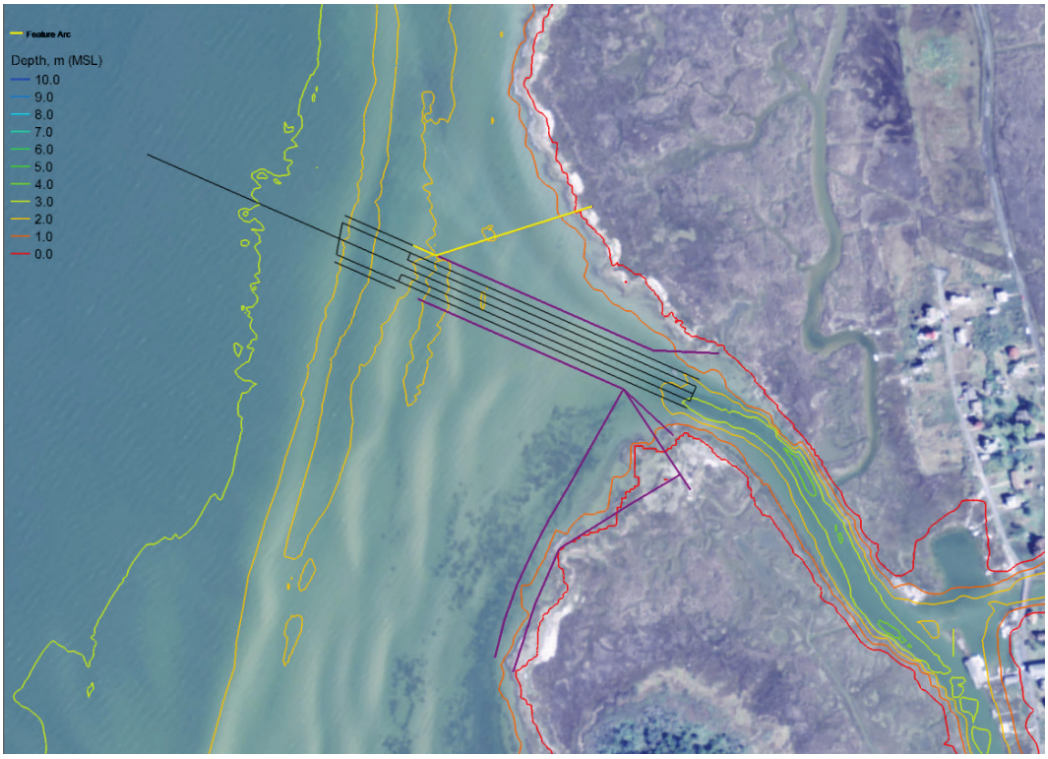

Figure 2-7. Sketch of shore-normal north jetty.

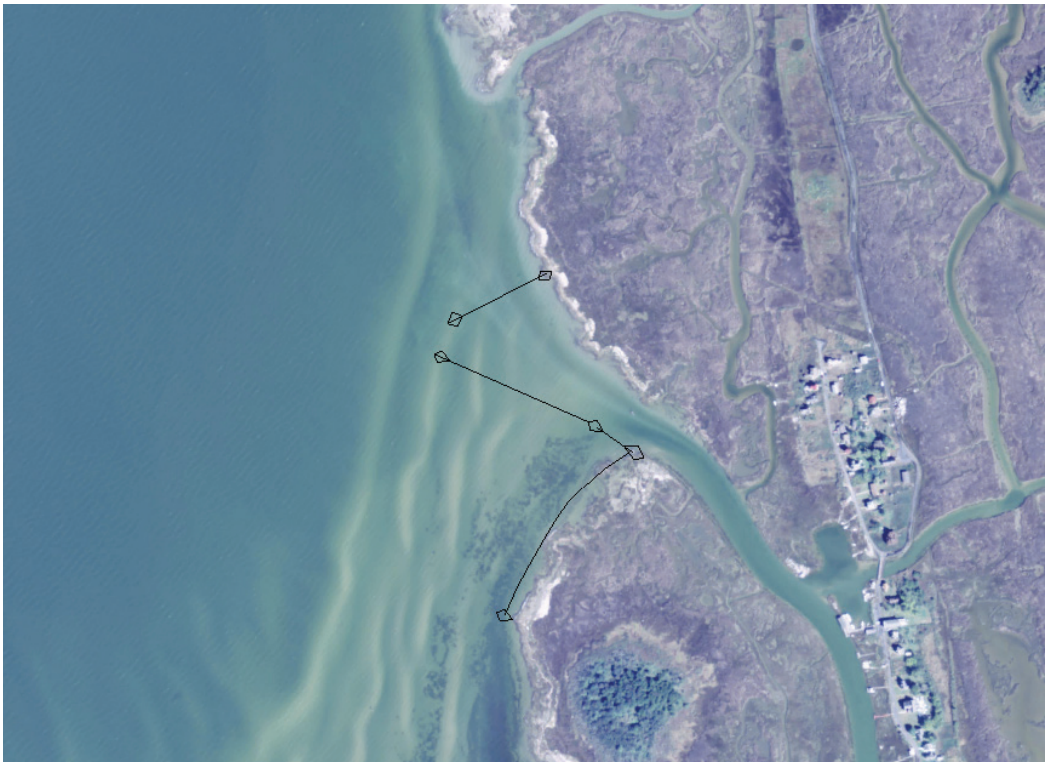

2.4 Metocean data

Figure 2-8 shows water level and wind stations available in the vicinity of the study area. These include the National Data Buoy Center (NDBC) buoy 44058 (Stingray Pt, VA), and NDBC buoy 44062 (Gooses Reef, MD), and six NOAA Coastal Stations: Rappahannock Light, VA (CB0801/RPLV2, NOAA Station 8632837); Cove Point LNG Pier, MD (CB1001/COVM2); Lewisetta, VA (LWTV2, NOAA Station 8635750); Bishops Head, MD (BISM2 8571421); Chesapeake Bay Bridge Tunnel, VA (CBBV2, NOAA Station 8638863); and Windmill Pt, VA (NOAA Station 8636580). Figures 2-9 and 2-10 show the time series of water level and wind data, respectively, for 2014 from these stations.

Figure 2-8. Water level and wind stations in the vicinity of study area.

Figure 2-9. Example water level time series for 2014 at Lewisetta, VA (8635750), and Chesapeake Bay Bridge Tunnel (8638863).

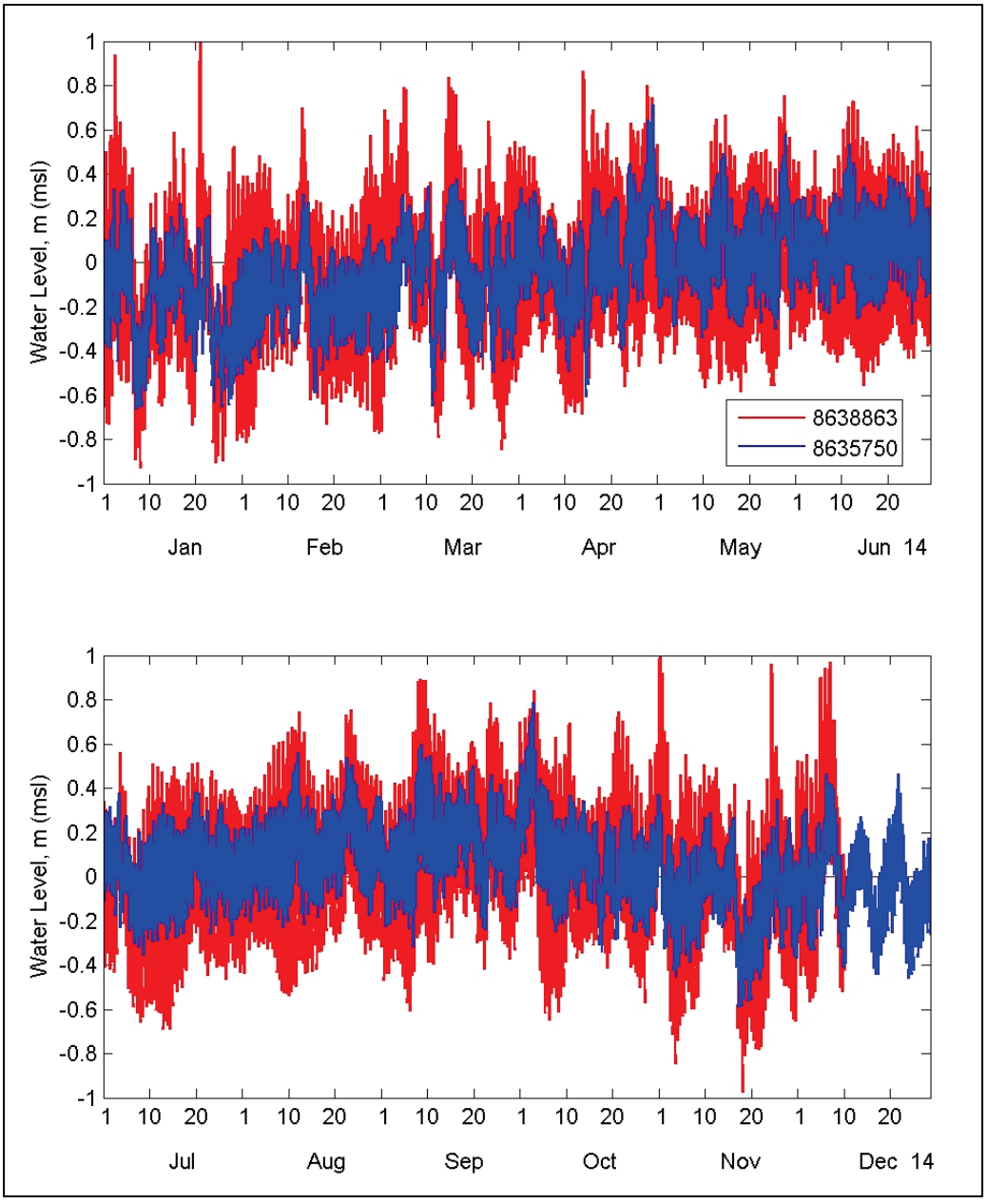

Because Smith Island and the middle portion of the Chesapeake Bay are not exposed to open ocean waves, locally generated waves affecting the west side of the Smith Island were developed by using local winds as input to CMS-Wave.

Figure 2-10. Wind data time series for 2014 at different stations.

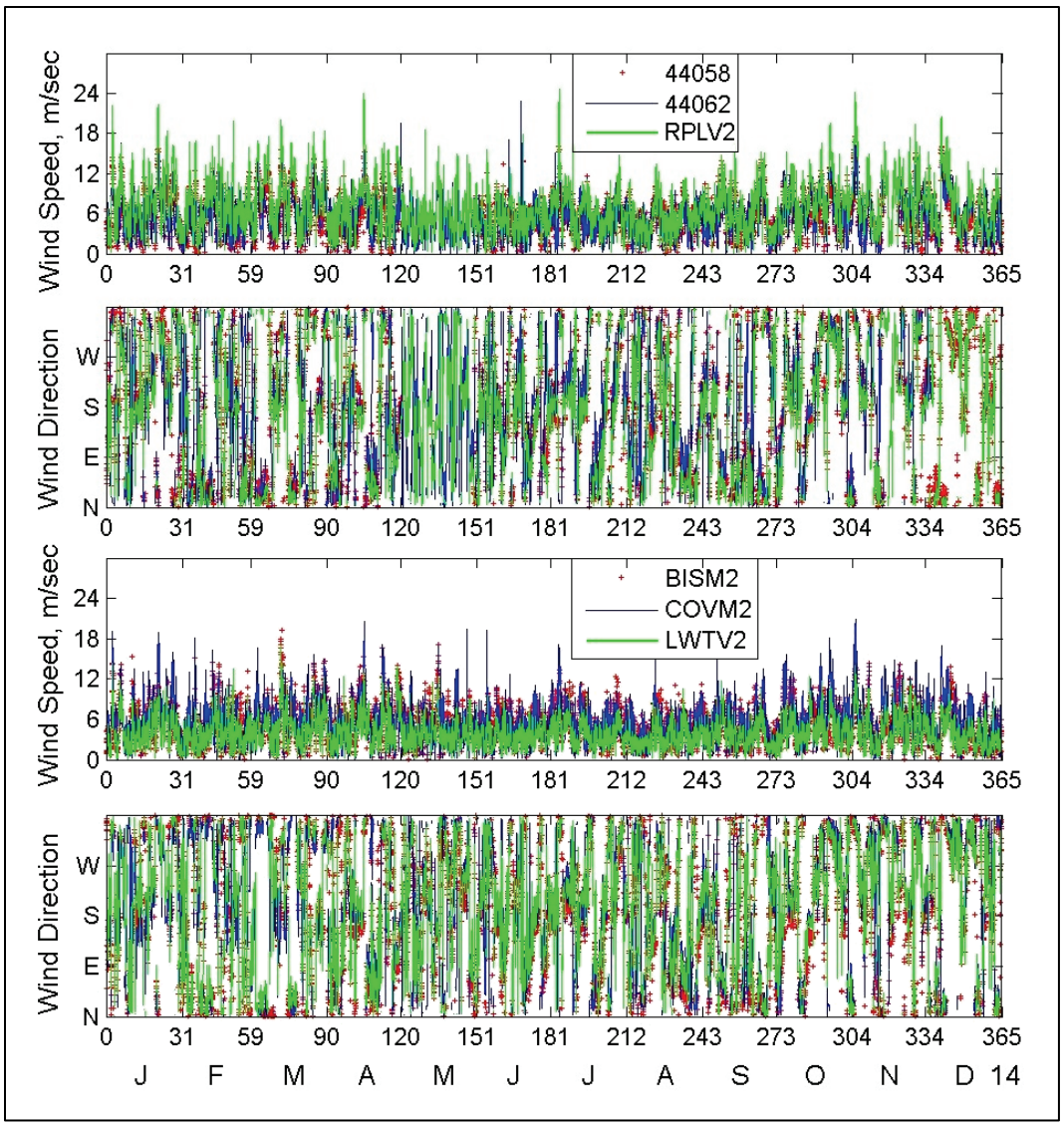

2.5 Model grids

Figure 2-11 shows the CMS modeling grid domains for the entire Chesapeake Bay (large rectangle box) and local Smith Island (small rectangle box). The bay-wide large grid domain covering approximately 60 by 180 miles (100 by 300 kilometer [km]), is referred to as the "regional grid." This Bay-scale grid has a constant grid cell size of 1,600 by 1,600 ft (500 by 500 m), and water depths in this grid vary from 0 to 150 ft (0 to 45 m). Figure 2-12 shows the water depth contour map associated with the regional grid.

Figure 2-11. Extent of regional (bay-wide) and local (Smith Island) modeling domain.

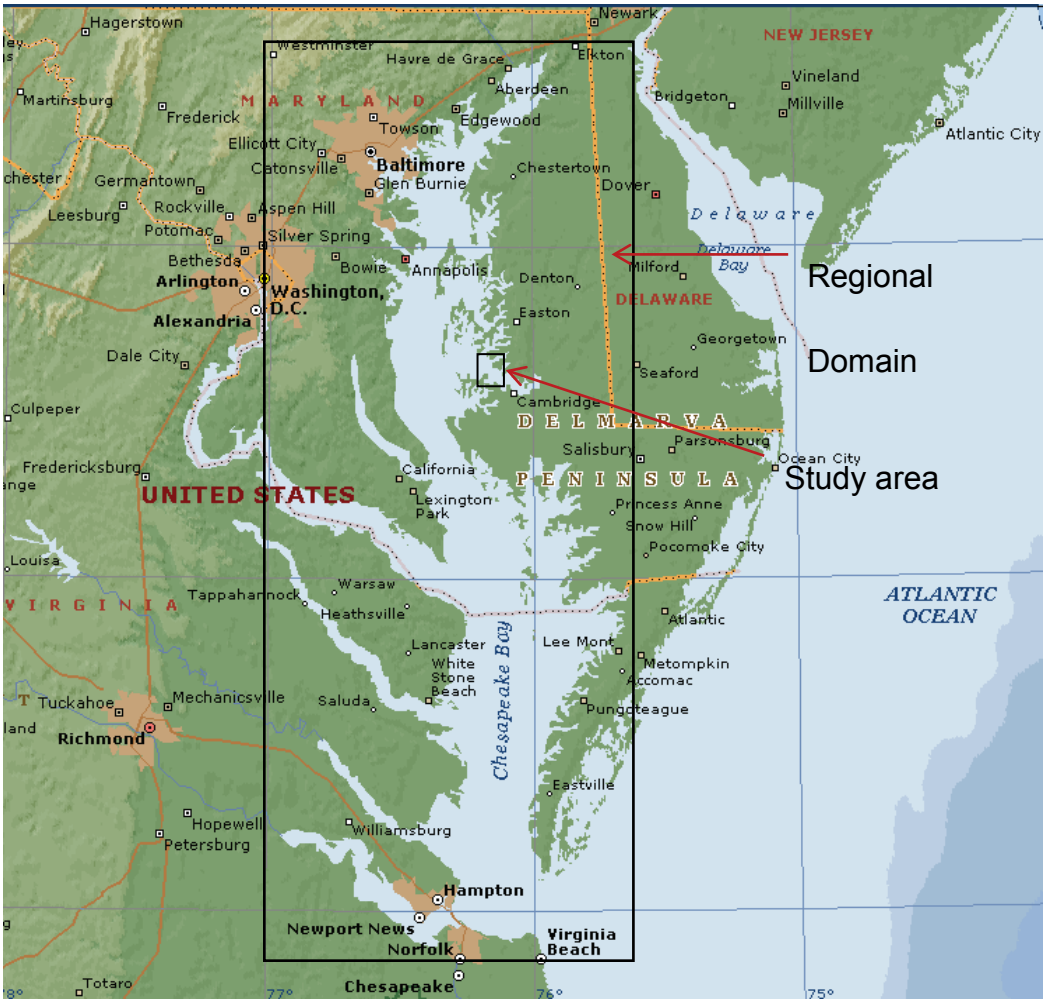

The Smith Island local grid domain is approximately 7.8 by 11.6 miles (12.5 by 18.5 km) with varying cell spacing ranging from 10 to 330 ft (3 to 100 m). Figure 2-13 shows the existing local grid depth contours and model domain covers the Smith Island.

Figure 2-14 shows the local CMS-Wave grid bathymetry representing the existing west channel configuration at Rhodes Point. The zoomed image in Figure 2-15 provides details of the depth contours at the west entrance channel and north and south shoreline seaward of the canal at Rhodes Point. This grid has a finer-resolution bathymetry on the west side of Smith Island and especially at the west channel of Rhodes Point. The water depths in the grid vary from 0 to 20 ft (0 to 6.1 m). This baseline geometry, designated as Alt-0, was used in the evaluation of the two proposed Alternatives (Alt-1 and Alt-2) which included jetty and revetment structures.

Figure 2-12. Regional Chesapeake Bay grid depth contour map.

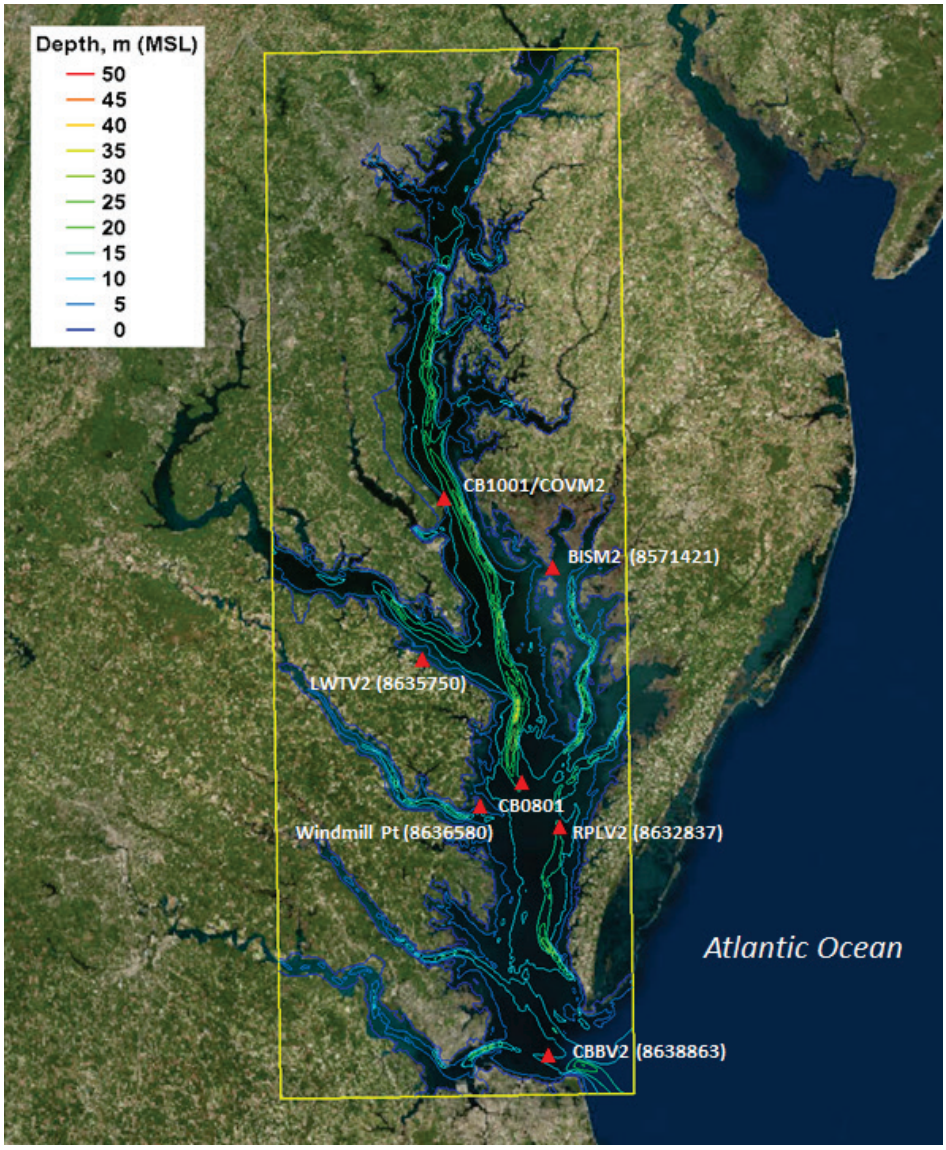

Figure 2-13. Local Smith Island grid depth contour map.

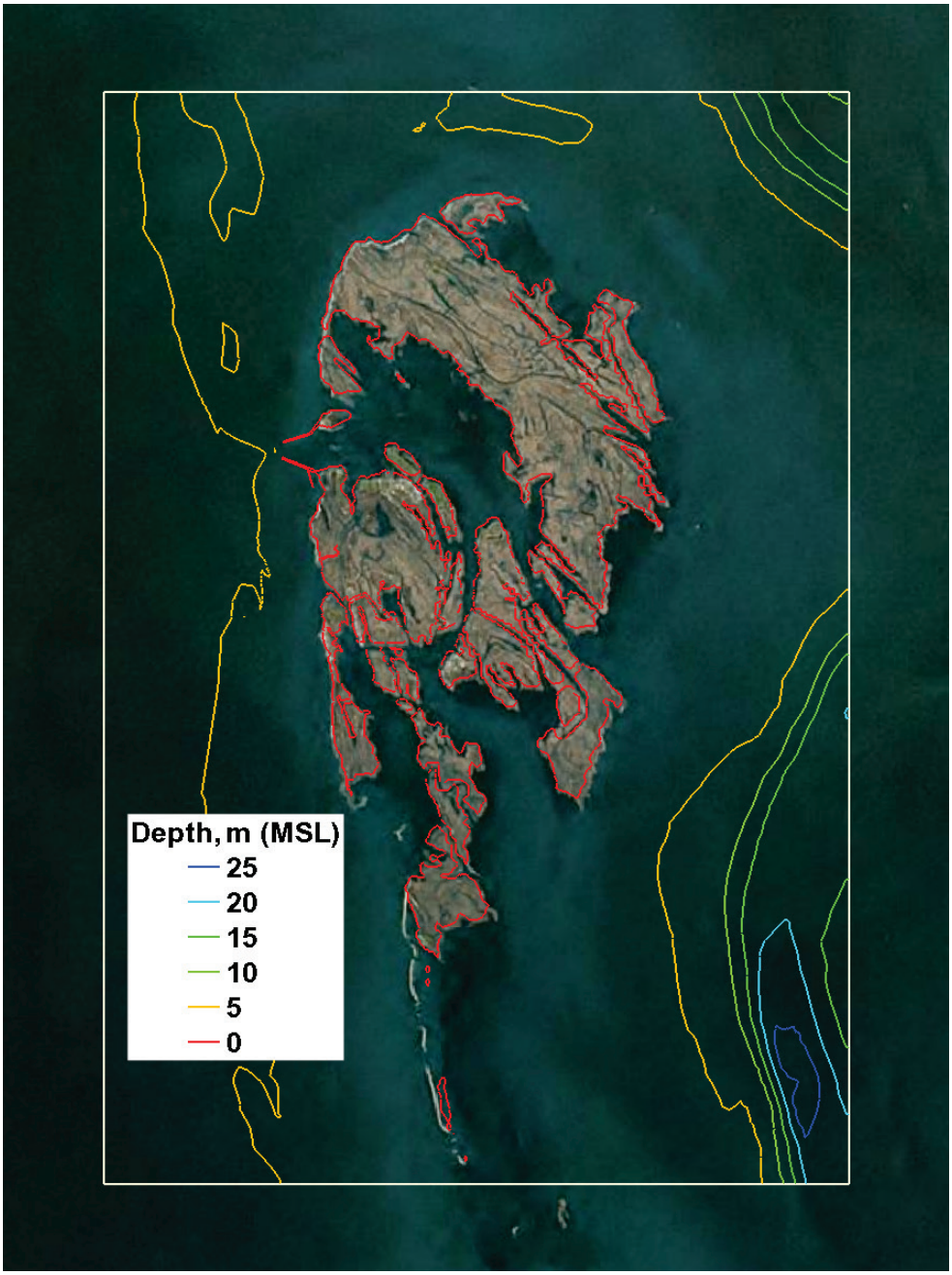

Figure 2-14. Local CMS-Wave grid depth contours at Rhodes Point and vicinity.

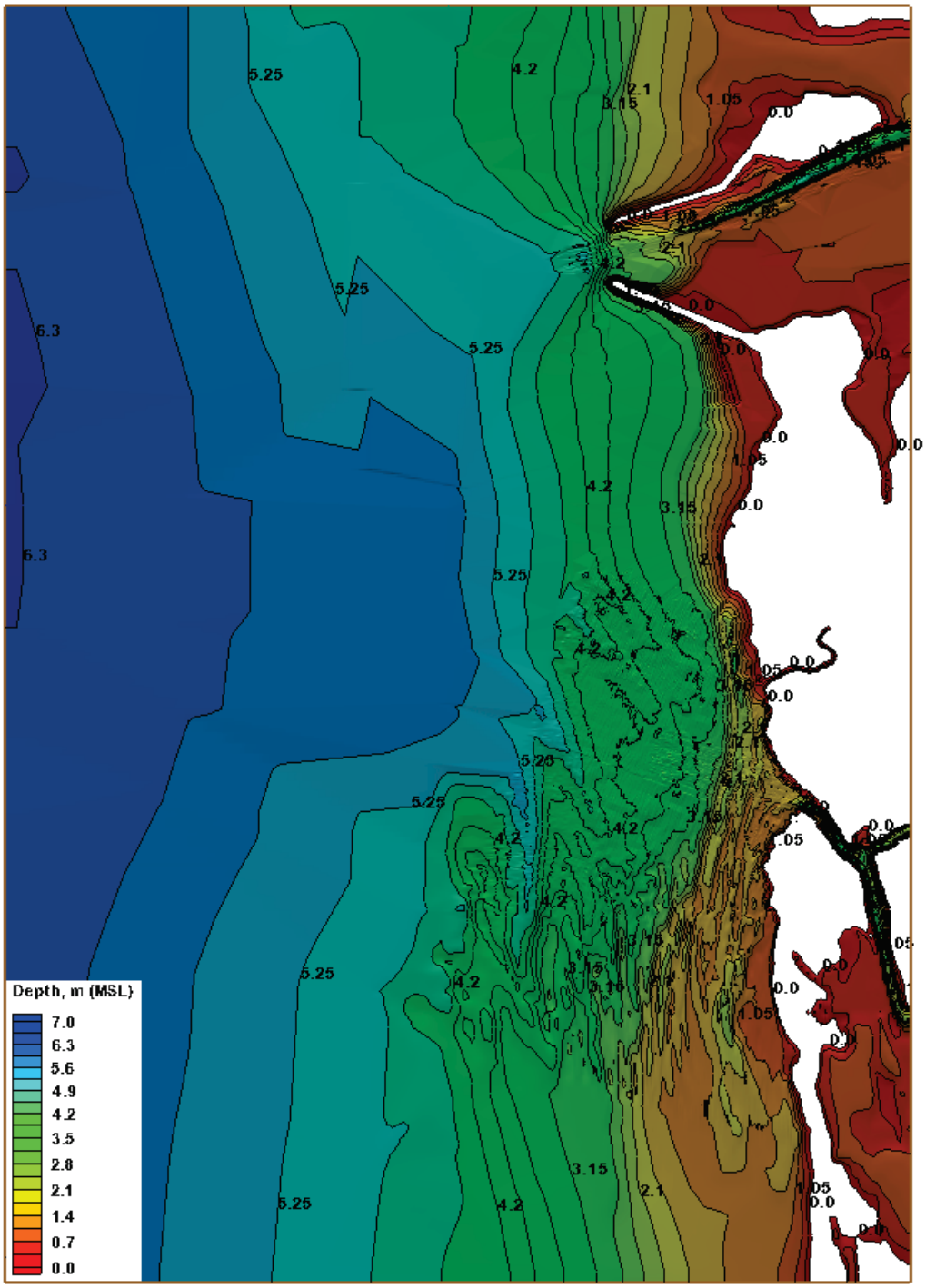

Figure 2-15. Depth contours covering the western channel and seaward areas of the canal entrance.

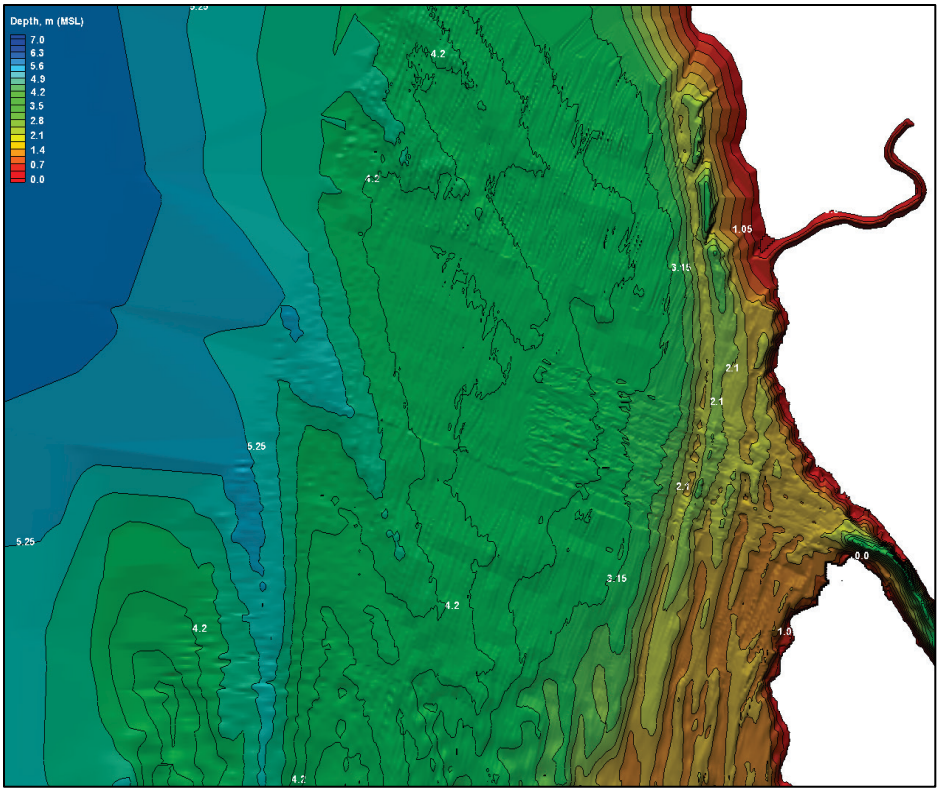

A modeling approach consistent with the main goal of the present study was used. This included quantitative estimates of waves and calculations of wave heights for no-project versus alternative condition, and preliminary jetty and revetment structure design calculations. The study team selected a 1-month simulation in summer, a 1-month simulation in winter, and Hurricane Sandy as the design storm condition. The months of August and February 2014 were selected for the 1-month simulations in summer and winter, respectively. Hurricane Sandy was simulated for a 6-day period (26–31 October 2012). Because of low wave energy (calm bay condition) during August 2014, only winds and tidal forcings were included in the simulation for this month (e.g., no wave input).

2.6 Existing channel and structural Alternatives

Additional information about the three channel configurations investigated is provided in this section. These included the existing channel geometry without structures and two Alternatives with jetty and revetment structures. The configurations were designated as Alt-0 (existing), Alt-1 and Alt-2, and are depicted in Figures 2-16, 2-17, and 2-18, respectively. The five transects,

T1 through T5, were created to extract model output as displayed on each figure with the channel centerline showing the location of channel.

Figure 2-16 shows the existing geometry (Alt-0). There is only a natural channel in the "without project" case, so an imaginary channel with five output transects is shown in reference to Alternatives. The numbering scheme used for save locations along each transect is noted. The output transects have the following stations: T1 (1–17), T2 (18–28), T3 (29–55), T4 (56–74), and T5 (75–95). The distance between stations on each transect was 10 m.

Figure 2-16. Existing channel geometry (Alt-0) with five transects (T1 to T5).

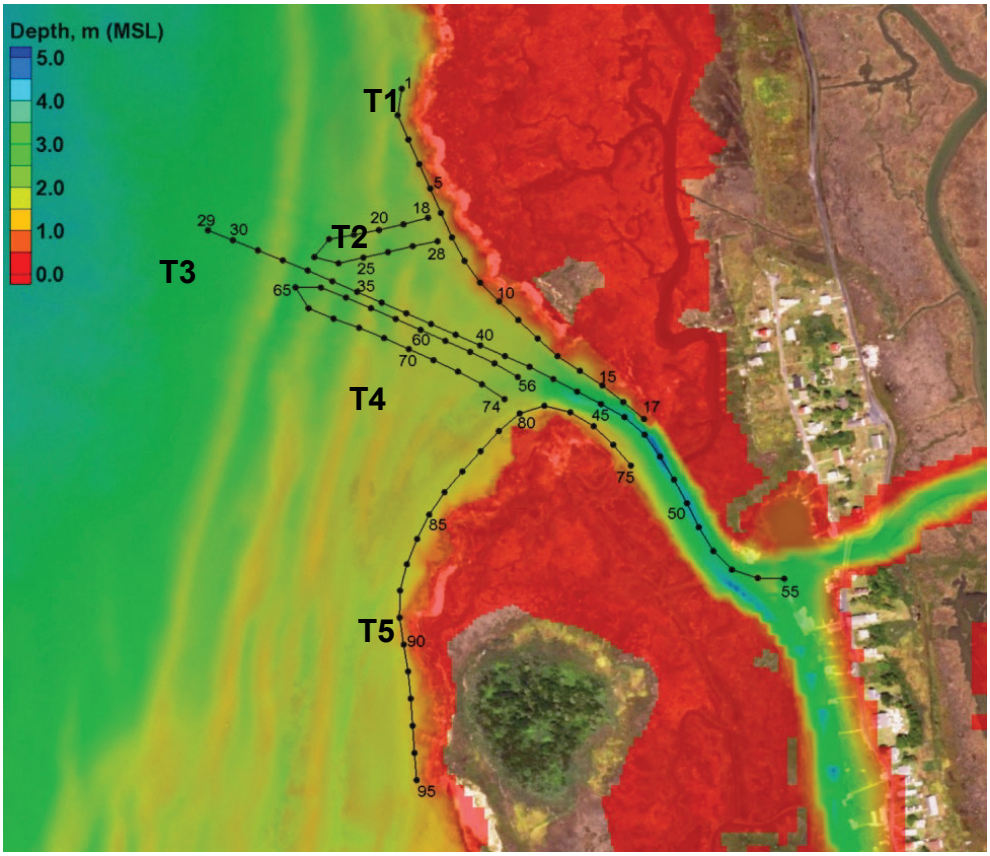

Figure 2-17. Alt-1 channel geometry (a) with a shore-normal north jetty and (b) five output transects (T1 to T5).

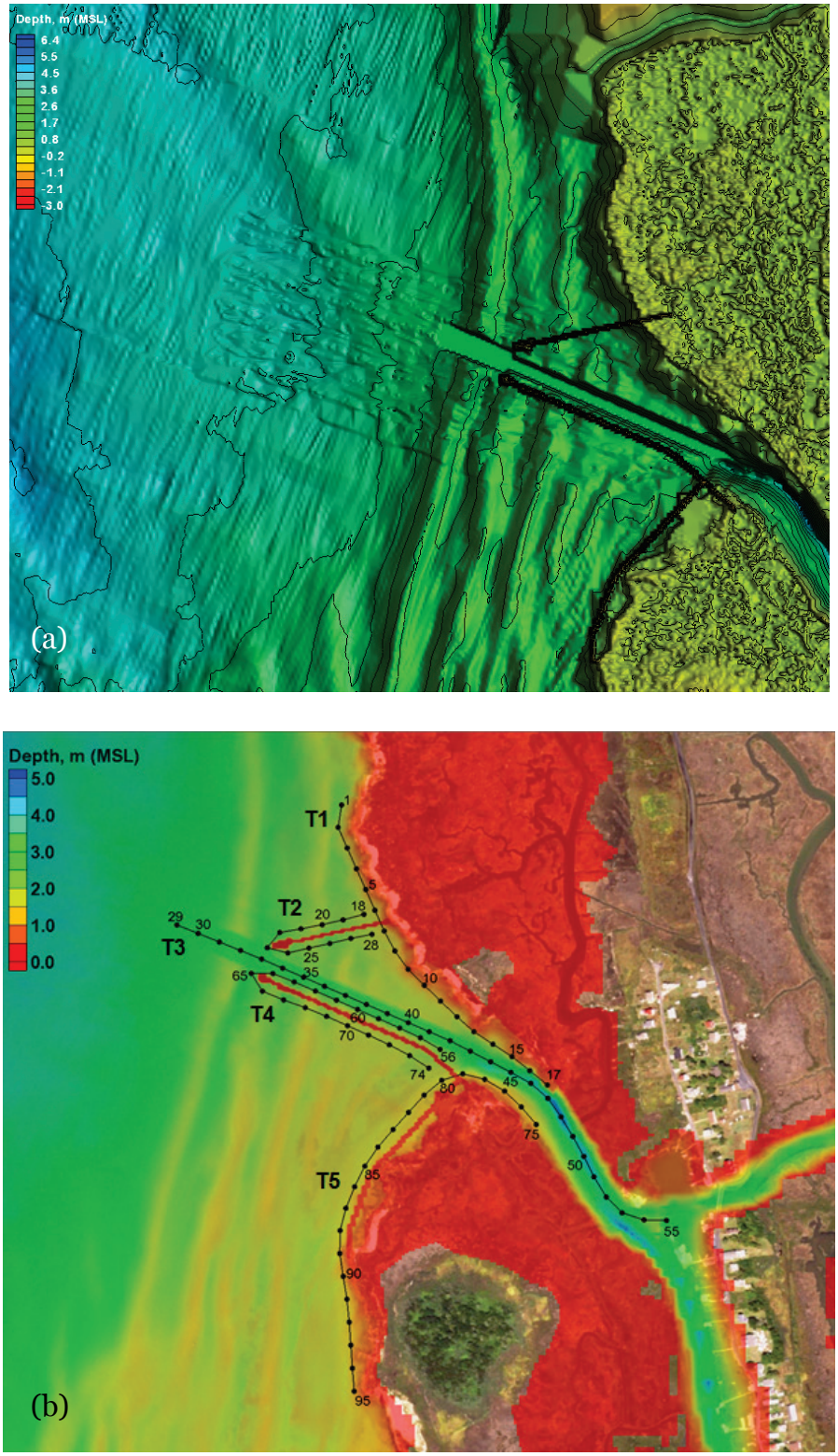

Figure 2-18. Alt-2 channel geometry (a) with a parallel north jetty and (b) five output transects (T1 to T5).

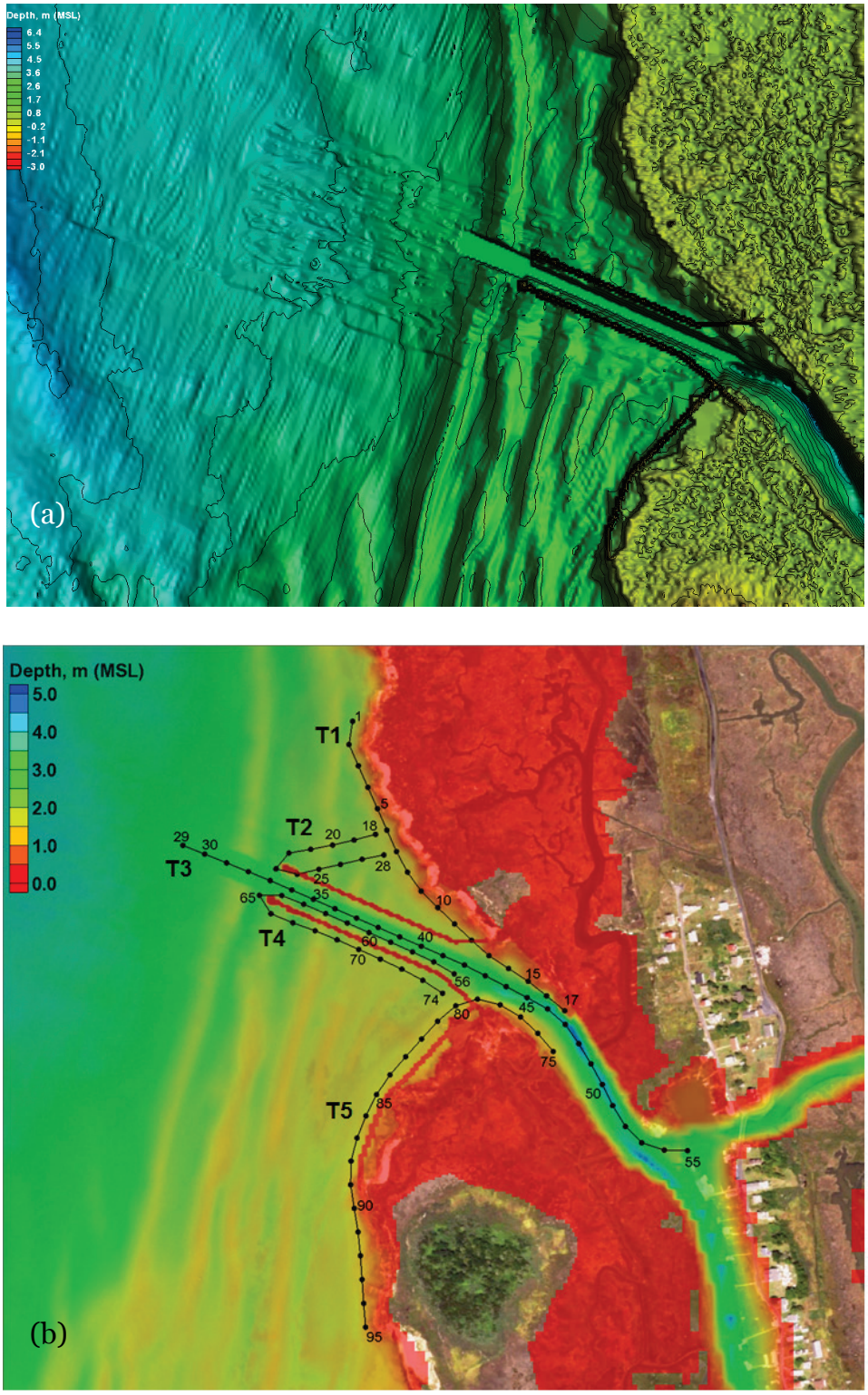

Alt-1 representing the new realigned channel geometry with a shore-normal north jetty is shown in Figures 2-17(a), and with the five output transects in Figure 2-17(b). The 688 ft (210 m) long north jetty was oriented in a SW to NE direction, with the last 130 ft (40 m) segment on land. The 820 ft (250 m) long first segment of the south jetty paralleling the channel centerline was oriented in a NW to SE direction. The second segment (tie-in) was 310 ft (95 m) long, with the last 165 ft (50 m) of this jetty structure on land. The low-crested revetment dike for protection of the south shorelines was 840 ft (280 m) long. Figures 2-16, 2-17, and 2-18 show the canal at Rhodes Point that splits Smith Island and establishes a water connection between the west and east sides of island.

Figure 2-18(a) and Figure 2-18(b) show the Alt-2 configuration and output transects T1 to T5, respectively. Alt-2 was considered in the 2009 feasibility project and was re-evaluated in the present study. It has two parallel jetties situated along north and south edges of the channel. The jetties are each 800 ft (245 m) long. Both the north and south parallel sections join with a dogleg segment (tie-in), connecting to the land north and south of the entrance. The second segment of the north jetty was 295 ft (90 m) long, with 82 ft (25 m) of it on land. The second segment of the south jetty was 345 ft (105 m) with 195 ft (60 m) of it on land. The low-crested revetment dike for protection of the south shorelines was 920 ft (280 m) long. The same output stations were used for all Alternatives.

The terminal ends of the north and south jetties at the shorelines were assumed to have appropriate land elevation to minimize the likelihood for destabilization and flanking. The north jetty in Alt-1 was a shorter structure because its land connection point was moved farther away from the mouth of canal. The shore connection points for the north and south jetties in Alt-2 were much closer to the entrance canal. The tie-in of the north jetty in Alt-2 connected to the north shoreline at a distance of 210 ft (70 m) from the canal entrance. The south jetty tie-in was 100 ft (30 m) from the entrance. The total length (linear footage) of the jetties was kept as short as possible to reduce the structural cost. The north jetty lengths for Alt-1 and Alt-2 were approximately 665 ft (200 m) and 1,000 ft (305 m), respectively. The south jetty was 1,000 ft (305 m) for both Alternatives. The jetties in both Alternatives were represented in the numerical model by a rubble-mound structure with a crest elevation of +5 ft (1.5 m) above MLLW and crest width of 8 ft (2.4 m). The water depths in the areas of interest ranged from 0 to 22 ft (0 to 6.5 m) in the west channel and seaward area of the Chesapeake Bay.

2.7 Forcing conditions

Rhodes Point and vicinity area are affected by annually and seasonally changing forcing conditions in the Chesapeake Bay. These include metocean events such as storms, northeasters, hurricanes, and normal winds, waves, and tidal conditions. The dominant winds are from the north and northwest in the winter and from the southwest in the summer while local breeze shifts the wind direction on a daily basis. Larger waves generally occur during northeasters and tropical storms when high winds blow across the bay. The west shoreline of Smith Island is exposed to open water in the lower Bay area where strong wind can generate large waves.

Figure 2-19 shows two sample wind roses for 2011 and 2012 from NOAA station 8632837 at Rappahannock Light, VA. Winds with magnitudes greater than 20 knots (~ 10 meters per second [m/sec]) mostly follow a longer fetch along the north–south direction in the lower bay. During northeasters with sustained winds of 30 to 40 knots (~ 15 to 20 m/sec), local wave heights ranging from 5 to 8 ft (~1.5 to 2.5 m) can occur along the west side of Smith Island.

A 6-day storm simulation (26–31 October 2012) covering the Hurricane Sandy period was selected to represent the 50-year return period event at Smith Island. This forcing condition was used for evaluating the effectiveness of the west entrance with jetties in reducing wave energy in the channel. For more common, less intense forcing conditions (typical conditions), the CMS simulations were conducted for one summer month (August 2014) and one winter month (February 2014).

The water level forcing from Station 9638863 (Chesapeake Bay Bridge Tunnel) and wind input from Station 8632837 (Rappahannock Light) were used in the bay-scale regional grid (parent grid) simulation (Figures 2-8 and 2-12). Results from this simulation were used for model calibration and driving the local Smith Island grid (child grid). For the model calibration, model-calculated water level results were saved at the location of three water level Stations (Bishops Head, 8571421; Lewisetta, 863570; Windmill Point, 8636580), and currents were saved at the two current data Stations (Cove Point, 8577018; Rappahannock Light, 8632837), and were compared with measurements.

Figure 2-19. Wind roses for 2011 and 2012 at Rappahannock Light, VA (8632837).

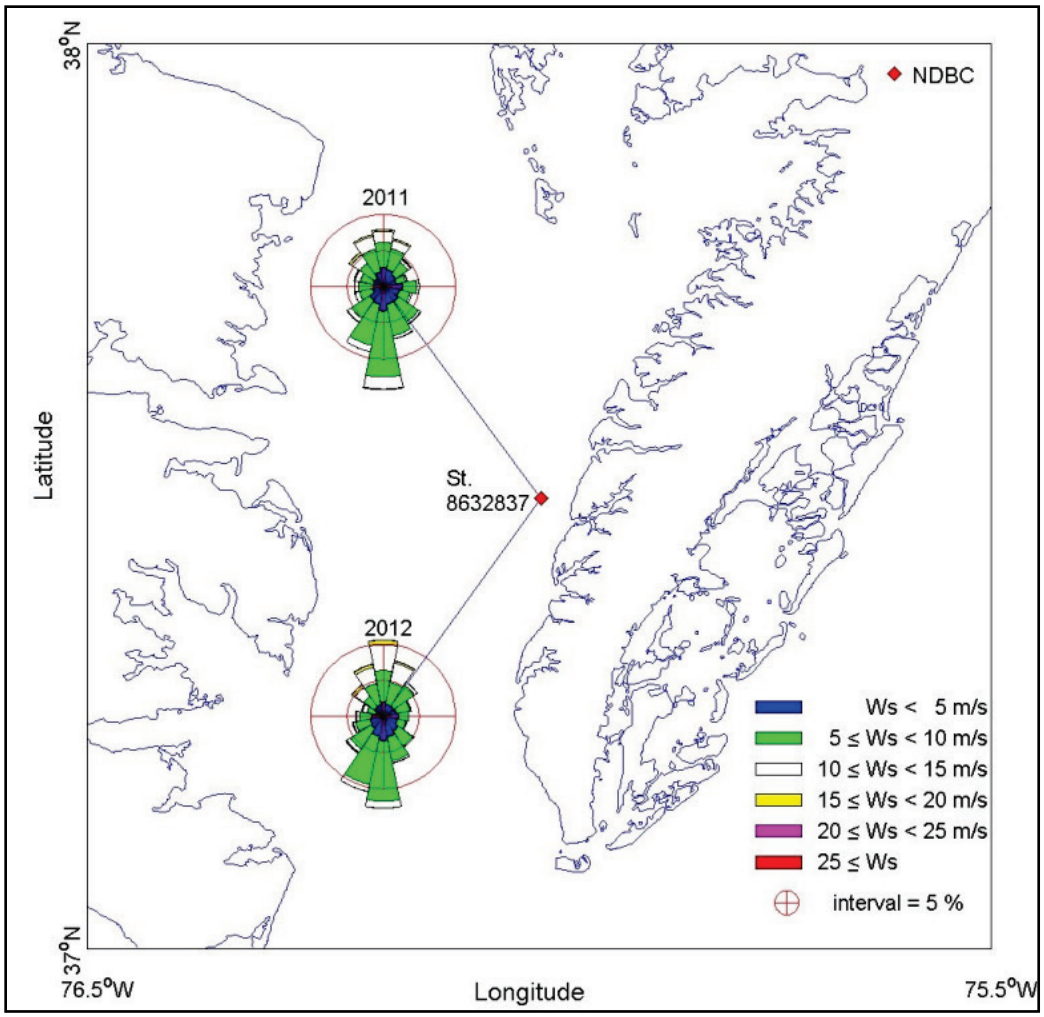

Figure 2-20 shows the model-data comparison of calculated water levels at Bishops Head, MD; Lewisetta, VA; and Windmill Pt, VA, near the project site. Good correlation between model water levels and data was obtained. The correlation coefficients between model water levels and data at Stations 8571421, 8635750, and 8636580 were 0.98, 0.97, and 0.93, respectively.

Figure 2-21 shows the model-data comparison of calculated currents along the east-west (E-W) and north-south (N-S) directions for NOAA stations at Rappahannock Light, VA, and Cove Point, MD. The correlation coefficients between calculated E-W components of currents and data at CB0801 and CB1001 were 0.27 and 0.88, respectively. The low correlation between calculated E-W current components and data at CB0801 was likely due to increased wind-wave interaction at lower current speeds. Higher correlation coefficients of 0.89 were obtained between calculated N-S components of

current and data at both CB0801 and CB1001. Overall, the model calibration results indicated a good model-data agreement for calculated water levels and current magnitudes in the bay.

Figure 2-20. Calculated and measured water levels for August 2014 at Bishops Head MD (8571421), Lewisetta VA (8635750), and Windmill Point VA (8636580).

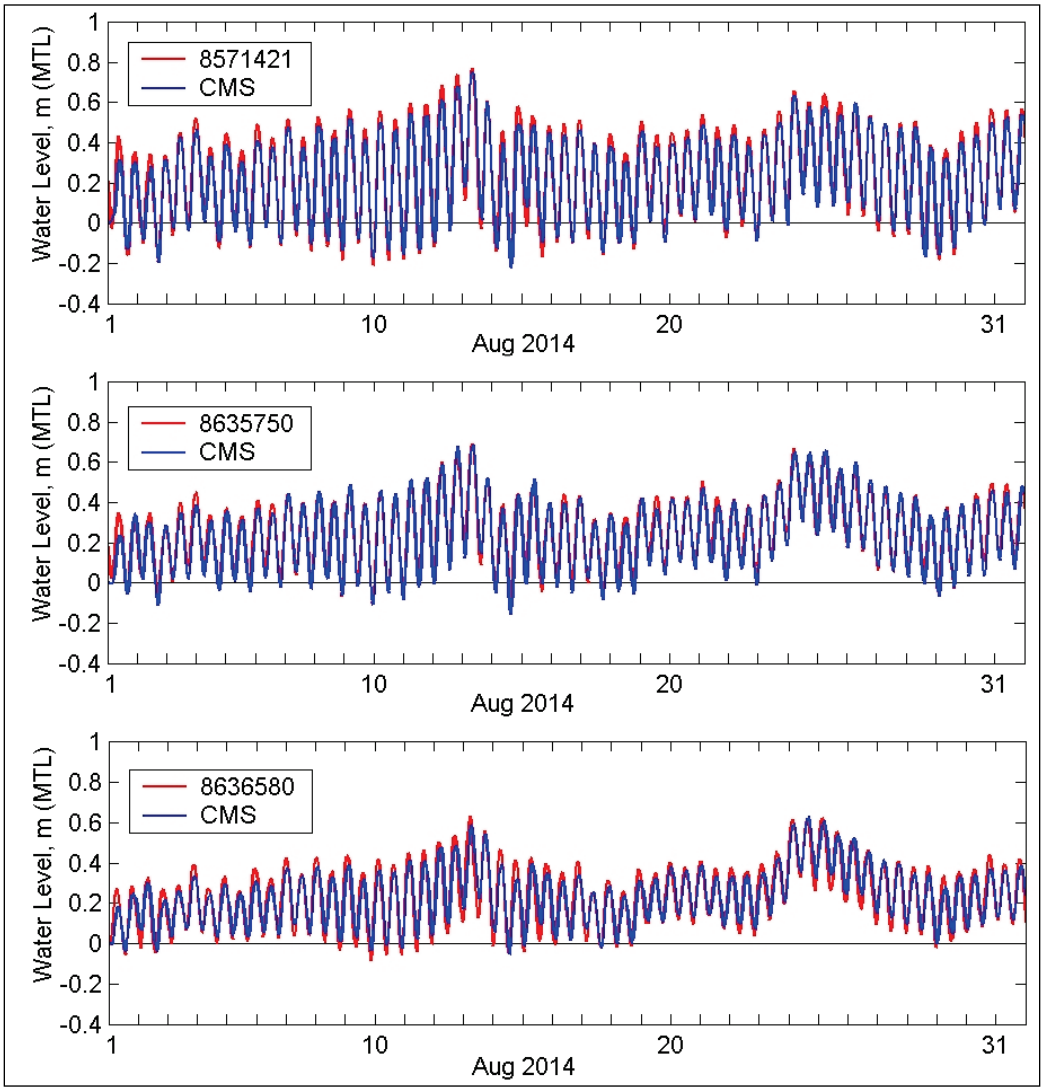

Figure 2-21. Calculated and measured currents for August 2014 at Rappahannock, VA (CB0801), and Cove Point, MD (CB1001).

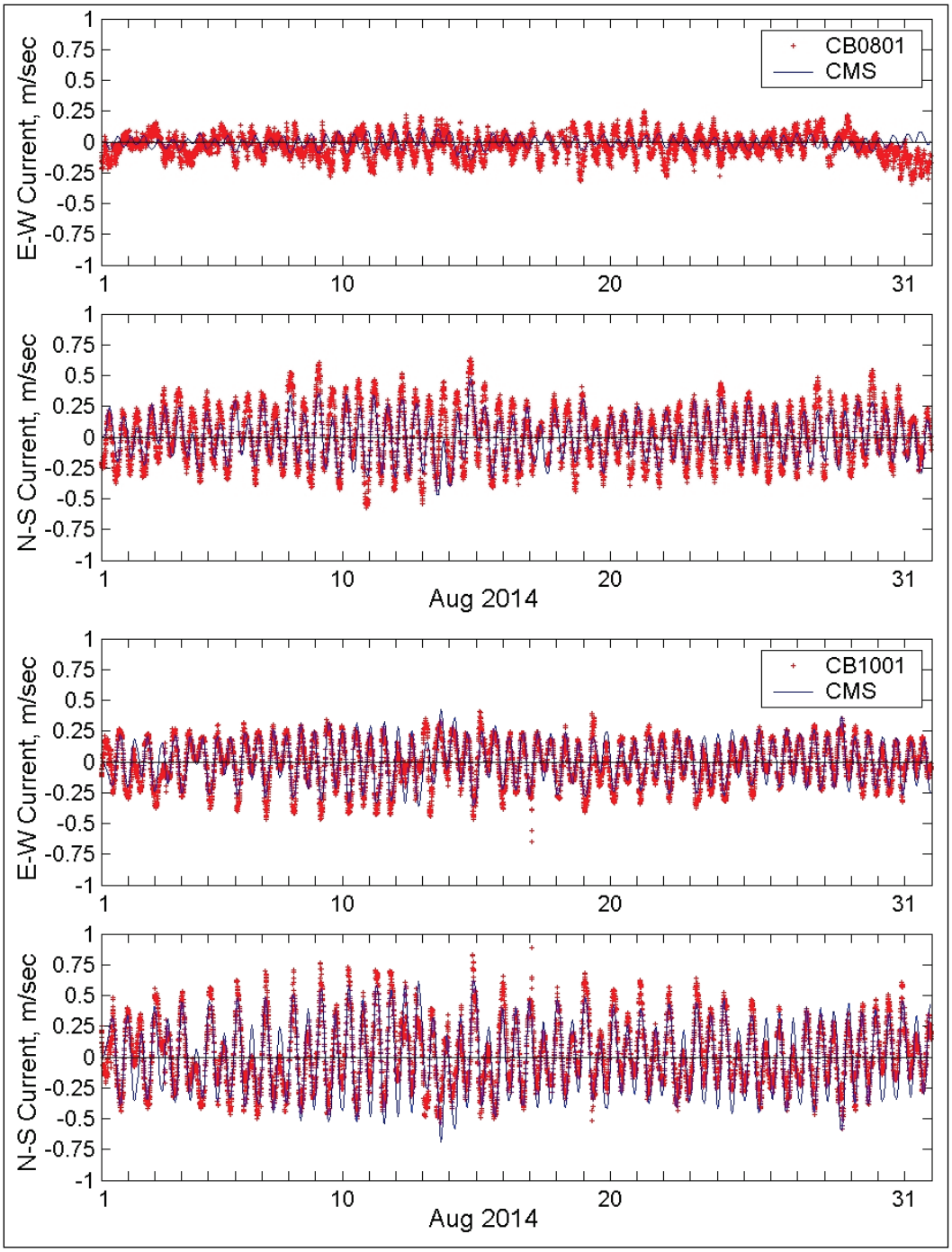

2.8 Save stations

Numerical model results were extracted along five transect lines (T1 to T5), covering the north and south jetties, channel centerline, and along the north and south shorelines. Figure 2-22 shows the five transects with save stations (points) on each transect. The spacing between the points is 100 ft (30 m). A total of 95 save stations was placed along the channel centerline, north and south shorelines, and around the perimeter of jetty and revetment structures. The save stations are shown in Figures 2-23, 2-24, and 2-25 for Alt-0, Alt-1, and Alt-2, respectively.

For clarity, all 95 save stations along five transects have been marked on Figures 2-23, 2-24, and 2-25, for Alt-0, Alt-1, and Alt-2, respectively. Only the start and end stations are labeled in these figures.

Figure 2-22. Transects (lines) for extraction of model results.

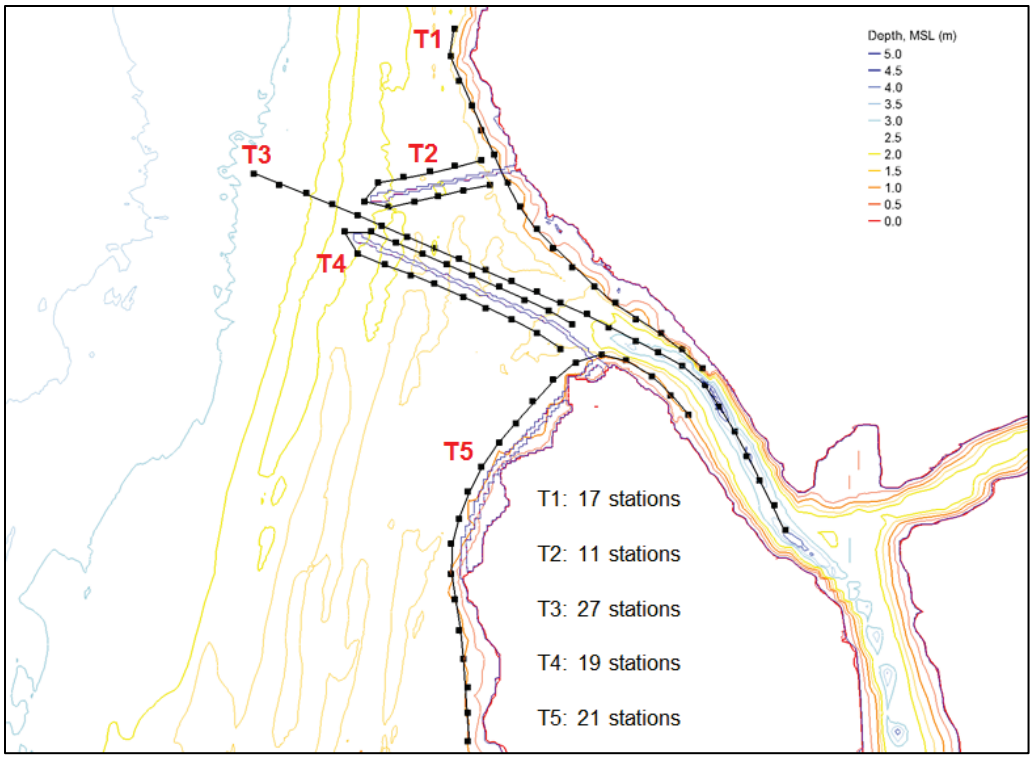

Figure 2-23. Save stations for Alt-0.

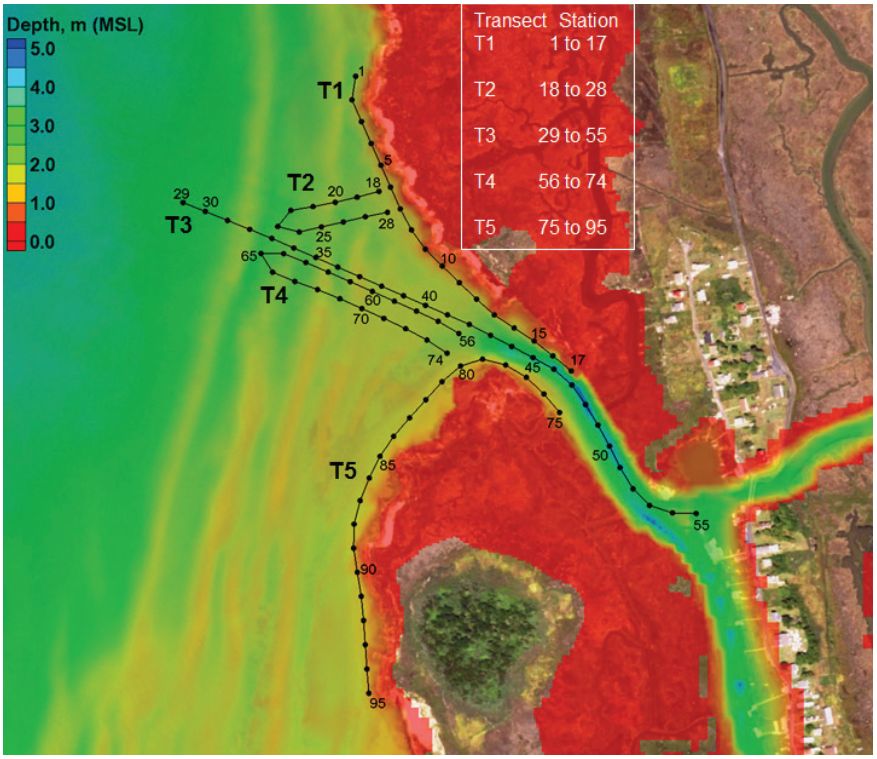

Figure 2-24. Save stations for Alt-1.

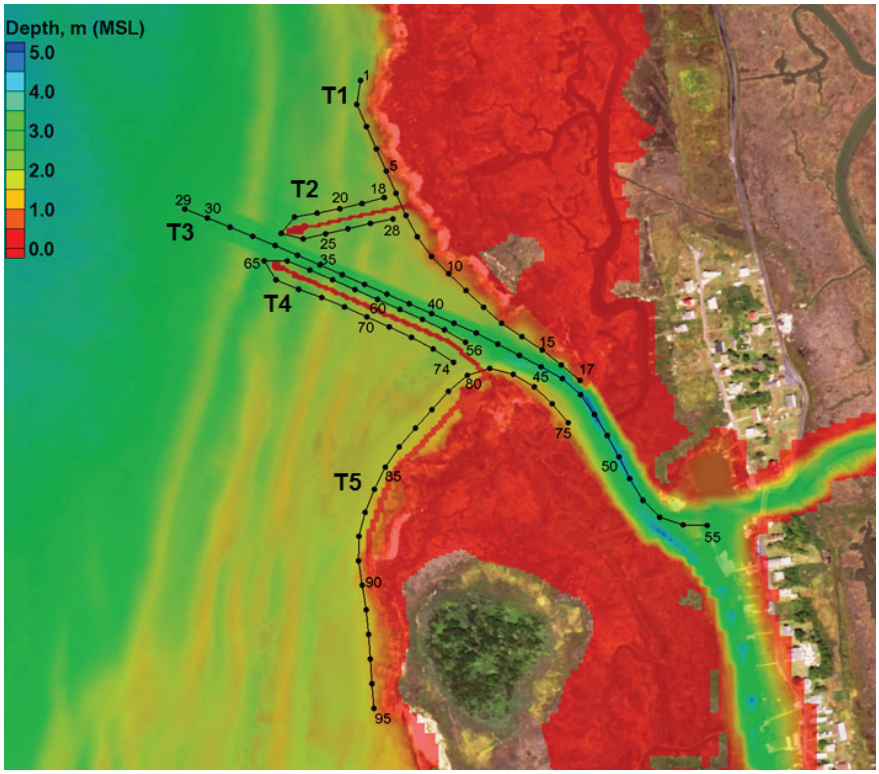

Figure 2-25. Save stations for Alt-2.

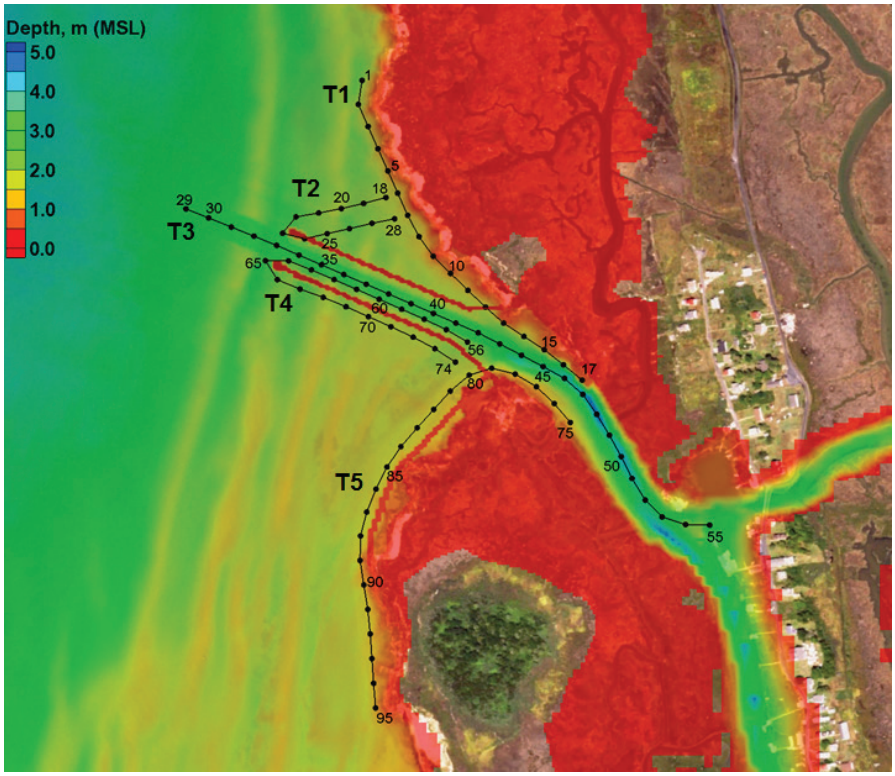

2.9 Simulated conditions

Combined CMS-Wave and CMS-Flow simulations were performed for Alt-0, Alt-1, and Alt-2 for the three conditions listed in Table 2-1. Condition 1 was for the month of August 2014, during which waves were small and not considered in this simulation. Because waves were small, model calculations only included winds, currents, and sediment transport. Condition 2 was for the month of February 2014, representing northeaster forcings common in the Chesapeake Bay during the winter season. Winds, waves, currents, and sediment transport were considered in this 1-month simulation. Condition 3 was for Hurricane Sandy, with a simulation time from 26–31 October 2012, and included winds, waves, flow, and sediment transport. Hurricane Sandy represented a 50-year tropical storm, and structural design calculations considered results of this simulation. For simulation of the three conditions, the gauge data including wind fields and water levels were used. Hurricane Sandy wind and pressure fields used as forcing for Condition 3 were extracted from the NACCS post-Sandy study database (Cialone et al. 2015).

Table 2-1. Simulation conditions.

Alt	Cond. 1: August 2014 (Flow and sediment transport)	Cond. 2: February 2014 (Flow, wave, and sediment transport)	Cond. 3: Hurricane Sandy 26-31 October 2012 (Flow, wave, and sediment transport)
0	x	x	x
1	x	x	x
2	x	x	x

Hurricane Sandy, representing a 50-year return period, was used in the numerical simulations for the existing west channel without a structure (without project) and for two Alternatives with jetty and revetment structures (with project). The model simulations were first conducted in the regional grid for waves and flow only, without sediment transport. The results from the regional simulations were provided as input to the local Smith Island grid for calculation of wave, flow, and sediment transport at the project site.

Three simulations were performed for three conditions (Table 2-1) using the large regional grid to develop spatially varying estimates of waves, water levels, and currents in the Chesapeake Bay. For example, Figure 2-26 shows the bay-wide wave-height field calculated by the regional model for Hurricane Sandy. Results indicate higher wave heights calculated outside Chesapeake Bay (red color region in Figure 2-26), which reduces significantly inside the Bay. Analysis of water levels for Hurricane Sandy indicated a maximum water level of 5 ft (~1.5 m) along the western shore of Smith Island.

2.10 Performance of Alternatives

Results from the wind-wave simulations for the entire bay were used as input to the fine-resolution local grid to develop the estimates of waves, flow, water levels, currents, and sediment transport at the project site. A total of nine simulations (three conditions × three Alternatives) was simulated with the local grid.

Figure 2-26. Calculated wave heights in the Chesapeake Bay for Hurricane Sandy: (a) 29 October 2012 at 0600 GMT and (b) 30 October 2012 at 0600 GMT.

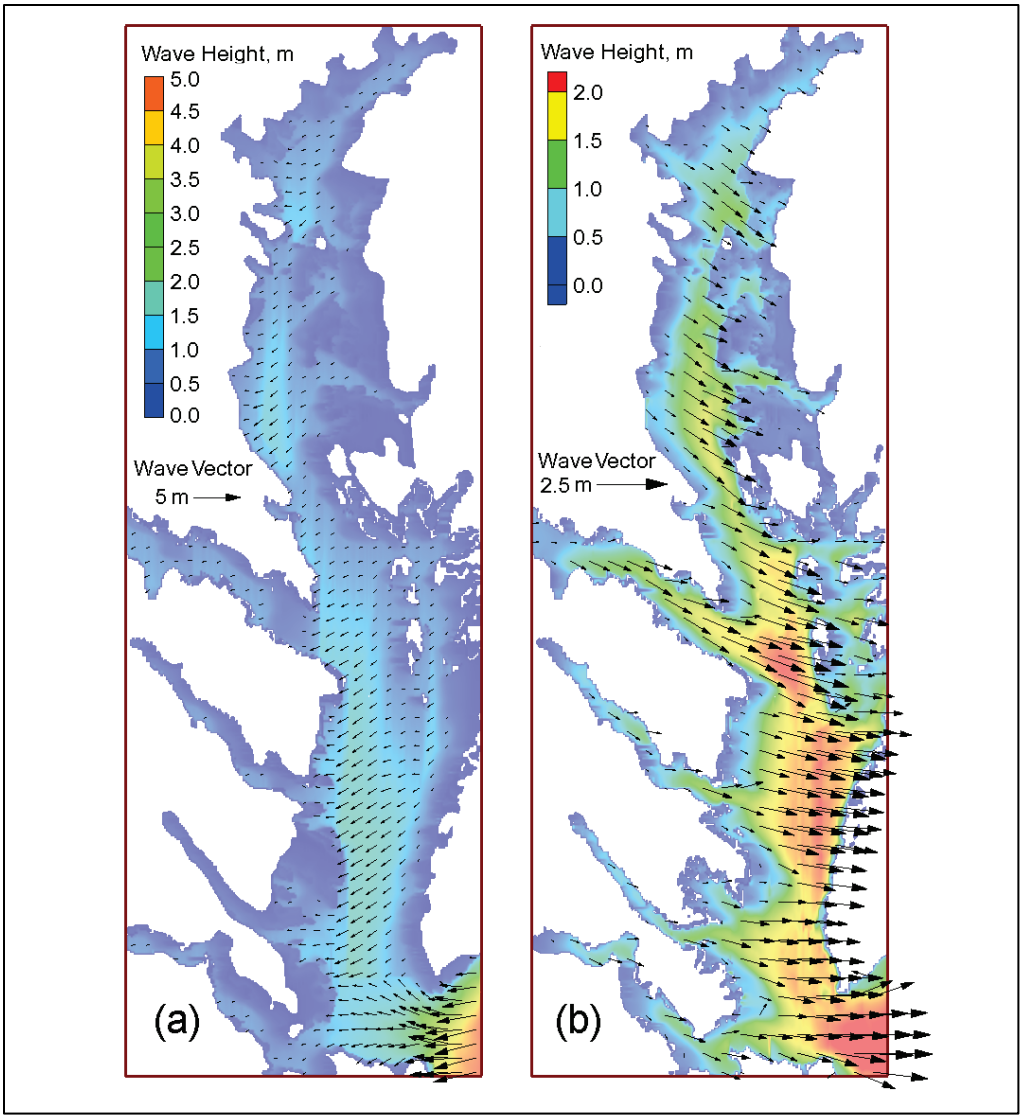

Figures 2-27, 2-28, 2-29 show the maximum wave fields for the three Alternatives Alt-0, Alt-1, and Alt-2, respectively, in the western channel of Sheep Pen Gut for a northeaster storm on 16 February 2014 at 0000 GMT.

Figures 2-30, 2-31, and 2-32 show the snapshots of wave height fields for the three Alternatives Alt-0, Alt-1, and Alt-2 on 30 October 2012 at 1200 GMT for Hurricane Sandy. These color-contours of wave fields provide a "big picture" of the wave height variation over the modeling domain, showing a direct comparison of the Alternatives evaluated.

Figure 2-27. Maximum wave height field for Alt-0 in the western channel (northeaster, 16 February 2014 at 0000 GMT).

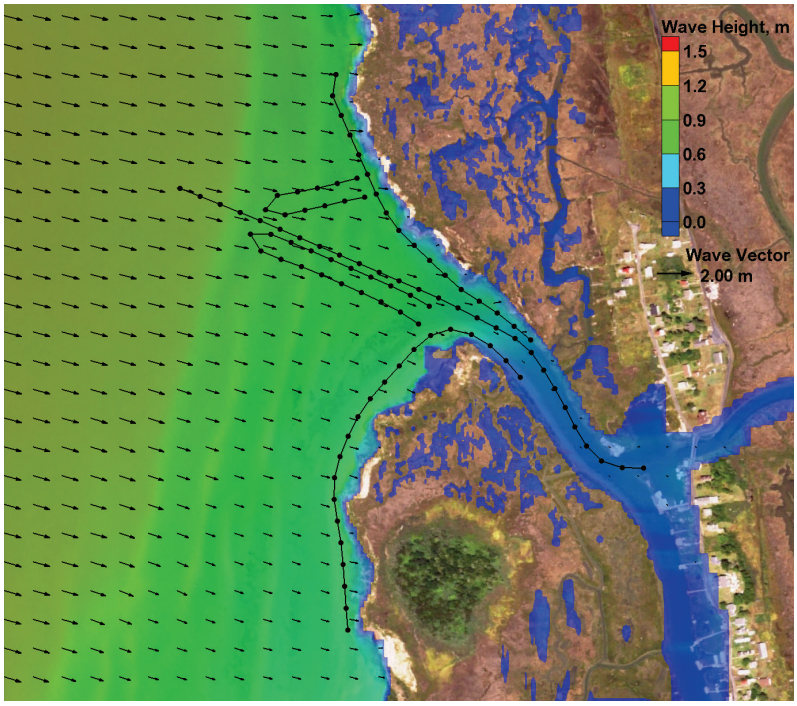

Figure 2-28. Maximum wave height field for Alt-1 in the western channel (northeaster, 16 February 2014 at 0000 GMT).

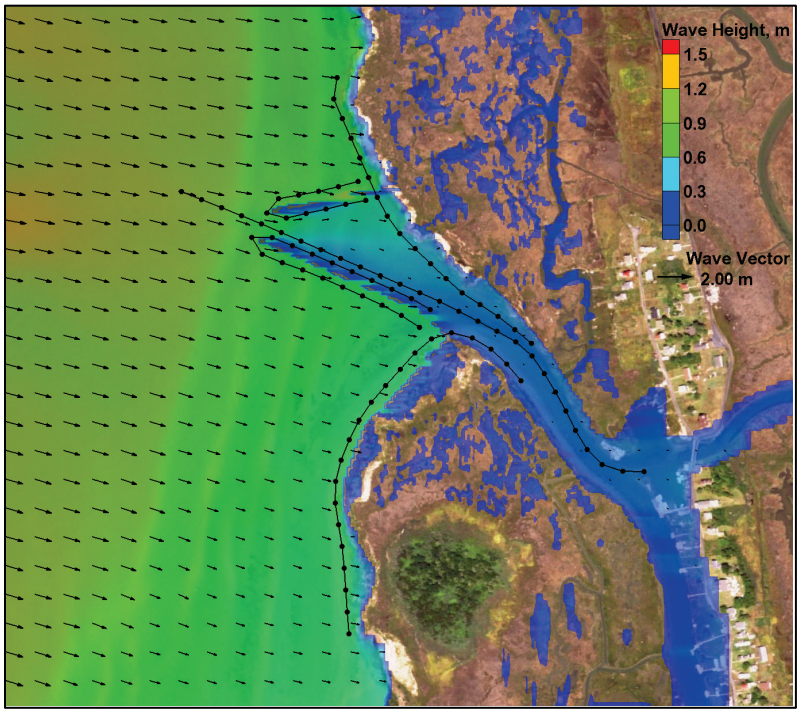

Figure 2-29. Maximum wave height field for Alt-2 in the western channel (northeaster, 16 February 2014 at 0000 GMT).

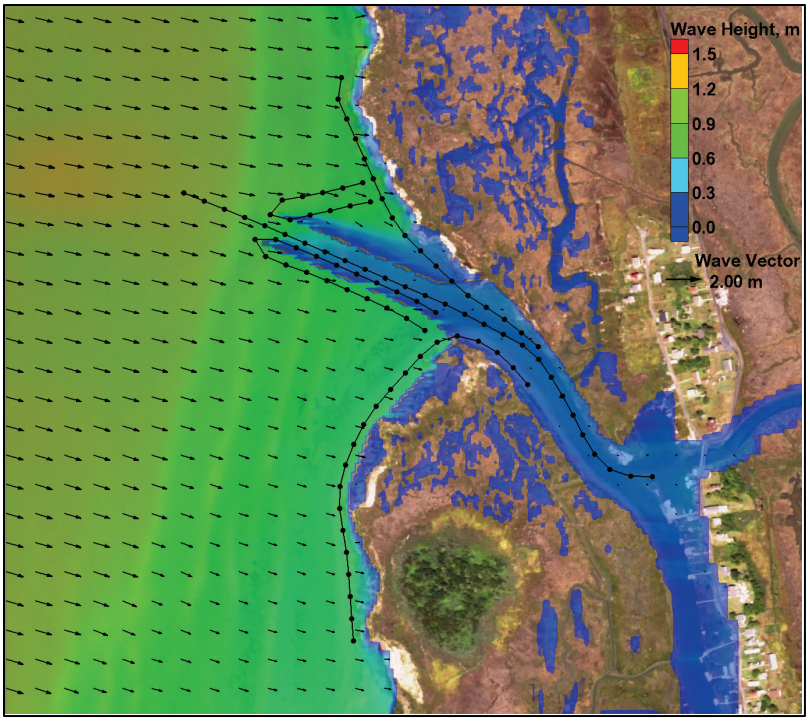

Figure 2-30. Maximum wave height field for Alt-0 in the western channel (Hurricane Sandy, 30 October 2012 at 1200 GMT).

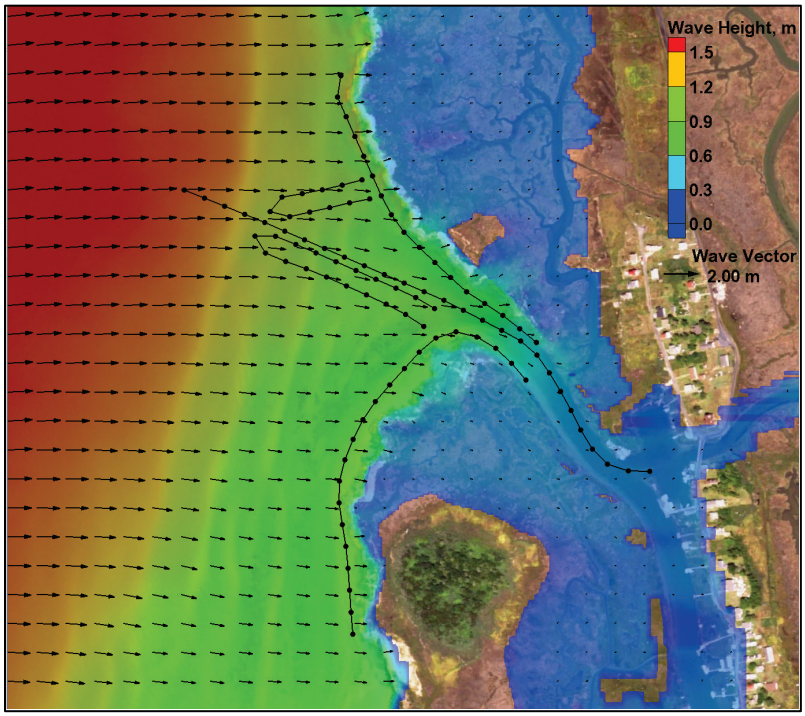

Figure 2-31. Maximum wave height field for Alt-1 in the western channel (Hurricane Sandy, 30 October 2012 at 1200 GMT).

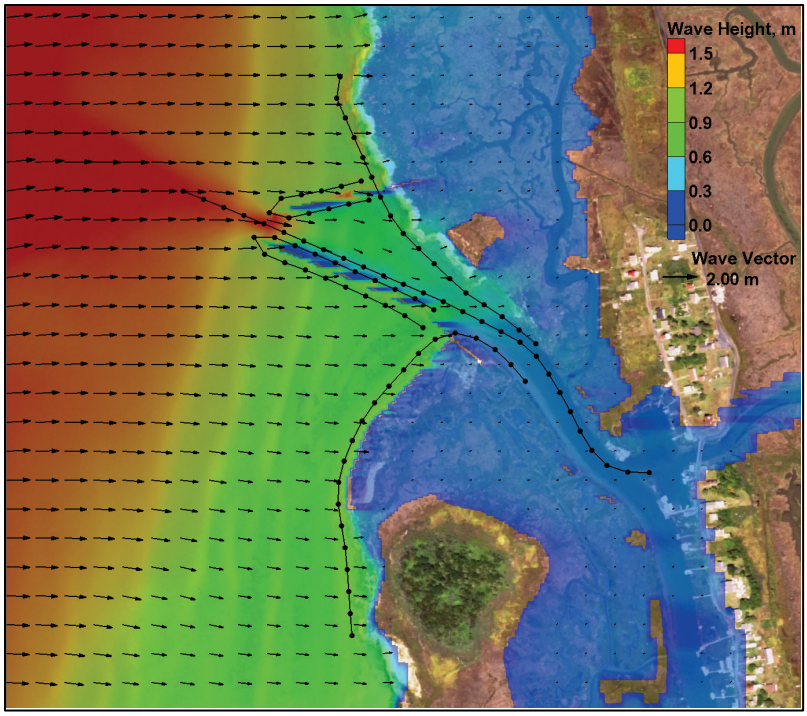

Figure 2-32. Maximum wave height field for Alt-2 in the western channel (Hurricane Sandy, 30 October 2012 at 1200 GMT).

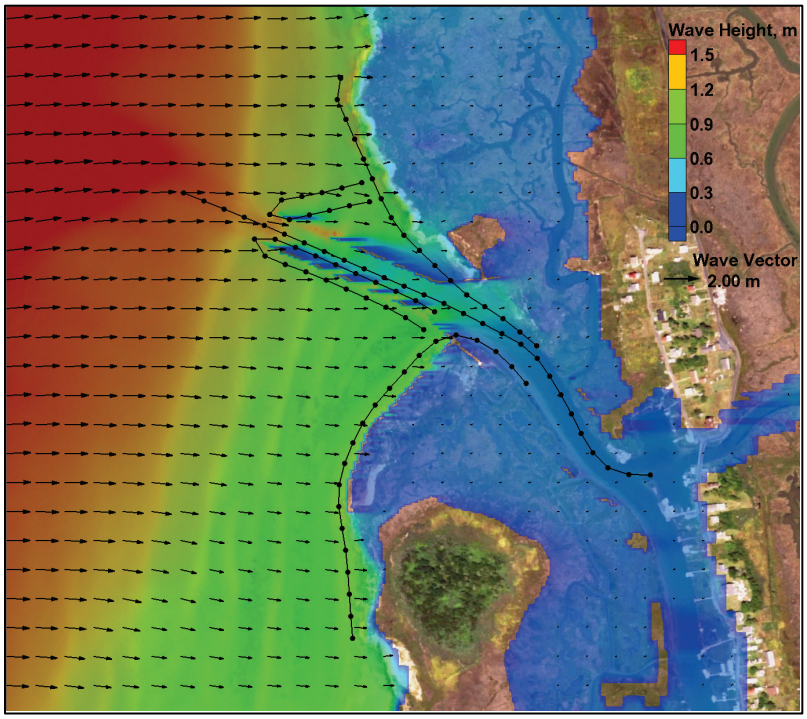

The red/orange color area in Figures 2-27 to 2-32 represents the largest wave heights, green represents moderate wave heights, and smaller wave heights are in the blue region. The largest wave heights are calculated seaward of the western channel, which are reduced through the channel eastward toward the narrow canal. These results confirm that the added jetties helped to reduce waves in the channel. The wave height reduction along the channel was similar for Alt-1 and Alt-2, with a slightly greater reduction occurring between the north jetty and shoreline for Alt-1.

Overall, wave heights for the existing (no-project) configuration were greater than wave heights for two Alternatives (with project) through the new realigned channel. These spatial plots indicated wave heights were greater seaward of the western channel, and jetties helped to reduce waves eastward throughout the channel.

2.11 Detailed analysis of results

Numerical model results along the north and south shorelines and the channel centerline were analyzed for Alt-0, Alt-1, and Alt-2 along the five transects described earlier (Figures 2-23, 2-24, 2-25) for the three chosen simulation conditions (see Table 2-1). The modeling results are compared here to investigate the performance of each Alternative in relation to wave-energy, current, and morphology change in the areas of primary interest. The goal of this detailed analysis was to determine the degree of protection offered by the proposed Alternatives as compared to the existing channel (Alt-0). A wave-reduction analysis was performed by comparing Alternatives (Alt-1 and Alt-2) to the existing channel (Alt-0). Wave height analysis results are provided for northeaster and tropical storms simulations because waves were not considered in Condition 1 (Table 2-1). These are followed by calculated current and morphology change estimates for all three conditions.

2.11.1 Comparison of Alternatives for wave heights

The wave height variations along the north shoreline (T1), channel centerline (T3), and south shoreline (T5), are displayed in Figures 2-33, 2-34, and 2-35, respectively. The locations where north and south jetties intersect with T1, T3, and T5 have been marked on these figures. These snapshots represent the maximum wave heights extracted from 1-month winter simulation (Condition 2 in Table 2-1) on 16 February 2014 at 0000 GMT. As shown in Figure 2-33, there is a noticeable variation in wave

height along T1 for the three Alternatives that ranged from 0.3 to 2.6 ft (0.1 to 0.8 m). The largest wave heights were calculated on the north segment of T1 at Stations 1 to 5. At Stations 7 to 9, calculated wave heights for Alt-2 were generally greater than wave heights for Alt-1 and slightly smaller at Stations 10 to 14.

Figure 2-33. Maximum wave height comparisons along the north shoreline transect T1 for a northeaster (16 February 2014 at 0000 GMT).

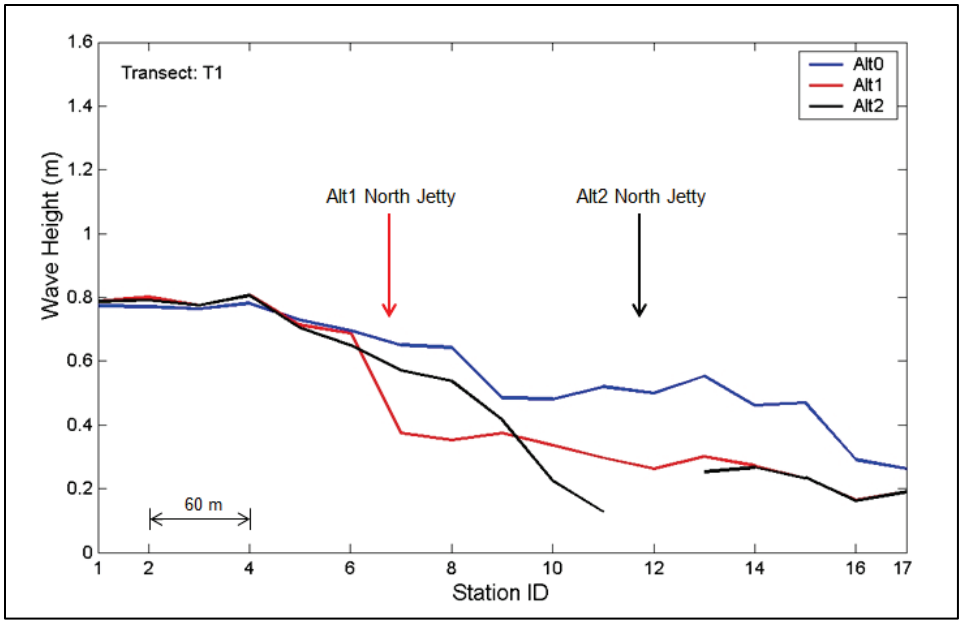

Figure 2-34. Maximum wave height comparisons along the channel centerline transect T3 for a northeaster (16 February 2014 at 0000 GMT).

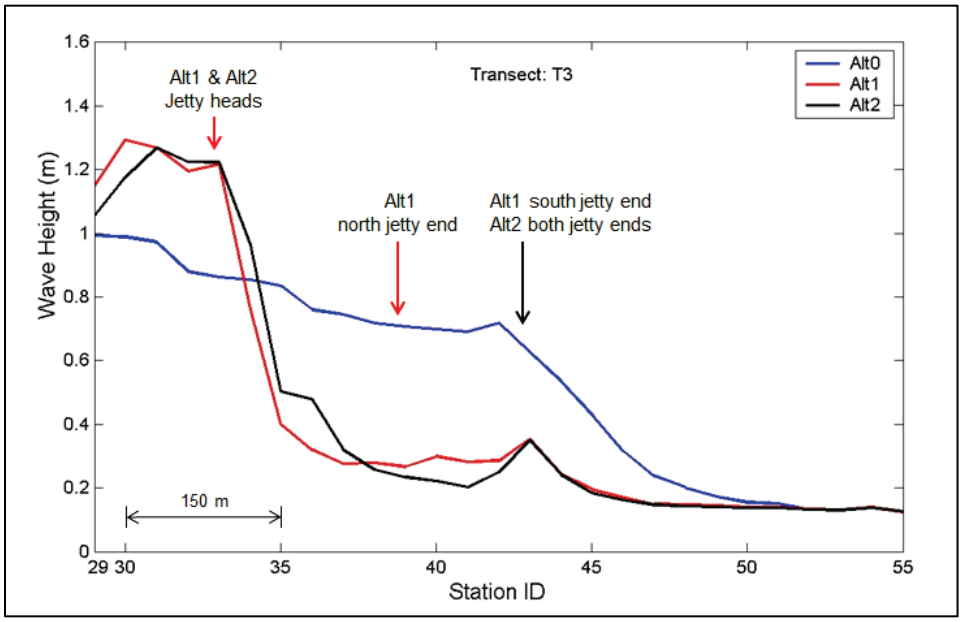

Figure 2-35. Maximum wave height comparisons along the south shoreline transect T5 for a northeaster (16 February 2014 at 0000 GMT).

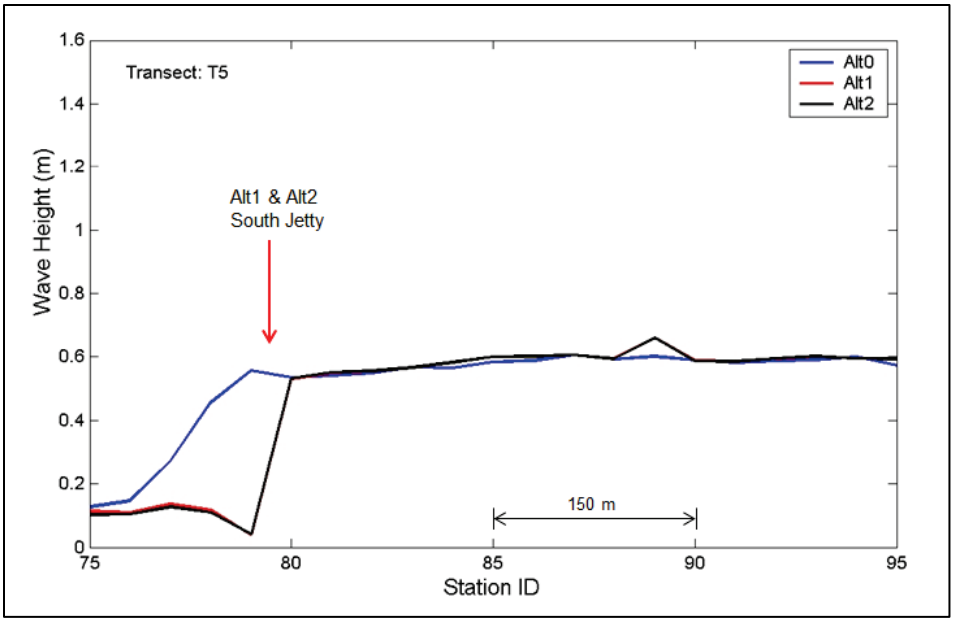

Calculated wave heights for the northeaster (Condition 2) along T3 are provided in Figure 2-34, representing the extracted maximum wave heights on 16 February 2014 at 0000 GMT. Comparison to Figure 2-33 shows wave heights exhibit similar variation along this transect (e.g., higher waves in Bay side along the channel and decreasing wave heights eastward along the channel). The range of wave heights varied from 0.3 to 4.3 ft (0.1 to 1.3 m), with larger wave heights at Stations 29 to 33. Overall, the calculated wave height reduction for Alt-1 was greater than that for Alt-2, where the channel was less protected by North Jetty in Alt-1. Results for Condition 2 along T5 are provided in Figure 2-35. Wave heights varied from 0 to 2 ft (0 to 0.6 m) along T5 for the northeaster. Wave heights along the channel centerline (T3) were greater than those along the north (T1) and south (T5) shoreline transects, respectively.

In summary, results for the three Alternatives indicated a significant variation in wave heights along T3. Larger wave heights were calculated along the seaward section of T3 (Stations 29 to 33).

Model results along T1, T3, and T5 for Hurricane Sandy (Condition 3) are provided in Figures 2-36, 2-37, and 2-38, respectively, for the maximum wave height field that occurred on 30 October 2012 at 1200 GMT. As expected, larger wave heights were obtained for Condition 3 than Condition 2. The north shoreline is more protected in Alt-1 and Alt-2 while the south

shoreline is not. Alt-1 and Alt-2 produced similar estimates along T5. This can be seen from comparison of results in Figures 2-36 vs. 2-38 and in Figures 2-33 vs. 2-35. The north shoreline can be expected to erode less with Alt-1 and Alt-2 than with Alt-0 because of the protection provided by jetties. The south shoreline is protected with the revetment in Alt-1 and Alt-2.

Figure 2-36. Maximum wave height comparisons along the north shoreline transect T1 for Hurricane Sandy (30 October 2012 at 1200 GMT).

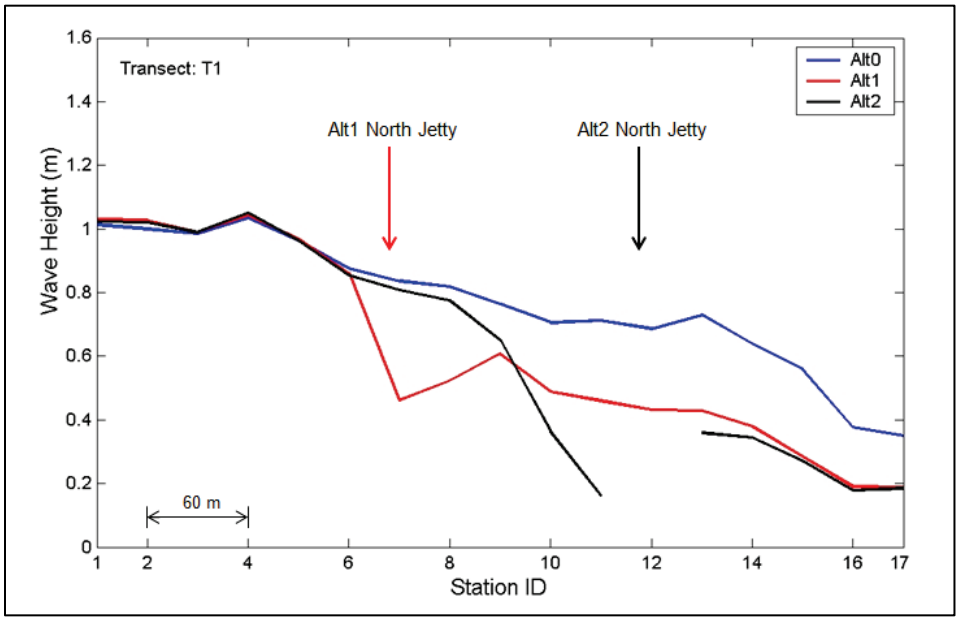

Figure 2-37. Maximum wave height comparisons along the channel centerline transect T3 for Hurricane Sandy (30 October 2012 at 1200 GMT).

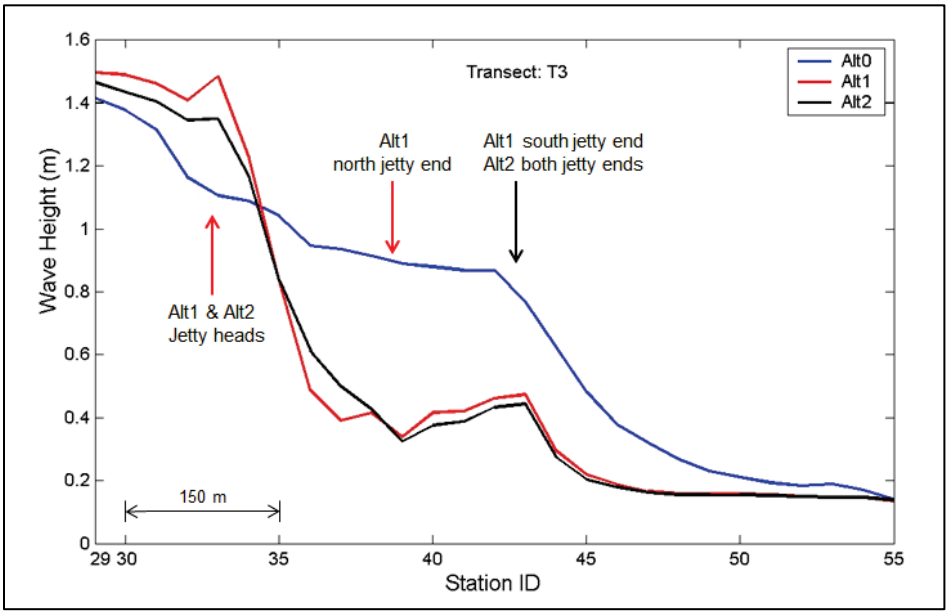

Figure 2-38. Maximum wave height comparisons along the south shoreline transect T5 for Hurricane Sandy (30 October 2012 at 1200 GMT).

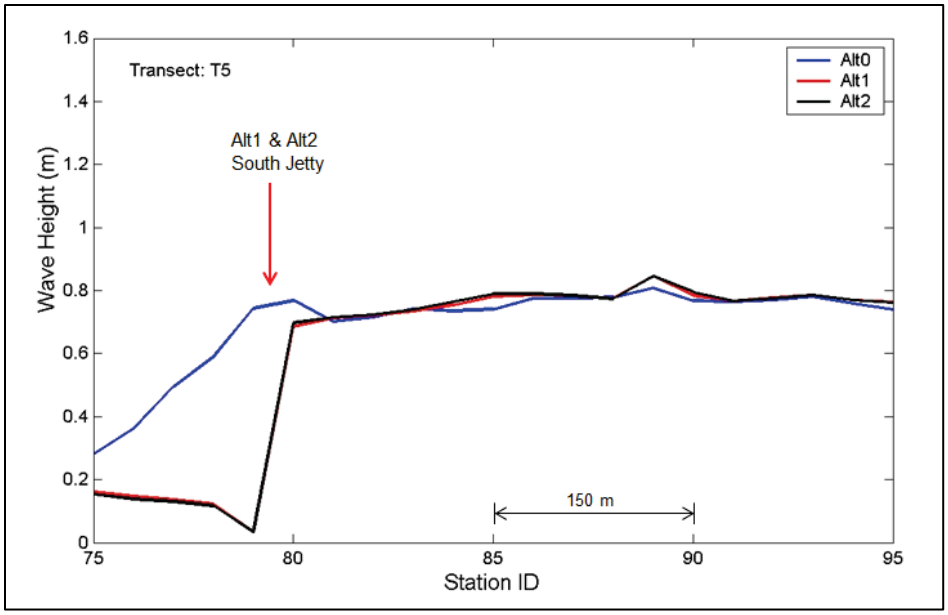

Model results (Figures 2-33 to 2-38) indicated that both Alt-1 and Alt-2 provided a significant reduction in wave height inside the jetty entrance along the channel (T3) as compared to Alt-0. Model wave heights from Alt-1 and Alt-2 increased more than 25% immediately seaward of the jetty entrance. Such an increase could be due to a combination of effects including convergence (focusing) of waves entering the channel at the jetty heads, waves against currents during ebb tidal flow, and wave reflection and diffraction effects by the jetties. In summary, wave heights reduced along the channel centerline for both Alt-1 and Alt-2 moving eastward between Stations 33 and 55. Although the north jetty in Alt-1 was approximately only half the length of north jetty in Alt-2, results for Conditions 2 and 3 indicated Alt-1 was as effective as Alt-2. Over the entire length of T3, Alt-1 yielded a slightly greater reduction in wave height than Alt-2. The largest wave heights were calculated along T3, smallest along T5, and values for T1 were in between.

Between the north and south jetties, wave heights reduced consistently along the channel centerline for both Alt-1 and Alt-2, with a 50% maximum wave height reduction attained. In general, Alt-1 and Alt-2 produced a similar reduction. For example, the wave height at Station 40 was 0.7 ft (0.2 m) for Alt-2, 1 ft (0.3 m) for Alt-1, and 2.5 ft (0.75 m) for Alt-0, respectively. These estimates indicated a three-fold wave height reduction was possible with the jettied channel geometries evaluated.

To interpret calculated wave heights and wave height reduction achieved with each Alternative, several statistics including the maximum and mean wave heights and percent reduction along T1, T3, and T5 were calculated for each Alternative. The analysis of wave-height reduction from Alt-1 and Alt-2 was based on a wave height reduction factor calculated as the percentage of wave-height reduction relative to the wave heights in the existing channel (Alt-0) without the project condition. This was defined as

$$\left|\frac{\text{(Wave Height for Alternative) - (Wave Height for Existing Channel)}}{\text{(Wave Height for Existing Channel)}}\right| \times 100\%$$

Tables 2-2, 2-3, and 2-4 provide a summary of wave height statistics for T1, T3, and T5, respectively, for February 2014 (Condition 2), and Tables 2-5, 2-6, and 2-7 for Hurricane Sandy (Condition 3). All Stations on each transect were included in the calculation of wave height and morphology change statistics provided in Tables 2-2 through 2-7. The zero value of wave height reduction was assigned if no reduction was calculated. The maximum wave height affects the operations and navigability while the mean wave height affects the sediment transport in the study area.

Along T1 (north shoreline) in Alt-1 and Alt-2, wave statistics were calculated separately for the west segment (Station 1 to Station 6) not protected by north jetty, and the east segment (Station 7 to 17), which was either fully or partially protected by north jetty. Wave statistics were similar for Alt-0, Alt-1, and Alt-2 along the unprotected west segment of T1. There was a significant wave height reduction along the protected east segment of Alt-1 and Alt-2 located in the lee of north jetty. Along the protected segment of T1, Alt-1 provided roughly 50% maximum and 40% average wave height reduction (Table 2-2) for Conditions 2 and 3. Alt-2 yielded 75% and 42% reduction, respectively (Table 2-5).

Along T3 (channel centerline) in Alt-1 and Alt-2, wave statistics were calculated separately for the west segment (Station 29 to Station 33) outside the jetty entrance (unprotected channel) and the east segment (Station 34 to 55) inside the jetty entrance (protected channel). Along the east segment of T3 (inside jetty entrance), the maximum and mean wave height reductions for both Alt-1 and Alt-2 were approximately 65% and 35%, respectively (Tables 2-3 and 2-6). Along the unprotected west segment (outside jetty entrance), model wave heights for Alt-1 and Alt-2 increased more than 25% as compared to Alt-0. This increase was due to a

combination of wave interaction with the jetty heads, waves against ebbing currents, and stronger wave reflection and diffraction effects at and around the tips of jetties.

Table 2-2. Calculated wave height statistics along T1 (16 February 2014 at 0000 GMT).

Alt	Max wave height (m)	Mean wave height (m)	Max wave height reduction* (%)	Mean wave height reduction* (%)
	Unprotected segment of North shoreline in Alt-1 and Alt-2 (Sta 1 to Sta 6)			
0	0.78	0.75	0	0
1	0.81	0.76	2.3	0
2	0.81	0.75	6.8	0.2
	Protected segment of North shoreline in Alt-1 and Alt-2 (Sta 7 to Sta 17)			
0	0.65	0.48	0	0
1	0.37	0.29	50.3	40.0
2	0.57	0.28	75.4	42.2

* Calculated as the percentage change of wave heights of Alt-1 and Alt-2 from Alt-0.

Table 2-3. Calculated wave height statistics along T3 (16 February 2014 at 0000 GMT).

Alt	Max wave height (m)	Mean wave height (m)	Max wave height reduction* (%)	Mean wave height reduction* (%)
	Along channel segment outside the jetty entrance in Alt-1 and Alt-2 (Sta 29 to Sta 33)			
0	1.00	0.94	0	0
1	1.29	1.22	0	0
2	1.27	1.19	0	0
	Along channel segment inside the jetty entrance in Alt-1 and Alt-2 (Sta 34 to Sta 55)			
0	0.85	0.46	0	0
1	0.76	0.24	63.0	35.5
2	0.96	0.25	70.7	35.0

* Calculated as the percentage change of wave heights of Alt-1 and Alt-2 from Alt-0.

Along T5 (south shoreline) in Alt-1 and Alt-2, wave statistics were calculated separately for the east segment (Station 1 to Station 6) protected by the south jetty and the south segment (Station 7 to Station 17), which is not protected by the south jetty. Along the protected segment of T5 (Station 75 to Station 79), maximum and mean wave height reductions were more than 90% and 50%, respectively (Tables 2-4 and 2-7). Overall, the unprotected segments of T1 and T5 were neither affected by the jetties or had a minor wave height increase/decrease primarily due to local wave processes. Along the unprotected segment of T3 outside the jetty entrance,

wave heights for Alt-1 and Alt-2 increased 25% or more due to waves interacting with the jetty heads, waves against ebbing currents, and wave reflection and diffraction around the jetty tips.

Table 2-4. Calculated wave height statistics along T5 (16 February 2014 at 0000 GMT).

Alt	Max wave height (m)	Mean wave height (m)	Max wave height reduction* (%)	Mean wave height reduction* (%)
	Protected segment of south shoreline in Alt-1 and Alt-2 (Sta 75 to Sta 79)			
0	0.56	0.31	0	0
1	0.14	0.10	92.8	50.4
2	0.13	0.10	92.6	54.0
	Unprotected segment of south shoreline in Alt-1 and Alt-2 (Sta 80 to Sta 95)			
0	0.60	0.58	0	0
1	0.66	0.59	0.8	0
2	0.66	0.59	0.8	0

* Calculated as the percentage change of wave heights of Alt-1 and Alt-2 from Alt-0

Table 2-5. Calculated wave height statistics along T1 (30 October 2012 at 1200 GMT).

Alt	Max wave height (m)	Mean wave height (m)	Max wave height reduction* (%)	Mean wave height reduction* (%)
	Unprotected segment of north shoreline in Alt-1 and Alt-2 (Sta 1 to Sta 6)			
0	1.03	0.98	0	0
1	1.04	0.99	1.6	0
2	1.05	0.98	2.3	0
	Protected segment of north shoreline in Alt-1 and Alt-2 (Sta 7 to Sta 17)			
0	0.84	0.65	0	0
1	0.61	0.40	50.0	40.0
2	0.81	0.39	77.2	43.1

* Calculated as the percentage change of wave heights of Alt-1 and Alt-2 from Alt-0.

Table 2-6. Calculated wave height statistics along T3 (30 October 2012 at1200 GMT).

Alt	Max wave height (m)	Mean wave height (m)	Max wave height reduction* (%)	Mean wave height reduction* (%)
	Along channel segment outside the jetty entrance in Alt-1 and Alt-2 (Sta 29 to Sta 33)			
0	1.42	1.28	0	0
1	1.50	1.47	0	0
2	1.47	1.40	0	0
	Along channel segment inside the jetty entrance in Alt-1 and Alt-2 (Sta 34 to Sta 55)			
0	1.09	0.57	0	0
1	1.23	0.34	61.8	36.2
2	1.17	0.34	63.7	36.9

* Calculated as the percentage change of wave heights of Alt-1 and Alt-2 from Alt-0.

Table 2-7. Calculated wave height statistics along T5 (30 October 2012 at 1200 GMT).

Alt	Max wave height (m)	Mean wave height (m)	Max wave height reduction* (%)	Mean wave height reduction* (%)
	Protected segment of south shoreline in Alt-1 and Alt-2 (Sta 75 to Sta 79)			
0	0.74	0.49	0	0
1	0.16	0.12	95.4	70.0
2	0.15	0.11	95.4	71.3
	Unprotected segment of south shoreline in Alt-1 and Alt-2 (Sta 80 to Sta 95)			
0	0.81	0.76	0	0
1	0.84	0.76	10.7	0
2	0.85	0.77	9.2	0

* Calculated as the percentage change of wave heights of Alt-1 and Alt-2 from Alt-0.

2.11.2 Comparison of Alternatives for currents and sediment transport

The current and morphology change calculated for the summer-month (August 2014) simulation are included in the results provided in this section. Figures 2-39 to 2-47 provide the variation of calculated current along the north shoreline (T1), channel centerline (T3), and south shoreline (T5), respectively, for the three conditions simulated. These snapshots represent the CMS-calculated maximum current extracted from the simulations for three conditions (Table 2-1) at the maximum flood/ebb stage.

Figure 2-39. Maximum currents along T1 (August 2014).

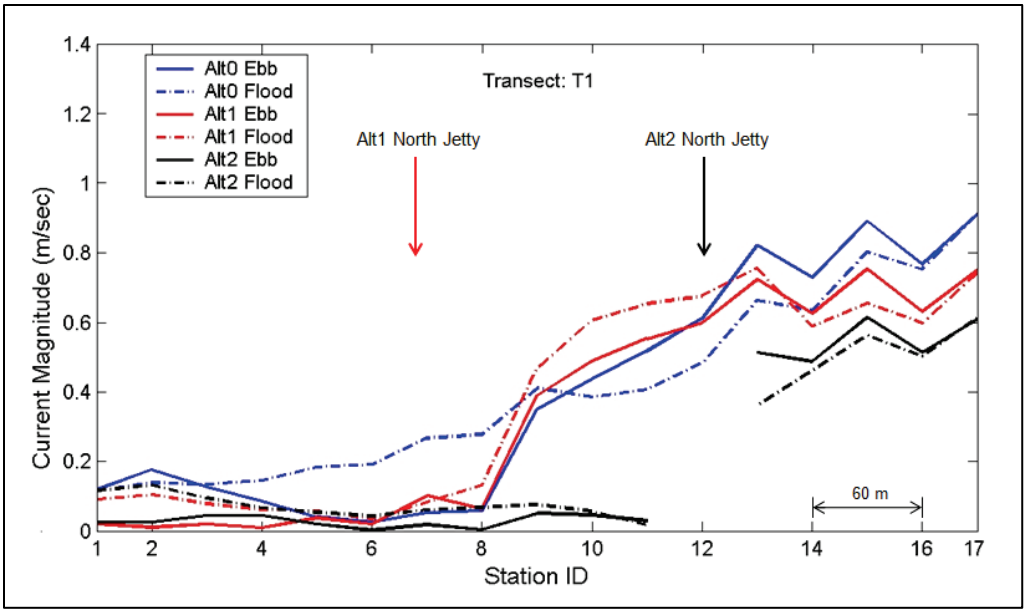

Figure 2-40. Maximum currents along T1 (February 2014).

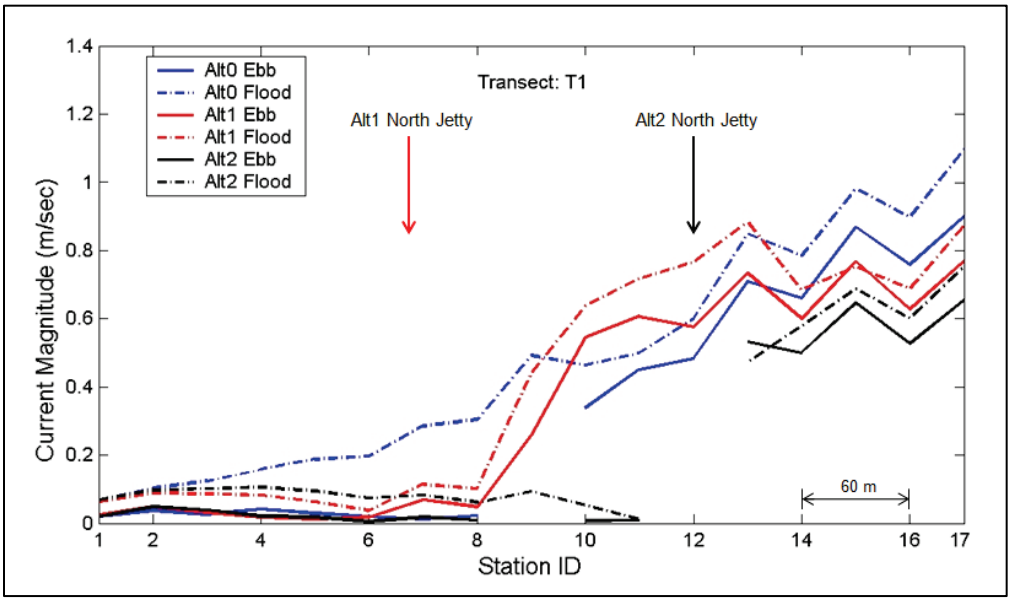

Figure 2-41. Maximum currents along T1 (Hurricane Sandy).

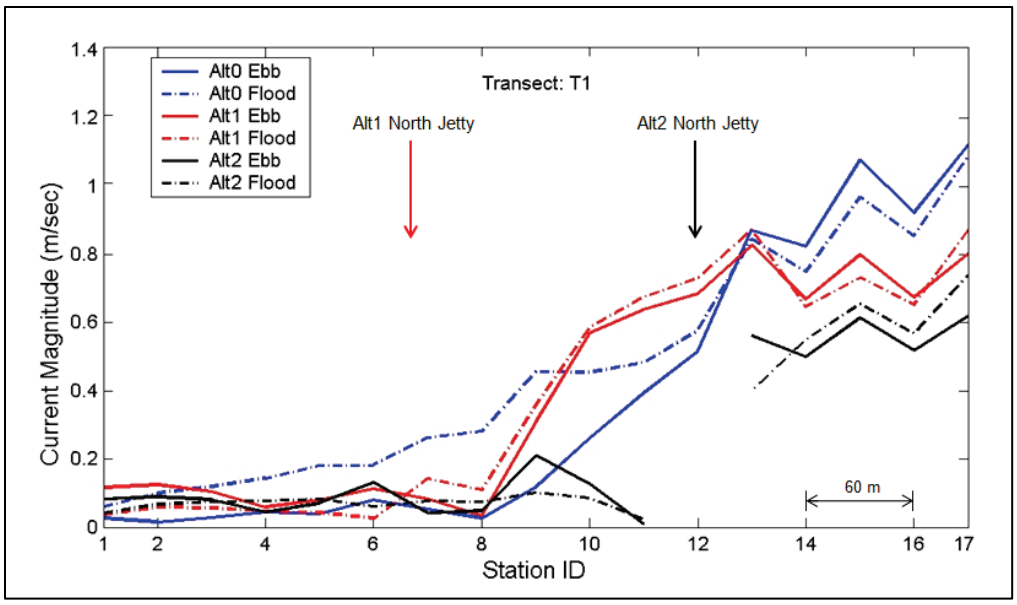

Figure 2-42. Maximum currents along T3 (August 2014).

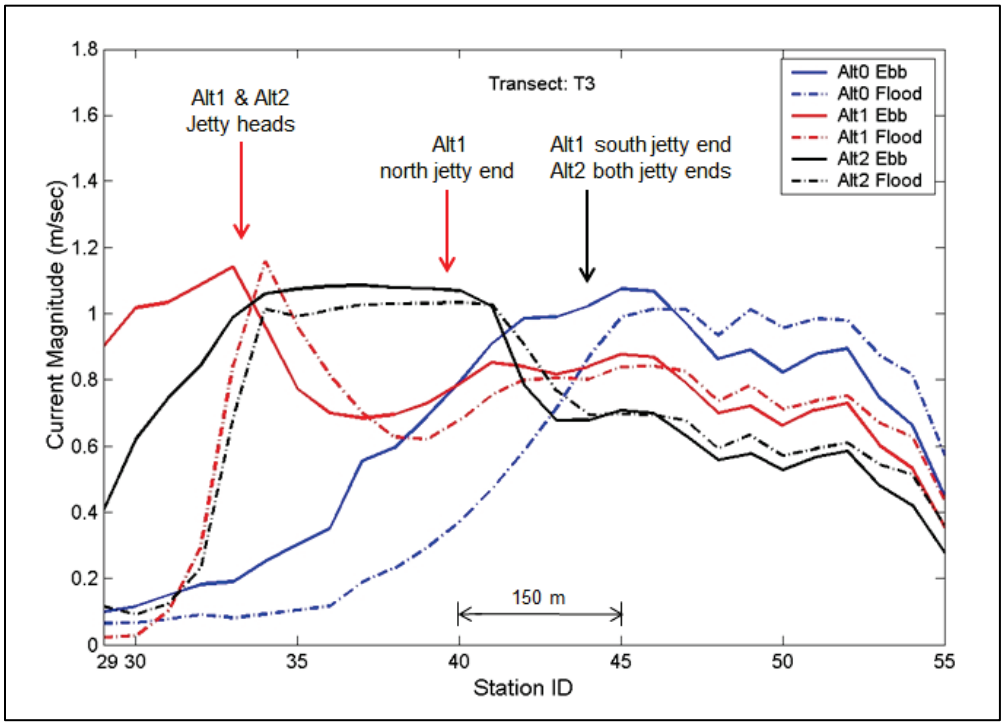

Figure 2-43. Maximum currents along T3 (February 2014).

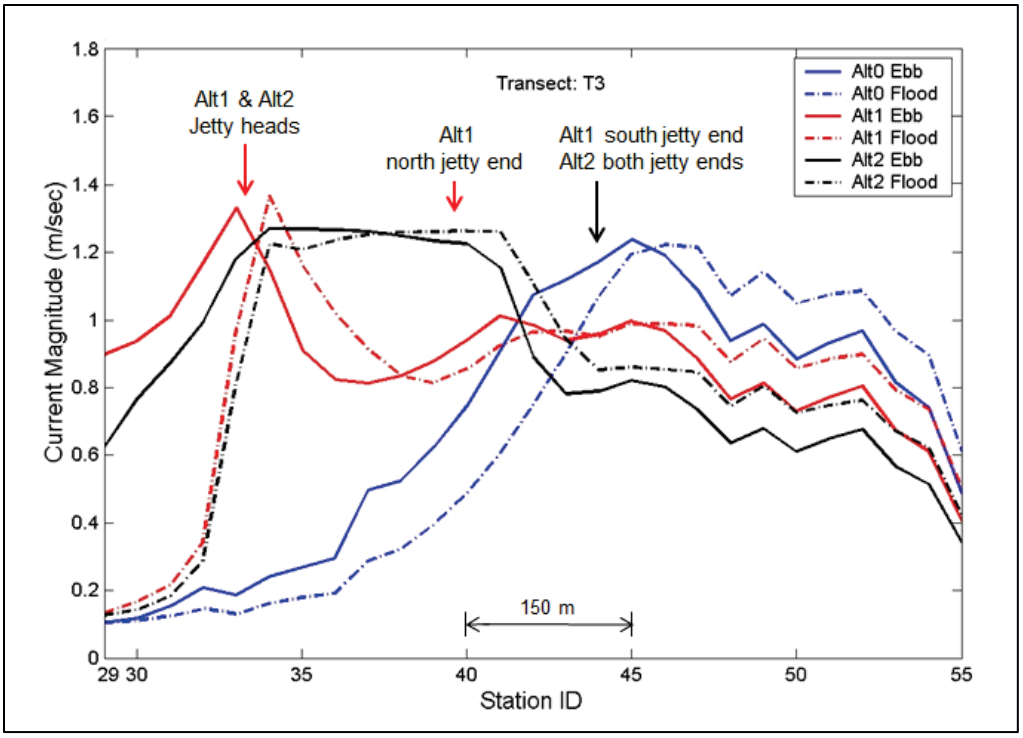

Figure 2-44. Maximum currents along T3 (Hurricane Sandy).

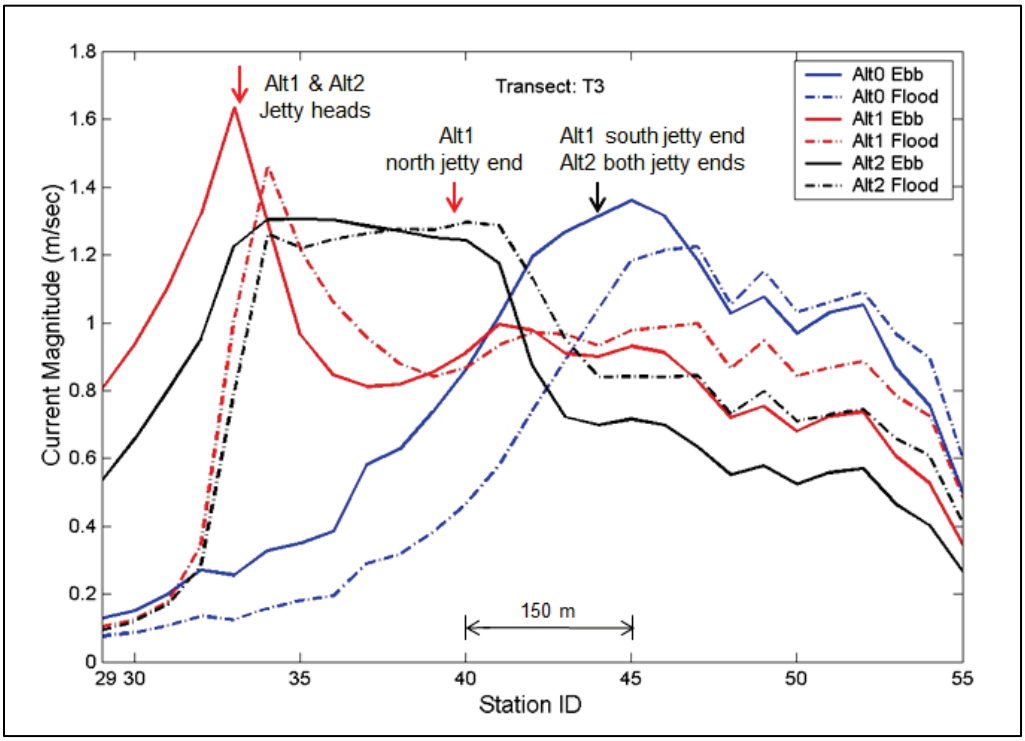

Figure 2-45. Maximum currents along T5 (August 2014).

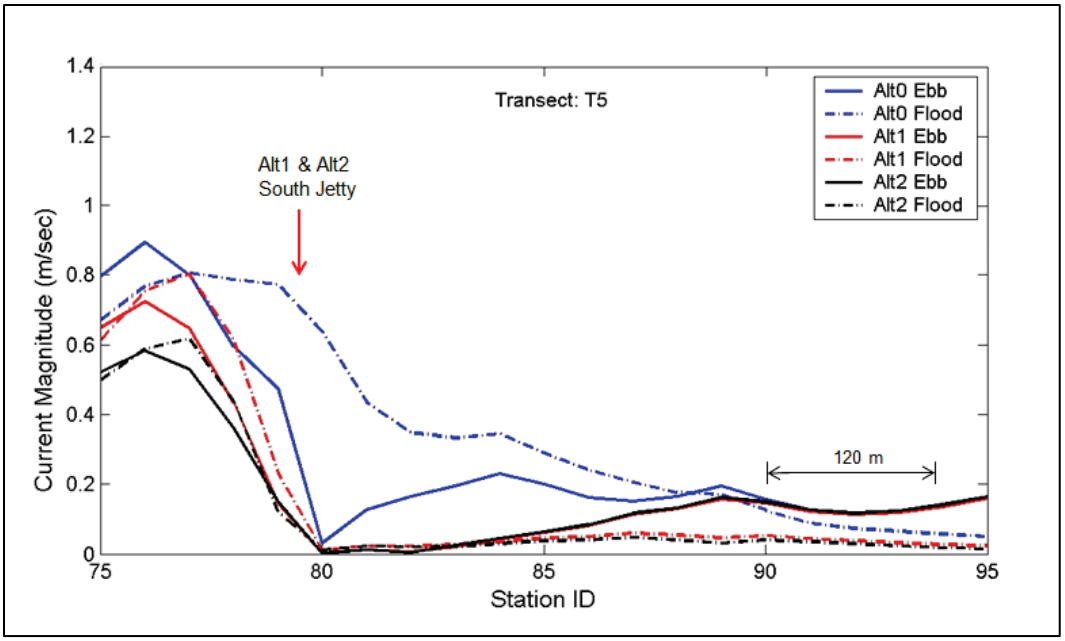

Figure 2-46. Maximum currents along T5 (February 2014).

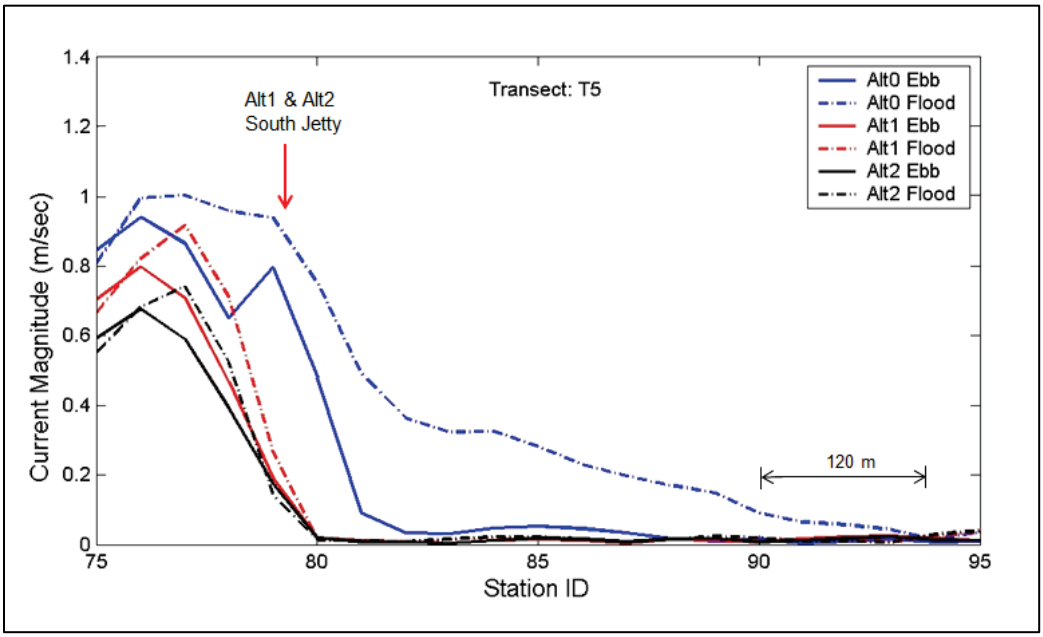

Figure 2-47. Maximum currents along T5 (Hurricane Sandy).

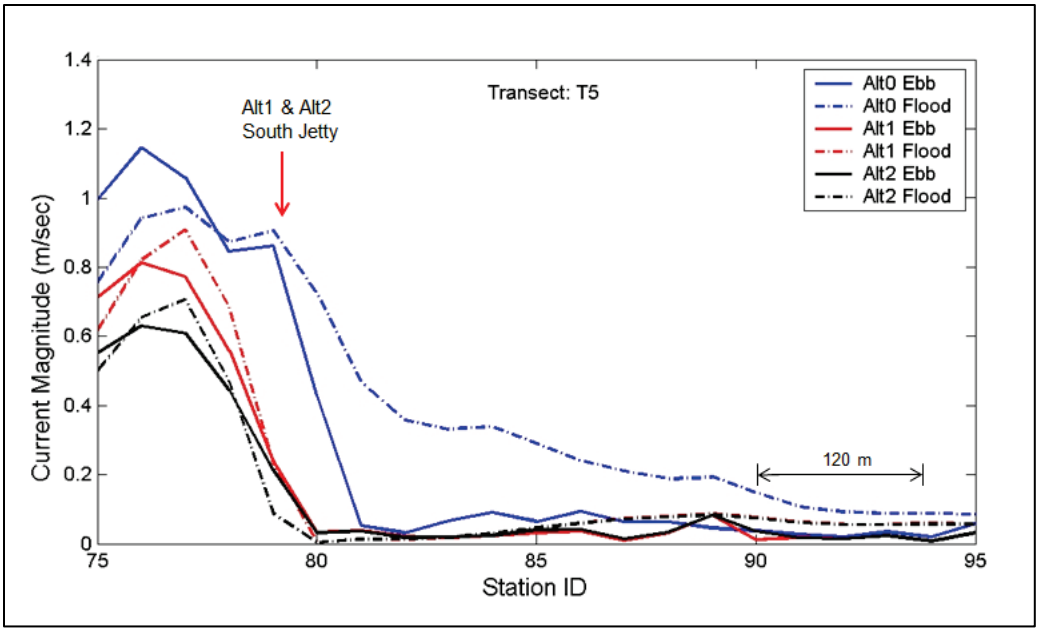

Figures 2-39, 2-40, and 2-41 show current magnitude along T1 at flood/ebb for the three Alternatives and three conditions (Table 2-1) simulated. Model calculated currents for August 2014, February 2014, and Hurricane Sandy were relatively weak (average less than 0.7 ft/sec [0.2 m/sec]) in the northern segment of T1 (Stations 1 to 8). Current speeds increased southward toward the canal throat from Stations 8 to 17, reaching a maximum of 3.3 ft/sec (1.1 m/sec). For August 2014, there is no clear trend between the flood and ebb current for any Alternative. However, for the February 2014 simulation, the current speeds along the entire length of T1 during flood flows were greater than ebb current for the three Alternatives. The difference in the maximum current between Alt-1 and Alt-2 was small and less than 0.5 ft/sec (0.15 m/sec) that would not affect the navigability of small boats. Concerning the potential for erosion of the north shoreline, currents generated with Alt-1 and Alt-2 were similar in the northern section of T1 but were different in the southern section, where difference increased closer to the canal entrance.

Figures 2-42, 2-43, and 2-44 show the variation in current magnitude along the channel centerline (T3). Maximum flood/ebb current for the three Alternatives is shown in these plots for the three conditions simulated. Model calculated currents for August 2014, February 2014, and Hurricane Sandy varied from 0.3 to 5.2 ft/sec (0.1 to 1.6 m/sec). For August 2014, the flood current in the channel was stronger close to the canal between Stations 45 to 55 while the ebb current increased westward.

The same trend in current speed was obtained for the February and August 2014 simulations, with the maximum current increasing to 4.3 ft/sec (1.3 m/sec). Both flood/ebb currents dropped sharply between Stations 33 to 35. The maximum current reached 5.2 ft/sec (1.6 m/sec) for Hurricane Sandy, and the difference between the flood and ebb currents increased and expanded along the channel as compared to currents for the February and August 2014 simulations.

Figures 2-45, 2-46, and 2-47 show the maximum flood/ebb current speed along the south shoreline (T5) for the three Alternatives (Alt-0, Alt-1, and Alt-2). The maximum currents of February and August 2014 and Hurricane Sandy ranged from 0 to 3.6 ft/sec (0 to 1.1 m/sec) along T5 for different Alternatives. The strong current speeds between Stations 75 to 80 decreased sharply along the south edge of canal and increased slowly over the rest of T5. Current speed was rather weak between Stations 80 and 95, with an average speed of 0.7 ft/sec (0.2 m/sec). Similar current speed estimates were obtained along the south and north shorelines, with stronger currents occurring along both shorelines closer to the canal entrance.

The sediment transport was calculated in the CMS-Flow local grid covering the Rhodes Point. Sediment grain size data from grab samples by NAB were obtained in June 2015. The sediment data consisted of primarily sand in the study area. A constant D_{50} of 0.2 mm was used in the present simulations.

Figure 2-48 shows estimates of the morphology change calculated along T1, T3, and T5 for the August 2014 simulation. These 1-month erosion and deposition estimates were less than 1.3 ft (0.4 m) for Alt-0, with the largest morphology change occurred along the channel centerline (T3).

The morphology change estimates for the February 2014 simulation along T1, T3, and T5 are provided in Figure 2-49. These erosion/deposition estimates for 1 month were similar in magnitude to August 2014 estimates, with a maximum value of 1.3 ft (0.4 m) for Alt-0 obtained along T3. However, the spatial variations along the three transects are different.

Figure 2-48. Morphology changes along T1, T3, and T5 (August 2014).

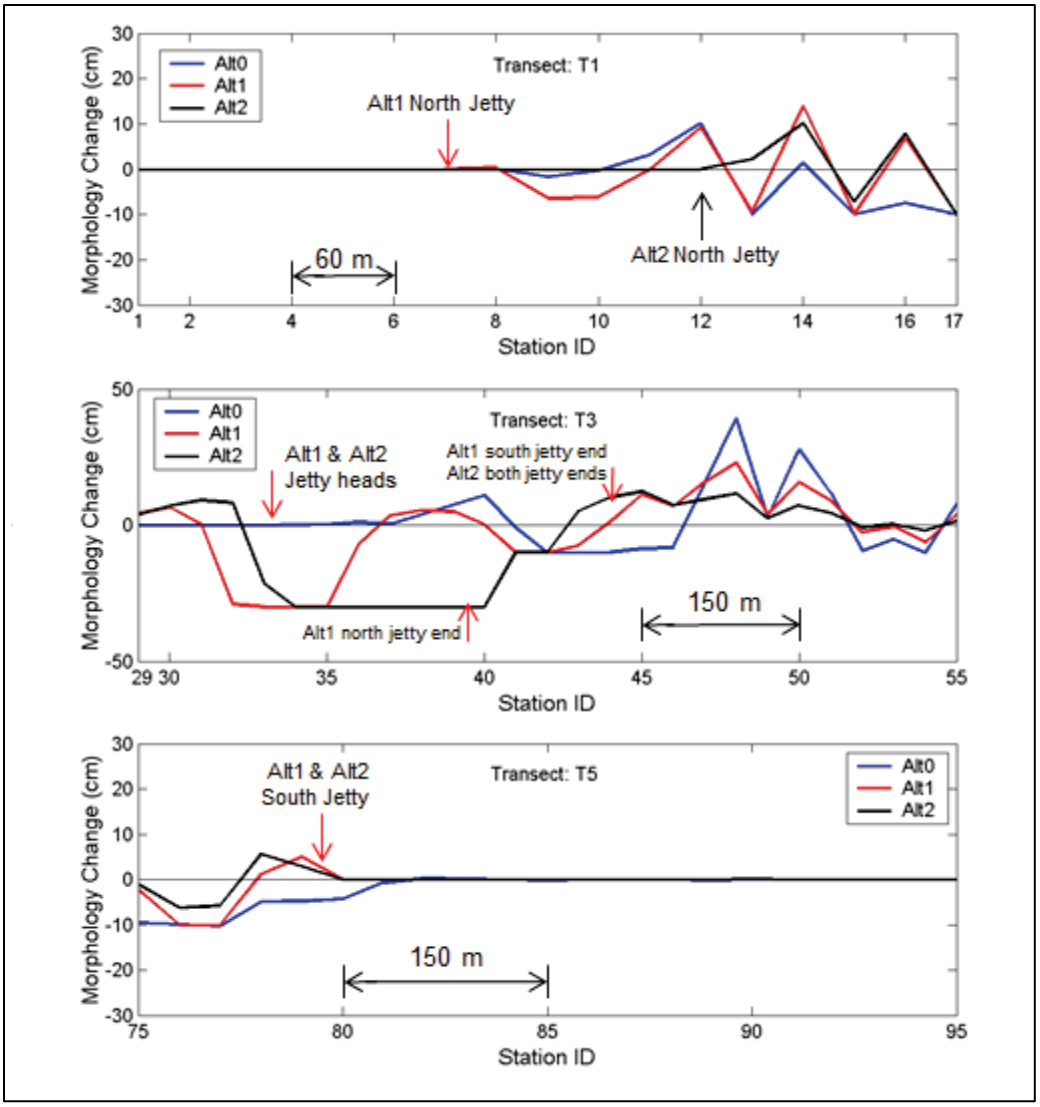

Figure 2-49. Morphology changes along T1, T3, and T5 (February 2014).

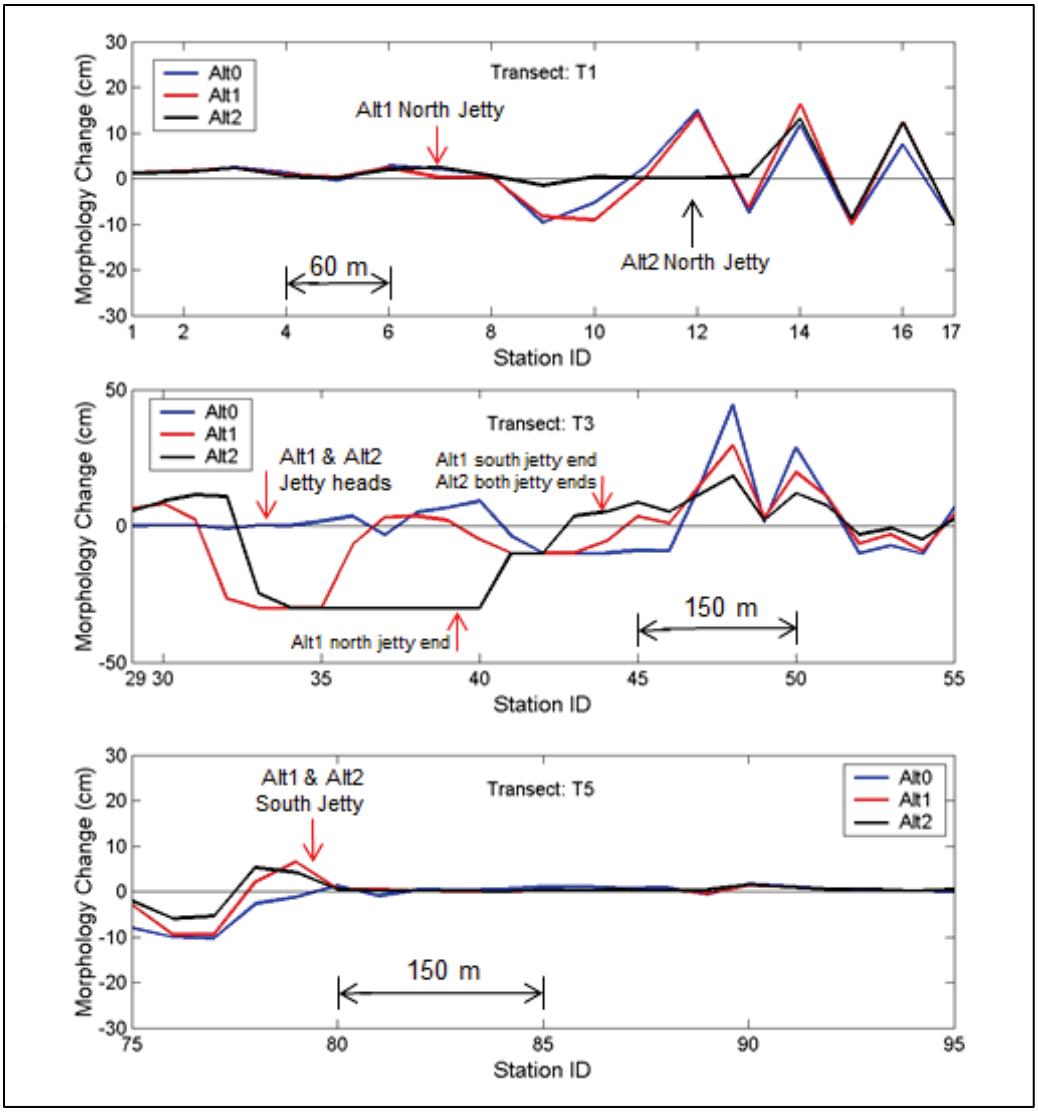

Figure 2-50 displays the morphology change estimates for Hurricane Sandy for the 26–31 October 2012 simulation. The spatial variation of erosion/deposition estimates along T1, T3, and T5 are provided. The maximum morphology change of approximately 0.7 ft (0.2 m) occurred along T3, where the maximum current was present. Although the calculated magnitudes of sediment transport are similar to August and February 2014 simulation results, the spatial variation of erosion and accretion along each transect was different.

Figure 2-50. Morphology changes along T1, T3, and T5 (Hurricane Sandy).

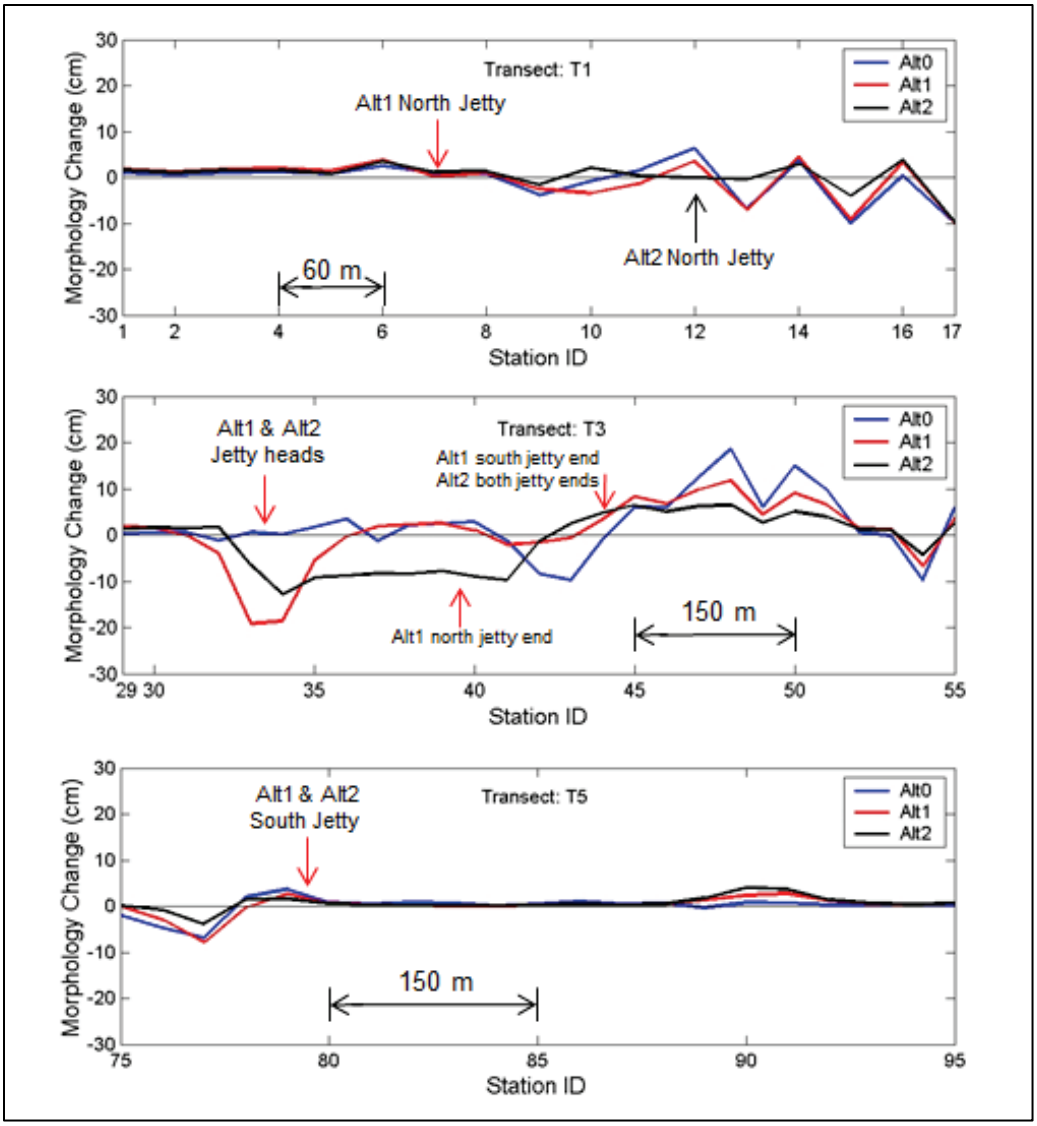

Figures 2-51, 2-52, and 2-53 show the spatial pattern of morphology change for Alt-0, Alt-1, and Alt-2, respectively, at the end of the August 2014 simulation with the peak ebb current field at 31 August 2014 at 1400 GMT, in which blue represents erosion and red represents deposition. Figure 2-54, 2-55, and 2-56 show the model morphology change pattern for Alt-0, Alt-1, and Alt-2, respectively, with the peak flood current field at 31 August 2014 at 2100 GMT with the same color legend.

Figure 2-51. Morphology change for Alt-0 (ebb current, 31 August 2014 at 1400 GMT).

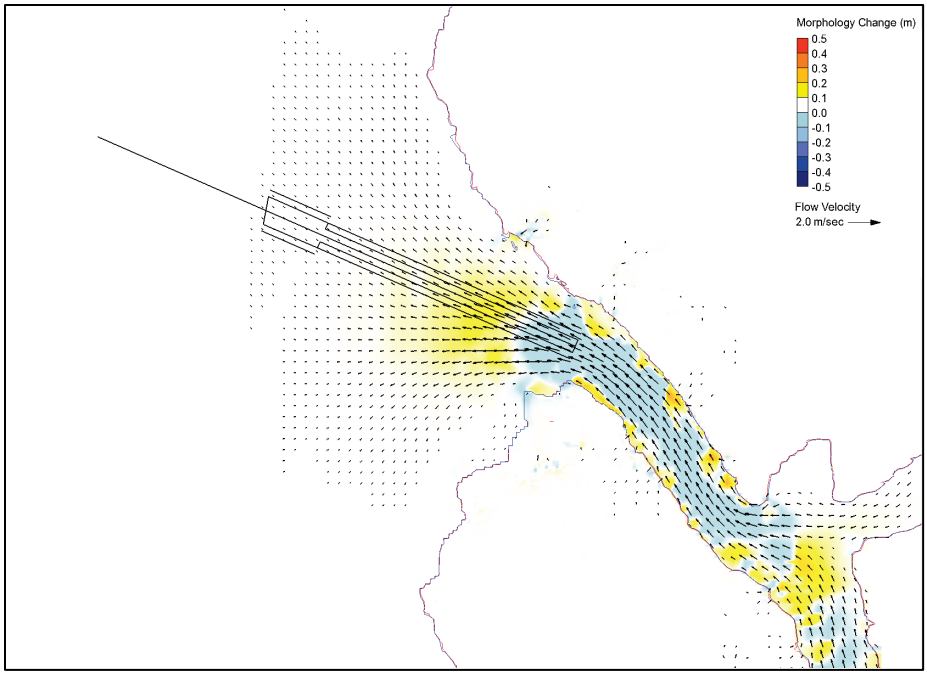

Figure 2-52. Morphology change for Alt-1 (ebb current, 31 August 2014 at 1400 GMT).

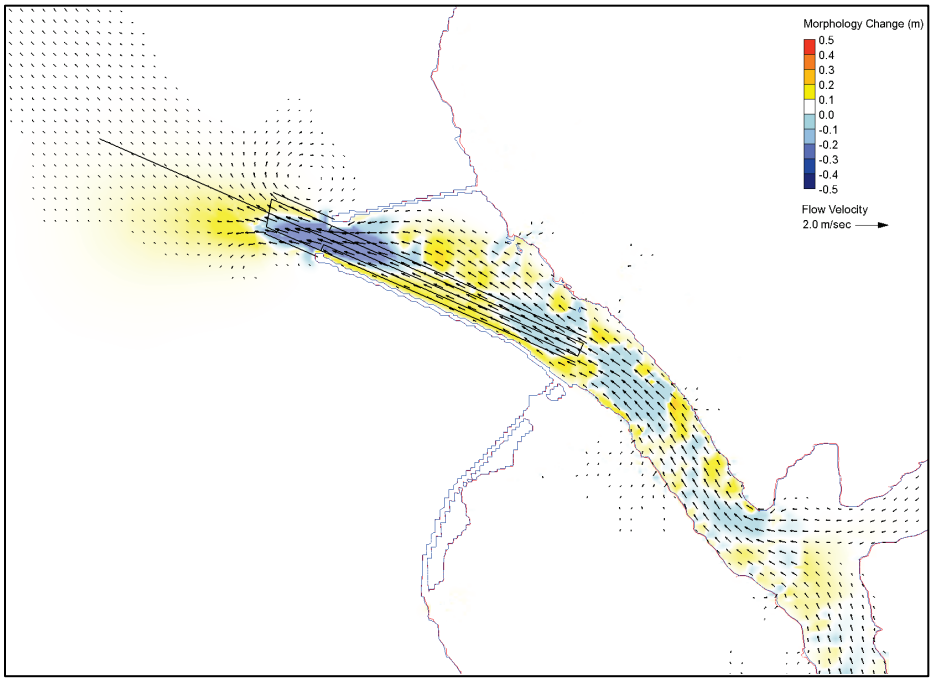

Figure 2-53. Morphology change for Alt-2 (ebb current, 31 August 2014 at 1400 GMT).

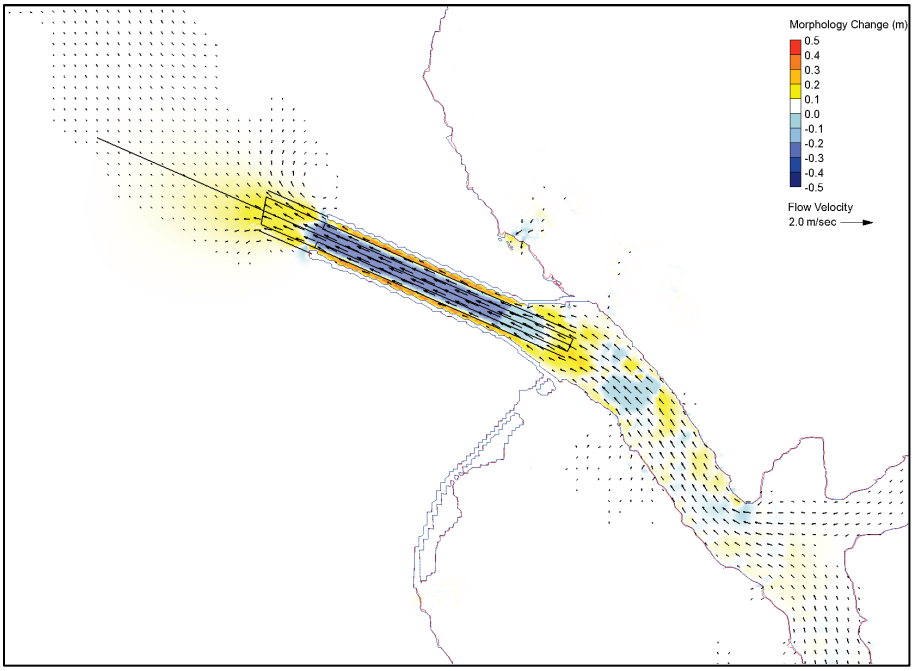

Figure 2-54. Morphology change for Alt-0 (flood current, 31 August 2014 at 2100 GMT).

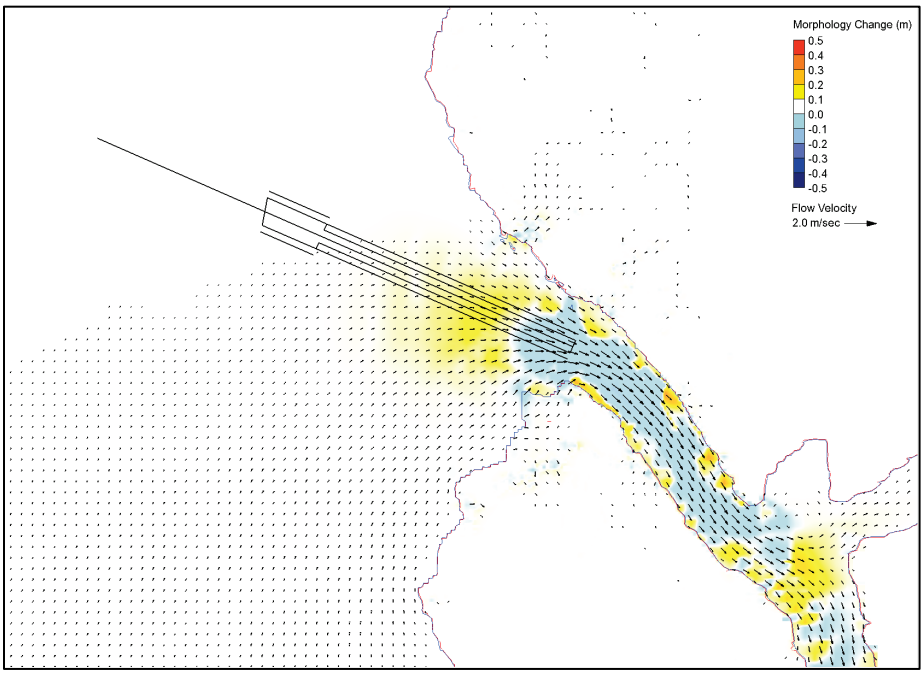

Figure 2-55. Morphology change for Alt-1 (flood current, 31 August 2014 at 2100 GMT).

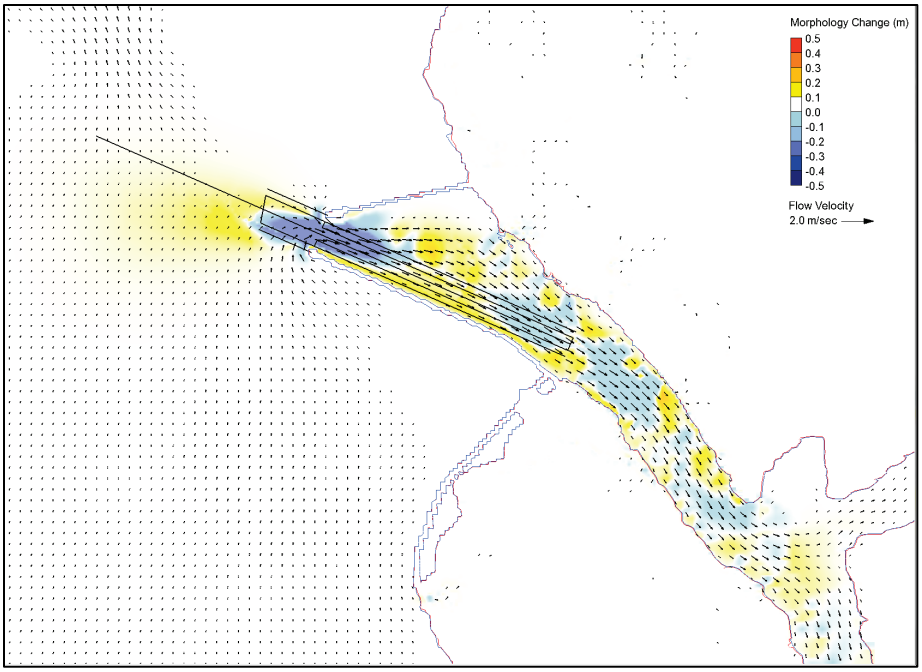

Figure 2-56. Morphology change for Alt-2 (flood current, 31 August 2014 at 2100 GMT).

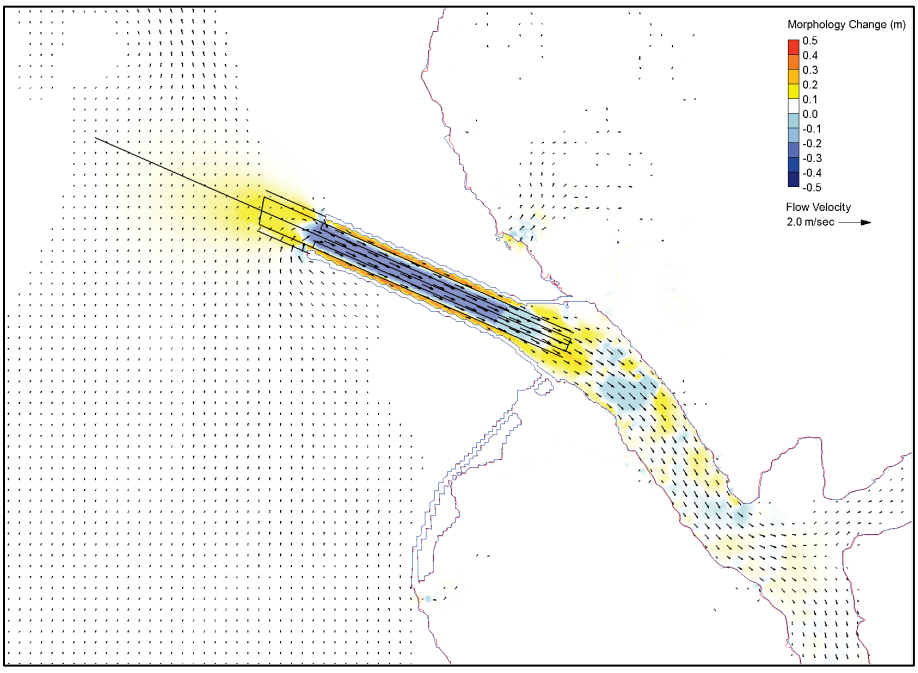

The summary statistics for morphology change are provided in Tables 2-8, 2-9, and 2-10 for Conditions 1, 2, and 3. Conditions 1 and 2 were 1-month-long simulations whereas Condition 3 was a 6-day simulation. The bed change along T1, T3, and T5 was calculated along these transects. The

purpose of the sediment transport calculations was to determine the effect of the jetties on channel erosion/accretion. The short-term estimates of morphology change based on a 1-month-long simulation with waves, currents, and sediment transport cannot be extrapolated to predict long-term channel shoaling rates. However, a 1-month simulation of sediment transport helps to determine sedimentation patterns in the channel and outside along neighboring shorelines.

Table 2-8. Calculated maximum bottom scour and accretion along T1.

Alt	Condition 1	Condition 2	Condition 3
0	-10 cm / 10 cm	-10 cm / 15 cm	-10 cm / 6 cm
1	-10 cm / 14 cm	-10 cm / 16 cm	-10 cm / 6 cm
2	-10 cm / 10 cm	-10 cm / 13 cm	-10 cm / 4 cm

Table 2-9. Calculated maximum bottom scour and accretion along T3.

Alt	Condition 1	Condition 2	Condition 3
0	-10 cm / 39 cm	-10 cm / 45 cm	-10 cm / 19 cm
1	-30 cm / 23 cm	-30 cm / 30 cm	-20 cm / 12 cm
2	-30 cm / 12 cm	-30 cm / 19 cm	-13 cm / 7 cm

Table 2-10. Calculated maximum bottom scour and accretion along T5.

Alt	Condition 1	Condition 2	Condition 3
0	-10 cm / 1 cm	-10 cm / 2 cm	-7 cm / 4 cm
1	-10 cm / 5 cm	-10 cm / 7 cm	-8 cm / 3 cm
2	-6 cm / 6 cm	-6 cm / 5 cm	-4 cm / 4 cm

The results in Tables 2-8, 2-9, and 2-10 indicate the maximum bottom erosion along T1, T3, and T5 remained less than 1.6 ft (0.5 m) within 1-month duration. A self-scouring channel with jetties is beneficial for the long-term channel maintenance. For the three Alternatives with three conditions simulated, the calculated maximum erosion and accretion along T1 were 0.3 ft (0.1 m) and 0.5 ft (0.16 m), respectively. Along channel centerline transect T3, maximum erosion/accretion were 1 ft (0.3 m) and 1.5 ft (0.45 m), respectively. The erosion and accretion along the south shoreline transect line T5 were 0.3 ft (0.1 m) and 0.2 ft (0.07 m), respectively. Model results indicated different sediment patterns developing along the north and south shorelines, with comparatively less erosion of the south shoreline.

For Alt-1 along the channel centerline, the sediment pattern shows increased bottom erosion around the jetty entrance. This is due to converging of flow and stronger interaction between waves and currents near the jetty heads. For Alt-2, the channel erosion increases between the parallel jetties due to constrained currents. The channel erosion in Alt-1 and Alt-2 is not linear with time as the channel cross section changes (e.g., channel becomes wider and deeper between jetties). The erosion in the channel is expected to reach equilibrium as coarser bed material is encountered. Because of lack of current field data and detail information about the channel bed layers, model predictions could not be calibrated and validated in the channel. Due to these uncertainties, both flow and sediment transport estimates can be over predicted. Local field data collection would help to address these uncertainties.

2.12 Estimates for structure design

The calculated wave-height, period, direction, and water-level estimates at locations on the windward side of the north and south jetties were extracted for structural calculations, as described in Chapter 3. Wave direction is in the meteorological convention (e.g., direction waves coming from).

3 Structural Design Calculations

3.1 Selection of design wave and water level

For design estimates of jetty stone size, the storm with a statistical return period of 50 years (Hurricane Sandy for this study) was used. Wave heights and wave periods for the 50-year event were described in Chapter 2. Although the tidal range is small in the area of Smith Island, a significant storm surge occurred during the design event. A still-water level rise of 5 ft (~1.5 m) for Hurricane Sandy was selected to include tidal fluctuations, storm surge, and wave setup.

All calculations have been expressed in the System International (SI) and American Customary (English) units. A table of conversions is included at the beginning of this report to assist in conversion between these units. The methodology used herein follows Melby (2010) and is updated in Melby et al. (2015).

3.2 Stability equations

3.2.1 Stable seaside armor stone size

Stable armor stone size is computed here based on 50-year return period wave and water level conditions. See Chapter 2 for details. The well-known Hudson equation has been used for years to determine armor stability (Hudson 1959; Department of the Army 1984). In stability number form, the Hudson equation is given by

$$N_s = \frac{H_{1/10}}{\Delta D_{n50}} = (K_D \cot\theta)^{1/3} \tag{3-1}$$

where N_s is the stability number, $H_{1/10}$ is the average height of the highest 10% of waves; $\Delta = S_r - 1$, with $S_r = \rho_r / \rho_w$ = immersed specific gravity of the armor stone with ρ_r = density of armor stone and ρ_w = density of water at the project site; D_{n50} is nominal stone size defined as $D_{n50} = (M_{50}/\rho_r)^{1/3}$, where M_{50} = median mass of armor stone; K_D is an empirical coefficient and θ is the seaside jetty structure slope angle. K_D takes into account all parameters not in the equation. The Hudson equation was originally developed for monochromatic waves, and use of the equation with

irregular wave height statistics has been discussed by many authors. The most common application of the equation utilizes $H_{1/10}$ for depth-limited wave conditions with the depth-limited breaker height limited to 0.78 * local water depth. Values published for K_D in the USACE *Coastal Engineering Manual* (USACE 2015) are appropriate. The Hudson equation assumes damage based on 0% to 5% eroded volume.

The seaside armor stability is computed based on the maximum wave momentum flux for nonlinear steep waves in shallow water (Melby and Kobayashi 2011). This corresponds to the case where armor stability is at its minimum. A non-linear wave momentum flux using Fourier solution (Melby and Hughes 2004) provides the following equation:

$$\left(\frac{M_F}{\rho_w g h^2}\right)_{\max} = A_0 \left(\frac{h}{g T_m^2}\right)^{-A_1}$$

$$A_0 = 0.639 \left(\frac{H_{m0}}{h}\right)^{2.026} \tag{3-2}$$

$$A_1 = 0.180 \left(\frac{H_{m0}}{h}\right)^{-0.391}$$

where M_F is the momentum flux as calculated in Equation (3-2), g is acceleration of gravity, h is local water depth, T_m is mean wave period, and $H_{mo} = H_s = 4\,(m_0)^{1/2}$ is the wave height of the zeroth moment of a wave energy spectrum. Note the n^{th} moment of the incident wave energy spectrum, $E(f)$, over frequency f is given by

$$m_n = \int_0^\infty f^n E(f) df \tag{3-3}$$

Two stability equations result from the fit of Equation (3-2) to data, which are

$$N_m = \frac{1}{a_m}\left(\frac{S}{K_s \sqrt{N_z}}\right)^{0.2} \tag{3-4}$$

and

$$N_m = \left(\frac{(M_F / \gamma_w h^2)_{\max}}{\Delta} \right)^{1/2} \frac{h}{D_{n50}} \tag{3-5}$$

The coefficient a_m for plunging waves is given by

$$a_m = \frac{1}{5P^{0.18}\sqrt{\cot\theta}} \qquad s_m \geq s_{mc} \tag{3-6}$$

and for surging waves, it is given by

$$a_m = \frac{s_m^{P/3}}{5P^{0.18}(\cot\theta)^{0.5-P}} \quad s_m < s_{mc} \tag{3-7}$$

where

$$s_m = H_{m0} / L_{m,} \qquad s_{mc} = -0.0035\cot\theta + 0.028 \tag{3-8}$$

Equating Equation (3-4) to Equation (3-5) yields the stable stone size as

$$D_{n50} = h a_m \left(\frac{S}{K_s \sqrt{N_z}} \right)^{-1/5} \left(\frac{(M_F / \gamma_w h^2)_{\max}}{\Delta} \right)^{1/2} \tag{3-9}$$

The variables S and A_e are related to damage level and illustrated in Figure 3-1. The remaining parameters that appear in Equation (3-4) to Equation (3-9) are as follows: N_m = the momentum flux stability number, P = notional permeability of the structure, $S = A_e/(D_{n50})^2$ = normalized eroded area (also known as the damage level, see Figure 3-1), A_e = eroded area, L_m = wave length, N_z = storm duration/T_m, K_s = an empirical parameter that accounts for accelerated damage occurring with constant wave conditions, $\gamma_w = \rho_w$ g = specific weight of water, s_m = local wave steepness, and s_{mc} = critical wave steepness.

The acceptable damage level (S) is dependent on the seaward slope angle. Recommended values of S by Van Gent and Pozueta (2004) for different structural slopes are as follows: S = 4 for 1V: 1.5H slope; S = 5 for 1V:2H slope; and S = 10 for 1V:4H slope.

Figure 3-1. Illustration of damage parameters.

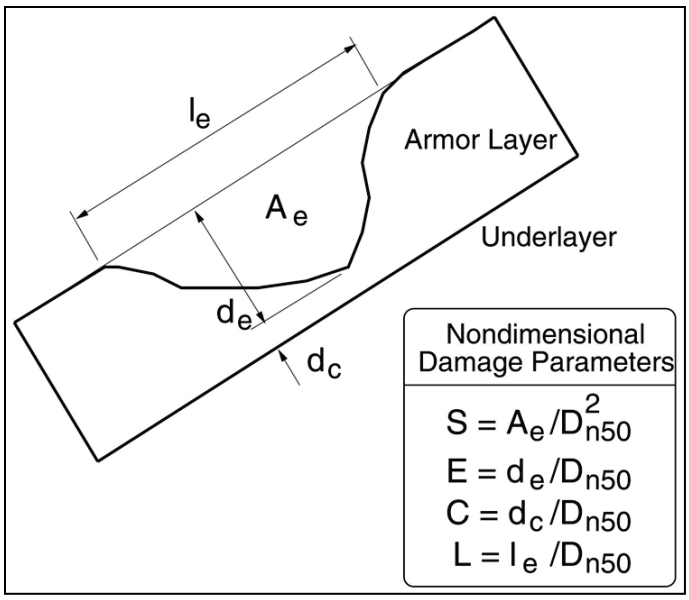

The permeability of the structure is defined by P. For an impermeable dike, P = 0.1. For a traditional multilayer breakwater, P = 0.4 – 0.6. Use of small core material that effectively restricts transmission would give a permeability of P = 0.4. In the absence of more detailed information, a value of P = 0.4 was used in this study.

3.2.2 Stable leeside armor stone size

The leeside stability equations given by Van Gent and Pozueta (2004) were reformulated by Melby (2010) to be similar to seaside equations defined as

$$D_{n50} = a_{ls}\left(\frac{S_{ls}}{K_{ls}\sqrt{N_z}}\right)^{-1/r}\left(\frac{u_{1\%}T_{m-1,0}}{125\sqrt{\Delta}}\right) \tag{3-10}$$

with

$$a_{ls} = (\cot\varphi)^{-2.5/r}[1+10\cdot\exp(-R_{c-rear}/H_s)]^{1/r} \tag{3-11}$$

where S_{ls} is the leeside damage, K_{ls} = 1 and r = 6 are empirical fit parameters for steady wave conditions, $u_{1\%}$ = maximum crest velocity exceeded by 1% of the waves, $T_{m\text{-}1,0} = m_{-1}/m_0$ of incident spectrum, $T_{m\text{-}1,0} = T_p/1.1$ for a JOint North Sea WAve Project (JONSWAP) incident wave spectrum (USACE 2015), ϕ = leeside slope angle, $R_{c\text{-}rear}$ = freeboard of leeside edge of crest, H_s

= H_{m0} of incident wave spectrum, and $(D_{n50})_{ls}$ = the nominal stone size, and Δ_{ls} = density parameter for the leeside armor, respectively.

Following Van Gent and Pozueta (2004), Melby (2010) introduced the leeside stability number, N_{ls}, and defined it as

$$N_{ls} = \left(\frac{u_{1\%} T_{m-1,0}}{125 (D_n \sqrt{\Delta})_{ls}} \right) = \frac{1}{a_{ls}} \left(\frac{S_{ls}}{K_{ls} \sqrt{N_z}} \right)^{1/r} \tag{3-12}$$

Based on Equation (3-11) and Equation (3-12), Melby (2010) expressed the storm leeside damage for constant wave conditions was expressed as

$$S_{ls} = K_{ls} \sqrt{N_z} \left(a_{ls} N_{ls} \right)^r \tag{3-13}$$

The crest velocity exceeded by 1% of the waves was estimated as

$$\frac{u_{1\%}}{\sqrt{g H_s}} = \frac{1.7 (\gamma_{f-C})^{0.5} \left(\frac{z_{1\%} - R_c}{\gamma_f H_s} \right)^{0.5}}{\left(1 + 0.1 \frac{B_c}{H_s} \right)} \tag{3-14}$$

where $\gamma_{f\text{-}C}$ = friction factor on crest, γ_f = friction factor on seaward slope, R_c = freeboard of seaside crest, B_c = breakwater crest width, and $z_{1\%}$ = run-up exceeded by 1% of incident waves. The friction coefficients ($\gamma_{f\text{-}C}$ and γ_f) and run-up ($z_{1\%}$) can be computed using the following equations:

$$\gamma_f = \gamma_{f-C} = \begin{cases} 0.55 & \xi_{s,-1} \le 2 \\ 0.05625 * (\xi_{s,-1} - 2) + 0.55 & 2 < \xi_{s,-1} < 10 \\ 1.0 & \xi_{s,-1} \ge 10 \end{cases} \tag{3-15}$$

and

$$\frac{z_{1\%}}{\gamma H_s} = \begin{cases} c_0 \, \xi_{s,-1} & for \; \xi_{s,-1} \le p \\ c_1 - c_2 / \xi_{s,-1} & for \; \xi_{s,-1} > p \end{cases} \tag{3-16}$$

where $c_2 = 0.25\ c_1^2/c_0$, $p = 0.5\ c_1/c_0$, $\gamma = \gamma_f \gamma_\beta$ is the reduction factor for roughness (γ_f) and angular wave attack (γ_β), and $\xi_{s,-1}$ is the Iribarren parameter based on the first negative moment wave period:

$$\xi_{s,-1} = \frac{\tan\varphi}{\sqrt{\frac{H_s}{L_{m-1,0}}}} \tag{3-17}$$

with

$$L_{m-1,0} = \frac{gT_{m-1,0}^2}{2\pi} \tag{3-18}$$

For the Rhodes Point jetties, values of $c_0 = 1.45$ and $c_1 = 5.1$ were selected (Van Gent and Pozueta 2004) for calculation of $z_{1\%}$ by Equation (3-16) and $\gamma_\beta = 1.0$ for normally incident waves. Substituting these values, Equation (3-16) becomes

$$\frac{z_{1\%}}{\gamma_f\ H_s} = \begin{cases} 1.45\xi_{s,-1} & for\ \xi_{s,-1} \le 1.76 \\ 5.10 - 4.485/\xi_{s,-1} & for\ \xi_{s,-1} > 1.76 \end{cases} \tag{3-19}$$

A schematic illustration of the seaside damage on a rubble-mound jetty structure is shown in Figure 3-2, indicated by Damage Conditions (DC) 1 and 2 in Figure 3-2. The DC 1 shows damage initiation that occurs as the armor is displaced near the still water line but has not extended into the filter layers. The DC 2 shows extensive damage over the entire active zone of the seaward side extending into the filter layers and even into the core and crest. Once seaside damage reaches DC 2, the jetty structure will breach during the storm. The leeside damage is illustrated in Figure 3-3, showing that damage begins on the rear crest and erodes seaward through the crest.

Figure 3-2. Illustration of damage on a rubble-mound structure (USACE 2015).

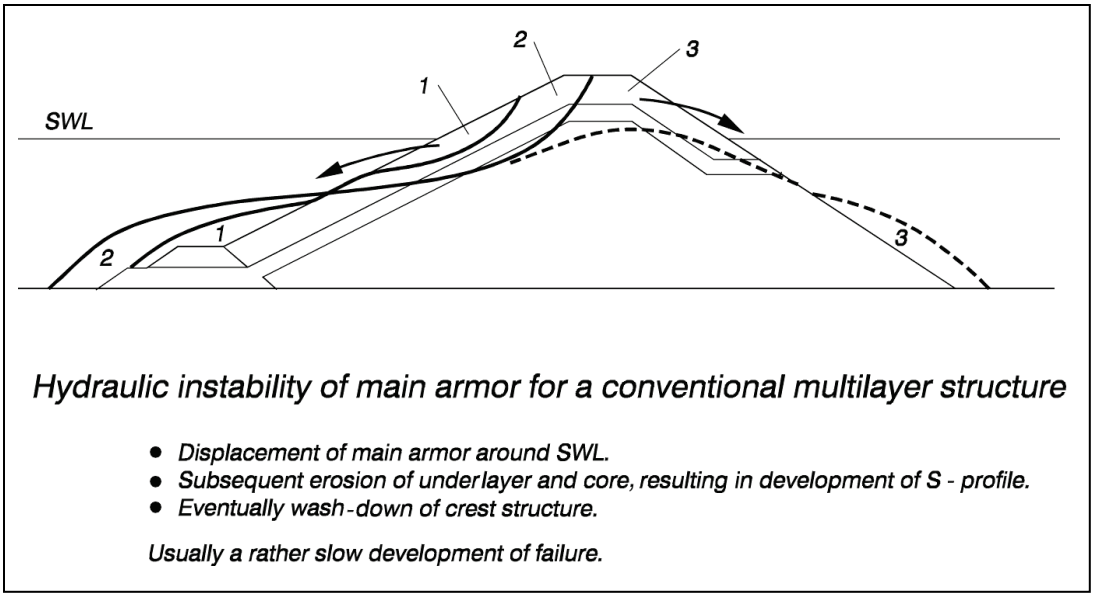

Figure 3-3. Leeside erosion of a rubble-mound breakwater (USACE 2015).

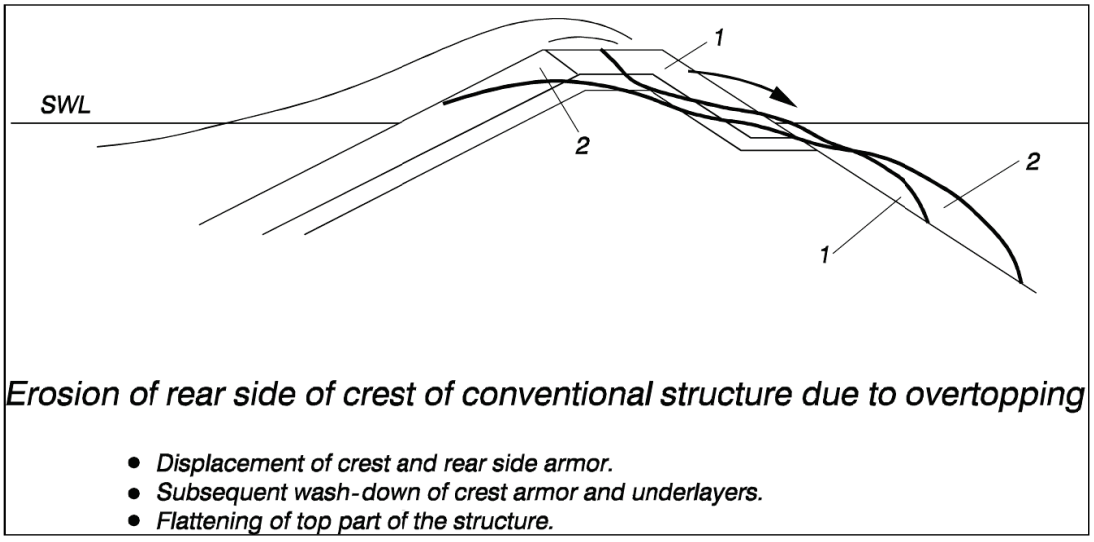

3.3 Wave overtopping transmission

Wave run-up (on a gentle slope) rubble-mound jetty structure is typically on the order of 1.5 to 1.6 times the incident wave height (USACE 2015). Wave run-up ($z_{1\%}$) is calculated using Equation (3-16). Wave overtopping occurs when $u_{1\%} > 0$ in Equation (3-14). The transmission due to overtopping represents the transformation of wave height from the seaside of the breakwater, $(H_s)_i$ or H_s , to the leeside of the jetty structure, $(H_s)_t$. This type of wave transmission is worse for heavily damaged sections that have lowered or submerged crest elevations. The transmission coefficient

$K_t = (H_s)_t/(H_s)_i$ is computed for permeable rubble-mound breakwaters using the following relations proposed by d'Angremond et al. (1996) as

$$K_t = -0.4\frac{R_c}{H_s} + 0.64\ [\frac{B_c}{H_s}]^{-0.31}(1 - e^{-0.5\xi_{s,-1}}) \tag{3-20}$$

Equation (3-20) is applicable to small crest width of $B_c/H_s < 8$.

3.4 Design structure

3.4.1 Assumptions

Incident wave direction was included in the stability calculations assuming waves approach normal to the structure ($\gamma_\beta = 1.0$).

Calculations assumed three values of side slopes; these were 1V:1.5H (θ=21.8 degrees [deg]), 1V:2H (θ=26.6 deg), and 1V:2.5H (θ=33.7 deg). In the absence of detailed information on stone that will be used, a specific rock weight (ρ_r g) of 165 pounds per cubic foot (lb/ft^3) or 0.0825 ton/ft^3 or 2.91 ton/m3 and a minimum damage level of $S = S_{ls} = 2$ were assumed. For short jetty structures, both seaside and leeside crest freeboards were assumed to be equal ($R_c = R_{c\text{-}rear}$).

3.4.2 Calculations

The design jetties had a constant crest height of 3.84 ft (1.17 m) above MSL and a constant crest width of 8 ft (2.4 m). Equation (3-9) and Equation (3-10) with the above assumptions were used to calculate stable armor stone sizes at each save location (Stations 19, 21, 23, 65, 68, and 71) shown in Figure 2-23 (Alt-0), Figure 2-24 (Alt-1), and Figure 2-25 (Alt-2). Tables 3-1, 3-2, and 3-3 present the calculated stone size/weight and transmitted wave heights associated with three breakwater side slopes: θ (= ϕ) = 21.8 deg (1V:2.5H), 26.6 deg (1V:2H), and 33.7 deg (1V:1.5H), respectively. The stone weight (ton) in these tables was calculated as ρ_r g $(D_{n50})^3$.

Table 3-1. Stone weights and transmitted wave heights (side slope 1V:2.5H).

Sta	Storm Water Level, MSL (ft)	Depth, MSL (ft)	Design Wave Ht (ft)	Design Wave Period (sec)	Sea-side Armor Diam (ft)	Sea-side Armor Weight (ton)	Lee-side Armor Diam (ft)	Lee-side Armor Weight (ton)	Trans Coef	Trans Wave Height (ft)
19	5.00	5.75	3.15	4.8	1.03	0.09	1.19	0.14	0.47	1.48
21	5.00	6.00	3.30	4.8	1.07	0.10	1.21	0.15	0.46	1.53
23	5.00	7.70	4.10	4.8	1.29	0.18	1.31	0.19	0.44	1.80
65	5.00	7.70	3.80	4.8	1.21	0.15	1.27	0.17	0.45	1.70
68	5.00	5.05	2.90	4.8	0.96	0.08	1.15	0.13	0.48	1.40
71	5.00	4.80	2.60	4.8	0.88	0.06	1.10	0.11	0.50	1.30
Max	5.00	7.70	4.10	4.8	1.29	0.18	1.31	0.19	0.50	1.80

Table 3-2. Stone weights and transmitted wave heights (side slope 1V:2H).

Sta	Storm Water Level, MSL (ft)	Depth, MSL (ft)	Design Wave Ht (ft)	Design Wave Period (sec)	Sea-side Armor Diam (ft)	Sea-side Armor Weight (ton)	Lee-side Armor Diam (ft)	Lee-side Armor Weight (ton)	Trans Coef	Trans Wave Height (ft)
19	5.00	5.75	3.15	4.8	1.15	0.13	1.41	0.23	0.51	1.60
21	5.00	6.00	3.30	4.8	1.20	0.14	1.44	0.24	0.50	1.66
23	5.00	7.70	4.10	4.8	1.44	0.25	1.56	0.32	0.48	1.97
65	5.00	7.70	3.80	4.8	1.35	0.20	1.52	0.29	0.49	1.85
68	5.00	5.05	2.90	4.8	1.08	0.10	1.36	0.21	0.52	1.50
71	5.00	4.80	2.60	4.8	0.99	0.08	1.30	0.18	0.53	1.39
Max	5.00	7.70	4.10	4.8	1.44	0.25	1.56	0.32	0.53	1.97

Table 3-3. Stone weights and transmitted wave heights (side slope 1V:1.5H).

Sta	Storm Water Level, MSL (ft)	Depth, MSL (ft)	Design Wave Ht (ft)	Design Wave Period (sec)	Sea-side Armor Diam (ft)	Sea-side Armor Weight (ton)	Lee-side Armor Diam (ft)	Lee-side Armor Weight (ton)	Trans Coef	Trans Wave Height (ft)
19	5.00	5.75	3.15	4.8	1.33	0.19	1.72	0.42	0.55	1.74
21	5.00	6.00	3.30	4.8	1.38	0.22	1.76	0.45	0.55	1.81
23	5.00	7.70	4.10	4.8	1.66	0.38	1.93	0.59	0.53	2.18
65	5.00	7.70	3.80	4.8	1.56	0.31	1.87	0.54	0.54	2.04
68	5.00	5.05	2.90	4.8	1.24	0.16	1.66	0.38	0.56	1.62
71	5.00	4.80	2.60	4.8	1.14	0.12	1.58	0.33	0.57	1.49
Max	5.00	7.70	4.10	4.8	1.66	0.38	1.93	0.59	0.57	2.18

3.4.3 Discussion

If waves overtop the jetty crest and are transmitted to the leeside of the structure, the design generally requires greater armor stone size on the leeside than the stone on the seaside of the structure. The steeper the jetty side slopes are, the greater the stable armor stone size would be both on the seaside and leeside of the jetty. Steeper side slopes also introduce stability problems and increase wave refraction, reflection, and diffraction.

Tables 3-1 to 3-3 indicate that the maximum design stone diameter occurs on the leeside of the jetty and increases from 1.31 to 1.93 ft (0.4 to 0.6 m) for side slopes 1V:2.5H and 1V:1.5H, respectively. The corresponding single stone weight on the leeside increases from 0.19 ton to 0.59 ton for the side slope of 1V:2.5H and 1V:1.5H, respectively. These estimates indicate that large stones would be required at the seaward end of the jetties (Station 23 and Station 65) where larger storm waves can break over the steeper structure slopes at deeper water depths.

3.5 Low-crested jetty

The calculations presented in the preceding sections developed a design for a traditional jetty with minimal damage during a 50-year storm event. The design structure has a constant crest height of 3.84 ft (1.17 m) above MSL and constant crest width of 8 ft (2.4 m). The structure had a constant crest height of 3.84 ft (1.17 m) and crest width of 8 ft (2.4 m). Because the design storm assumed a water level of 5 ft (1.53 m) MSL, the design structure would be submerged under this condition, making it a low-crested structure. At this water elevation, much of the island where the north and south jetties are located will be inundated, and there is little point in having a jetty that is higher than the surrounding land mass. As the water depth over a structure increases, the effects of waves on the structure decrease. A low-crested jetty was therefore considered.

There is only limited research on the armor layer stability of submerged structures. CIRIA (2007) presents results from Vidal et al. (1995) for stability of submerged structures. Nominal stone diameter, D_{n50}, is calculated by solving the linear quadratic equation below:

$$\frac{H_s}{\Delta D_{n50}} = A + B\frac{R_c}{D_{n50}} + C\left(\frac{R_c}{D_{n50}}\right)^2 \tag{3-21}$$

where A, B, and C are coefficients that vary with the level of damage and the segment of the structure. For example, the coefficients for the initial damage on structures having seaside and leeside slopes of 1V:1.5H are given in Table 3-4.

Table 3-4. Coefficients for initial damage estimate of submerged rubble-mound structure.

Segment	A	B	C
Front slope	1.831	-0.245	0.0119
Crest	1.652	0.0182	0.159
Back slope	2.575	-0.54	0.115
Total section	1.544	-0.23	0.053

Results of the stone size calculations are shown below in Tables 3-5, 3-6, and 3-7 with three breakwater side slopes: θ (= ϕ) = 21.8 deg (1V:2.5H), 26.6 deg (1V:2H), and 33.7 deg (1V:1.5H), respectively. In general, the overall maximum stone diameters and weights calculated from the submerged jetty structure equation, Equation (3-21), are smaller than those calculated from Equation (3-9) and Equation (3-10). The results of the submerged jetty analysis confirm that the armor stone weights calculated for a low-crested jetty should be stable at the design water level. Results indicate stone weight increases with increasing structure side slopes.

Table 3-5. Low-crest structure stone weights (side slope 1V:2.5H).

Sta	Storm Water Level, MSL (ft)	Depth, MSL (ft)	Design Wave Ht (ft)	Design Wave Period (sec)	Sea-side Armor Diam (ft)	Sea-side Armor Weight (ton)	Crest Armor Diam (ft)	Crest Armor Weight (ton)	Lee-side Armor Diam (ft)	Lee-side Armor Weight (ton)
19	5.00	5.75	3.15	4.8	0.68	0.03	0.90	0.06	0.97	0.07
21	5.00	6.00	3.30	4.8	0.72	0.03	0.96	0.07	1.02	0.09
23	5.00	7.70	4.10	4.8	0.92	0.07	1.24	0.16	1.33	0.19
65	5.00	7.70	3.80	4.8	0.85	0.05	1.14	0.12	1.22	0.15
68	5.00	5.05	2.90	4.8	0.61	0.02	0.81	0.04	0.87	0.05
71	5.00	4.80	2.60	4.8	0.53	0.01	0.68	0.03	0.75	0.03
Max	5.00	7.70	4.10	4.8	0.92	0.07	1.24	0.16	1.33	0.19

Table 3-6. Low-crest structure stone weights (side slope 1V:2H).

Sta	Storm Water Level, MSL (ft)	Depth, MSL (ft)	Design Wave Ht (ft)	Design Wave Period (sec)	Sea-side Armor Diam (ft)	Sea-side Armor Weight (ton)	Crest Armor Diam (ft)	Crest Armor Weight (ton)	Lee-side Armor Diam (ft)	Lee-side Armor Weight (ton)
19	5.00	5.75	3.15	4.8	0.76	0.04	0.96	0.07	1.00	0.08
21	5.00	6.00	3.30	4.8	0.80	0.04	1.02	0.09	1.05	0.09
23	5.00	7.70	4.10	4.8	1.03	0.09	1.32	0.19	1.36	0.21
65	5.00	7.70	3.80	4.8	0.95	0.07	1.21	0.15	1.25	0.16
68	5.00	5.05	2.90	4.8	0.69	0.03	0.86	0.05	0.89	0.06
71	5.00	4.80	2.60	4.8	0.60	0.02	0.74	0.03	0.77	0.04
Max	5.00	7.70	4.10	4.8	1.03	0.09	1.32	0.19	1.36	0.21

Table 3-7. Low-crest structure stone weights (side slope 1V:1.5H).

Sta	Storm Water Level, MSL (ft)	Depth, MSL (ft)	Design Wave Ht (ft)	Design Wave Period (sec)	Sea-side Armor Diam (ft)	Sea-side Armor Weight (ton)	Crest Armor Diam (ft)	Crest Armor Weight (ton)	Lee-side Armor Diam (ft)	Lee-side Armor Weight (ton)
19	5.00	5.75	3.15	4.8	0.88	0.06	1.04	0.09	1.02	0.09
21	5.00	6.00	3.30	4.8	0.93	0.07	1.11	0.11	1.08	0.10
23	5.00	7.70	4.10	4.8	1.19	0.14	1.43	0.24	1.40	0.23
65	5.00	7.70	3.80	4.8	1.09	0.11	1.31	0.18	1.28	0.17
68	5.00	5.05	2.90	4.8	0.79	0.04	0.94	0.07	0.92	0.06
71	5.00	4.80	2.60	4.8	0.69	0.03	0.81	0.04	0.79	0.04
Max	5.00	7.70	4.10	4.8	1.19	0.14	1.43	0.24	1.40	0.23

3.6 Revetment

The proposed jetty systems for Rhodes Point include a rock revetment for protecting the shoreline along the south side of the inlet. However, there is not much information available in the literature about the size and weight of submerged structures during storms at different water depths under the combined effects of different water levels, waves, and currents. Consequently, a range of 600 to 1,000 lb (0.3 to 0.5 ton) for armor stone weight for the south shoreline revetment is recommended. This recommendation was based on a similar recommendation for a recent study involving revetment design at Tangier Island (Demirbilek et al. 2015), where armor stone with weight ranging from 600 to 1,000 lb (0.3 to 0.5 ton) was suggested for the design of a revetment.

At Tangier Island, there is evidence that some of the revetment stones have moved. Overall, the rock revetment protecting the west side of the south shoreline of Tangier Island (it is located just south of Rhodes Point) has performed extremely well. No design records were found, and a letter indicated the revetment at Tangier Island used armor stone from 600 to 1,000 lb (0.3 to 0.5 ton) with 75% greater than 750 lb (~0.4 ton). Assuming this represented the design of the as-built structure, the design would yield average armor stone of 800 lb (0.4 ton). This is approximately half the seaside armor weight estimates for a low-crested structure (Tables 3-5, 3-6, and 3-7). On the basis of information for the Tangier Island revetment structure, and given the absence of any other design guidance, a 1,000 lb (0.5 ton) armor stone is recommended for the south shoreline revetment. Considering uncertainties involved with the design of revetment structures and for avoiding potential movement of the stones as occurred at Tangier Island, a safety factor of 1.25 may be used. This would increase the average armor stone to 1,250 lb (0.625 ton) for Rhodes Point south shoreline revetment as an upper bound design estimate.

3.7 Jetty response with sea level rise (SLR)

The effects of SLR on the performance and stability of the jetties were investigated for three estimates of projected SLR trends (Houston 2012; Church and White 2011; USACE 2011; Demirbilek et al. 2005) as follows:

1. National Research Council (NRC)-I
2. NRC-II
3. NRC-III.

The SLR in meters was computed using the following equation:

$$\overline{\eta}(Y_2) - \overline{\eta}(Y_1) = a_0(Y_2 - Y_1) + b_0[(Y_2 - Y_0)^2 - (Y_1 - Y_0)^2] \quad (3\text{-}22)$$

where Y_0 , Y_1 , and Y_2 are times in years, $\overline{\eta}(Y_2) - \overline{\eta}(Y_1)$ is the mean SLR from Y_1 to Y_2. The coefficients a_0 and b_0 were calibrated based on the data set with the starting year (a reference year) Y_0 in the data set. (See USACE [2011]) for additional information. For the Chesapeake Bay, a_0 = 1.7 mm/year, b_0 = 0.0271 mm/year^2 for NRC-I, b_0 = 0.07 mm/year^2 for NRC-II, and b_0 = 0.113 mm/year^2 for NRC-III with Y_0 = 1992. Figure 3-4 shows SLR scenarios for 2015 to 2065 (Y_1 to Y_2), converted to feet.

Figure 3-4. Sea level rise based on NRC-I, NRC-II, and NRC-III.

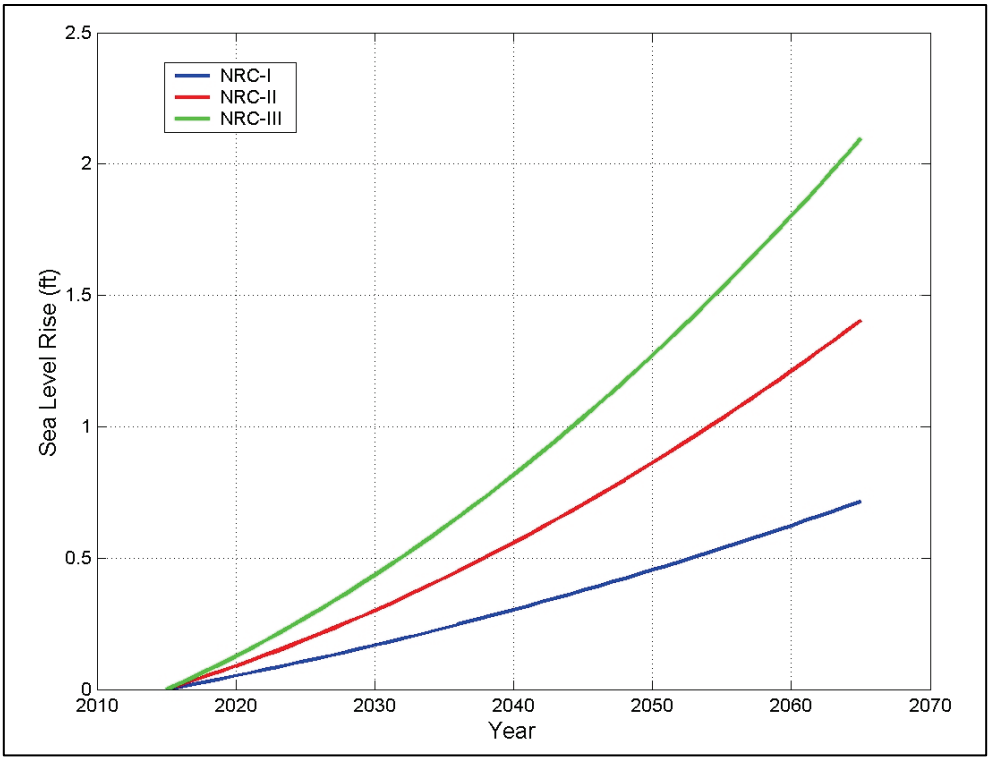

Boon et al. (2010) and Church and White (2011) reported that the mean SLR in the Chesapeake Bay area was approximately 0.015 ft/year (4.5 mm/year), which corresponded to a rise of 0.74 ft (0.2 m) over 50 years. Therefore, NRC-I provides a reasonable approximation of the most likely SLR scenario if the past is an indicator of future conditions (0.72 ft [0.22m] over 50 years) and the NRC-II serves as a reasonable upper bound (1.4 ft [0.43 m] over 50 years). For 100-year design, the SLR estimates for NRC-I and NRC-II are 1.9 ft (0.6 m) and 4.0 ft (1.2 m), respectively. Boon et al. (2010) also estimated subsidence in the Chesapeake Bay area of -4 mm/year, which corresponded to an increase in depth of 0.65 ft (0.2 m) over 50 years and 1.3 ft (0.4 m) for 100 years.

Assuming the NRC-I SLR as the most likely to occur, and adding 0.65 ft (0.2 m) for bay wide subsidence, the water depth at the jetty structure will increase by 1.37 ft (0.4 m) in 50 years, assuming adequate foundation materials are used to place the jetty stone and weight-induced subsidence would not be an issue. In this case, the crest elevation would reduce from 3.84 ft (1.2 m) to 2.47 ft (0.8 m) above the MSL. Assuming the NRC-II as the upper bound of the expected SLR, and adding 0.65 ft (0.2 m) for subsidence, the depth at the jetty structure would increase by as much as

2.04 ft (0.6 m) in 50 years. In this case, the crest elevation would be 1.8 ft (0.5 m) above the MSL.

If the water level increases, the jetty freeboard is reduced by the same amount. The seaside armor stone calculations are not sensitive to the change of freeboard, but the leeside armor stones can become unstable if the freeboard is reduced (Demirbilek et al. 2015). Tables 3-8, 3-9, and 3-10 present calculated leeside armor stones and transmitted waves at each of the save locations (Stations 19, 21, 23, 65, 68, and 71) if the depth increases by 1.37 ft (0.4 m) (NRC-I plus subsidence) or 2.04 ft (0.6 m) (NRC-II plus subsidence) for three breakwater side slopes: θ (= $\emptyset$) = 21.8 deg (1V:2.5H), 26.6 deg (1V:2H), and 33.7 deg (1V:1.5H), respectively. The calculation results indicate maximum transmitted wave heights are approximately 12% greater for NRC-I plus subsidence and 20% greater for NRC-II plus subsidence, as compared to no-SLR scenarios. Using these estimates, the maximum stone size (diameter) increased by 12% to 15% for NRC-I plus subsidence and by 18% to 22% for NRC-II plus subsidence.

Table 3-8. Leeside stones estimates with SLR (side slope 1V:2.5H).

Sta	Storm Water Level, MSL (ft)	Design Wave Ht (ft)*	Depth, MSL (ft)	Lee-side Armor Diam (ft)	Lee-side Armor Weight (ton)	Trans Wave Ht (ft)	Depth, MSL (ft)	Lee-side Armor Diam (ft)	Lee-side Armor Weight (ton)	Trans Wave Ht (ft)
			Depth increases by 1.37 ft				Depth increases by 2.04 ft			
19	5.00	3.15	7.12	1.40	0.23	2.03	7.80	1.51	0.28	2.30
21	5.00	3.30	7.37	1.42	0.24	2.08	8.04	1.52	0.29	2.34
23	5.00	4.10	9.07	1.50	0.28	2.34	9.74	1.60	0.34	2.61
65	5.00	3.80	9.07	1.47	0.26	2.24	9.74	1.57	0.32	2.51
68	5.00	2.90	6.42	1.37	0.21	1.94	7.10	1.48	0.27	2.21
71	5.00	2.60	6.17	1.33	0.19	1.84	6.84	1.45	0.25	2.11
Max	5.00	4.10	9.07	1.50	0.28	2.34	9.74	1.60	0.34	2.61

* Design wave period = 4.8 sec. Depth increases of 1.37 ft (NRC-I) and 2.04 ft (NRC-II) include subsidence in Chesapeake Bay.

Table 3-9. Leeside stones estimates with SLR (side slope 1V:2H).

Sta	Storm Water Level, MSL (ft)	Design Wave Ht (ft)*	Depth, MSL (ft)	Lee-side Armor Diam (ft)	Lee-side Armor Weight (ton)	Trans Wave Ht (ft)	Depth, MSL (ft)	Lee-side Armor Diam (ft)	Lee-side Armor Weight (ton)	Trans Wave Ht (ft)
			Depth increases by 1.37 ft				Depth increases by 2.04 ft			
19	5.00	3.15	7.12	1.64	0.36	2.15	7.80	1.75	0.45	2.42
21	5.00	3.30	7.37	1.66	0.38	2.21	8.04	1.78	0.46	2.47
23	5.00	4.10	9.07	1.77	0.46	2.52	9.74	1.87	0.54	2.78
65	5.00	3.80	9.07	1.73	0.43	2.40	9.74	1.84	0.51	2.67
68	5.00	2.90	6.42	1.60	0.33	2.05	7.10	1.72	0.42	2.32
71	5.00	2.60	6.17	1.54	0.30	1.93	6.84	1.67	0.39	2.20
Max	5.00	4.10	9.07	1.77	0.46	2.52	9.74	1.87	0.54	2.78

Design wave period = 4.8 sec. Depth increases of 1.37 ft (NRC-I) and 2.04 ft (NRC-II) include subsidence in Chesapeake Bay.

Table 3-10. Leeside stones estimates with SLR (side slope 1V:1.5H).

Sta	Storm Water Level, MSL (ft)	Design Wave Ht (ft)*	Depth, MSL (ft)	Lee-side Armor Diam (ft)	Lee-side Armor Weight (ton)	Trans Wave Ht (ft)	Depth, MSL (ft)	Lee-side Armor Diam (ft)	Lee-side Armor Weight (ton)	Trans Wave Ht (ft)
			Depth increases by 1.37 ft				Depth increases by 2.04 ft			
19	5.00	3.15	7.12	1.98	0.64	2.29	7.80	2.11	0.78	2.55
21	5.00	3.30	7.37	2.01	0.67	2.36	8.04	2.14	0.81	2.62
23	5.00	4.10	9.07	2.16	0.83	2.73	9.74	2.28	0.98	3.00
65	5.00	3.80	9.07	2.11	0.77	2.59	9.74	2.23	0.92	2.85
68	5.00	2.90	6.42	1.93	0.59	2.17	7.10	2.07	0.73	2.44
71	5.00	2.60	6.17	1.86	0.53	2.03	6.84	2.01	0.66	2.30
Max	5.00	4.10	9.07	2.16	0.83	2.73	9.74	2.28	0.98	3.00

Design wave period = 4.8 sec. Depth increases of 1.37 ft (NRC-I) and 2.04 ft (NRC-II) include subsidence in Chesapeake Bay.

The subsidence mentioned in Tables 3-8, 3-9, and 3-10 refers to the general subsidence of the Chesapeake Bay and does not address local subsidence caused by the weight of the jetty compressing the underlying soil substrate. The design jetty crest elevation should be increased to the desired crest elevation after the structure has settled. Also, no wave data were available to calibrate the numerical model, which lends potentially large uncertainty to this analysis. Therefore, the jetty and revetment design presented in this report may require further revision to account for possible settlement of the structure.

3.8 Cross-section design

The cross section is considered to include a core plus underlayers covered by two layers of armor stone. For simplicity, the volume of the under layers will be included with the core volume. Sufficient crest width needs to have at least three armor stones. If the leeside armor stones are different from the seaside armor stones, the crest width is based on one smaller stone and two larger stones, regardless of whether the larger stones are on the seaside or leeside (Demirbilek et al. 2015).

Figure 3-5 shows idealized cross-sectional areas with the seaside armor stone layer, leeside armor stone layer, and core beneath armor stone layer for jetty structure side slope = 1V:2H. Armor (1) is the cross-sectional area of the seaside armor, where a(ss) is the nominal diameter of the seaside armor stone. Armor (3) is the cross-sectional area of the leeside armor, where a(ls) is the nominal diameter of the leeside armor stone. Armor (2) is in the transition between Armor (1) and Armor (2). Therefore, because the leeside stone would be larger than the seaside stone, it is divided into one-third seaside armor and two-thirds leeside armor. The core stone is typically significantly less expensive than the armor stone and less expensive to place.

Figure 3-5. Idealized cross-section of jetty (side slope 1V:2H).

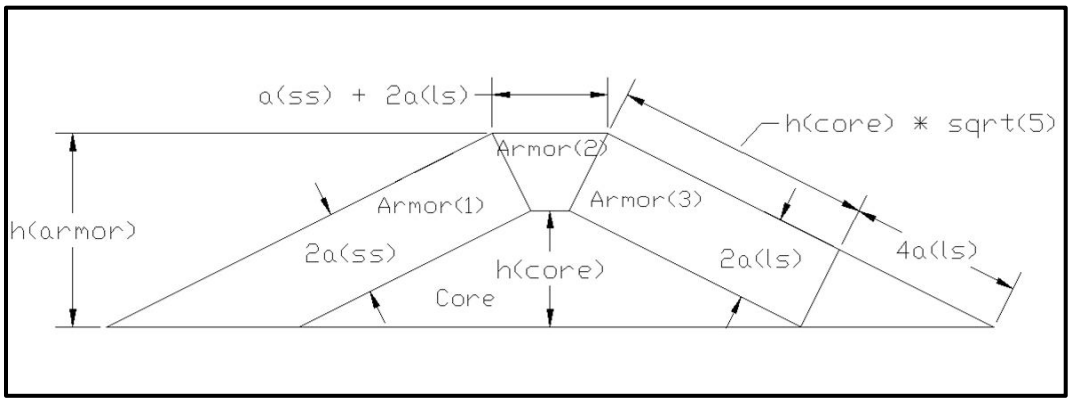

Tables 3-11 and 3-12 present the idealized cross-section areas of armor stone and core at each of the save locations (Stations 19, 21, 23, 65, 68, and 71) if the depth increases by 1.37 ft (0.4 m) (NRC-I plus subsidence) or 2.04 ft (0.6 m) (NRC-II plus subsidence), respectively, for the breakwater side slope angle of θ = 26.6 deg (1V:2H).

Table 3-11. Cross sections of armor stone and core for 1.37 ft depth increase by NRC-I plus subsidence (side slope 1V:2H).

Sta	h* (armor) (ft)	Seaside Stone Diam (ft)	Leeside Stone Diam (ft)	Total Area Seaside Armor (ft^2)	Total Area Leeside Armor (ft^2)	Total Area Crest Layer Armor (ft^2)	Area of Core + Underlayers (ft^2)
Depth increases by 1.37 ft; *h = crest elevation above MSL (2.47 ft) + depth.							
19	9.60	1.15	1.64	44.1	59.7	23.1	134.3
21	9.84	1.20	1.66	47.1	62.0	23.7	140.0
23	11.54	1.44	1.77	66.0	78.8	26.7	187.2
65	11.54	1.35	1.73	62.4	77.3	26.0	193.0
68	8.89	1.08	1.60	38.3	53.4	22.1	115.5
71	8.64	0.99	1.54	34.3	50.0	21.1	113.0

Table 3-12. Cross sections of armor stone and core for 2.04 ft depth increase by NRC-II plus subsidence (side slope 1V:2H).

Sta	h* (armor) (ft)	Seaside Stone Diam (ft)	Leeside Stone Diam (ft)	Total Area Seaside Armor (ft^2)	Total Area Leeside Armor (ft^2)	Total Area Armor Stone (ft^2)	Area of Core + Underlayers (ft^2)
Depth increases by 2.04 ft; *h = crest elevation above MSL (1.8 ft) + depth.							
19	9.60	1.15	1.75	44.1	62.9	24.1	130.1
21	9.84	1.20	1.78	47.1	65.7	24.6	135.1
23	11.54	1.44	1.87	66.0	82.5	27.4	182.7
65	11.54	1.35	1.72	62.4	76.9	25.9	193.5
68	8.89	1.08	1.67	38.3	55.2	22.7	113.0
71	8.64	0.99	1.87	34.3	58.3	24.1	101.8

The calculations of armor stone stability in Equation (3-2) to Equation (3-19) do not consider the jetty heads. In the Hudson equation, Equation (3-1), the stability coefficient K_D = 2.0 for jetty trunks with breaking waves and two layers of armor stone while for jetty heads with a 1:2 slope, the recommended coefficient (two layers of armor and breaking waves) is K_D = 1.6 (USACE 2015). This resulted in a 25% increase in stone size. In the absence of other guidance, armor stone sizes on the jetty heads (Stations 23 and 65) were calculated in the same manner as on the jetty trunks and were increased by 25%.

4 Conclusions

This report documents numerical wave, flow, and morphology change modeling for evaluation of the effectiveness of jetties for a shallow draft navigation channel at Rhodes Point, MD. U.S. Army Engineer District, Baltimore (NAB), is considering realignment of the western entrance channel protected by jetties and a revetment to protect the eroding south shoreline. The sheltering by jetties of the new (realigned) channel is expected to reduce wave energy in the channel and in areas in the lee of these structures. The jetties also provide an indirect protection to the north and south shorelines. The two Alternatives and existing channel geometry investigated by numerical models included north and south jetties connecting to north and south shorelines. Both Alternatives included the same revetment structure for protecting the south shoreline.

The Coastal Modeling System (CMS, including CMS-Wave and CMS-Flow) was used in this study. A number of advances to CMS-Wave were necessary to address this project's special needs. The Coastal Inlets Research Program (CIRP) funded these developments to improve the model's capabilities. These included development and testing of the full-plane and parent-child capability for hurricanes and northeasters in this estuary setting, developing pre- and post-processing analysis codes for model setup, and developing wave and water levels parameters for structural design calculations required at and around jetty and revetment structures.

Structural designs were estimated based on numerical wave and hydrodynamic modeling conducted for a 50-year design based on Hurricane Sandy wind speed, wave, and water-level conditions. A still-water level of 5 ft (1.5 m) was selected to include tide, storm surge, and wave setup. Two structure Alternatives were evaluated to identify an optimal design as determined by the level of wave-energy reduction in the navigation channel. The hydrodynamic modeling study results (e.g., wave height, period, direction, and water level) along the western side of the proposed jetty footprint were used in the preliminary structural design calculations. These calculations included jetty stability, run-up/overtopping, and transmission through and over the structure.

Results shown in Chapters 2 and 3 indicated performance of Alt 1 and Alt-2 were similar for the conditions evaluated. Negligible differences were obtained between these Alternatives in terms of their effects on waves, currents, and sediment transport calculated in the western channel and along the north and south shorelines. Both Alternatives are recommended as viable options to consider based on the level of wave reduction results provided in Chapter 2. A comparison of the two Alternatives indicated each performed equally well in reducing wave energy in the channel (Chapter 2). Without any jetty structure, results indicated wave dampening is comparatively less in the western channel and comparatively larger wave heights reached the north and south shorelines. Alt-1 with a shorter shore-normal north jetty of 650 ft (200 m) provided as much wave-reduction benefits as the longer 1,000 ft (305 m) north jetty in Alt-2.

Results indicated that for either Alternative with jetties, waves are strongly reduced from the jetty heads through the western portion of the channel. Wave energy dissipated to the extent that wave heights were reduced as compared to incident waves in the bay. Model results also indicated that the greatest benefits to be accrued by the Alternatives will occur in this western channel. Towards the east, the impacts of jetties on waves, currents, and shoaling in the narrow canal were relatively much less. For Condition 2 (February 2014) representing a northeaster month, the maximum and mean wave heights of 5.6 ft (1.7 m) and 1 ft (0.3 m) were estimated in the channel centerline, and the corresponding wave height reductions were 78% and 35.5%, respectively. For Hurricane Sandy, maximum and mean wave heights were 5 ft (1.52 m) and 1.8 ft (0.55 m), and wave reduction factors were 60% and 26%, respectively. For Condition 1 (August 2014), Condition 2 (February 2014), and Condition 3 (Hurricane Sandy), the maximum flood/ebb currents in the channel centerline were 3.6, 4.3, and 5.2 ft/sec (1.1, 1.3, and 1.6 m/sec), respectively. Both Alternatives exhibited the same trend in current fields, with stronger currents occurring between the jetty heads at the entrance to the channel. Currents were generally stronger along the north shoreline as compared to south shoreline, with stronger currents near along the shoreline closer to the canal entrance. While the numerical modeling results suggested a jettied channel provides significant wave-reduction benefits, it is recognized that other criteria may be used in selection of an optimal alternative. The construction cost for Alt-1 would be significantly less because of a shorter north jetty, so for this reason Alt-1 might be the preferred Alternative.

The results for morphology change indicated that the magnitude of change was small for three conditions simulated. The maximum change of 1 ft (0.3 m) occurred along the channel centerline. The spatial morphologic variation along three transects (north shoreline, channel centerline, and south shoreline) had different erosion/deposition patterns. Generally, sediment transport/morphology change for the three conditions followed the variation in the associated current fields.

Preliminary estimates for structural design of jetties and revetments were provided in this report to assist NAB in the selection between the two Alternatives evaluated. The information provided may be used in the estimate of jetty and revetment structure construction costs involved. Estimates include the stable armor stone sizes for both the seaside and leeside of a conventional multilayer rubble-mound jetty. Calculations were performed for a +5 ft (1.5 m, MLLW) or 3.84 ft (1.17 m, MSL) baseline structural crest elevation and three jetty side slopes of 1V:1.5H; 1V:2H; and 1V:2.5H. A 5 ft (1.52 m, MSL) still-water elevation was used for storm surge plus subsidence. Stone weights and transmitted waves heights for these slopes were calculated. Based on the size of the armor stones, cross-sectional areas were calculated for the seaside armor, leeside armor, and a combined core plus under layers. With a 5 ft (1.52 m) MSL surge plus subsidence, the relative jetty crest elevation will be reduced substantially or submerged completely. This would be a concern because structures with low crest elevation are particularly susceptible to leeside damage by overtopping waves. For this reason, the armor stone sizes for the seaside and leeside have to be recalculated if NAB decides to decrease the crest elevation of jetties.

The stone weights and transmitted wave heights for side slopes of 1V:2.5H, 1V:2H, and 1V:1.5H were provided in Chapter 3 in Tables 3-1, 3-2, and 3-3, respectively. Seaside armor weights for these three slopes were 360, 500, and 760 lb (0.18, 0.25, and 0.38 ton), and the corresponding leeside armor weights were 0.19, 0.32, 0.59 ton. Maximum transmitted wave heights for these slopes were 5.9, 6.5, and 7.1 ft (1.8, 1.97, and 2.18 m), respectively. Transmitted wave heights were calculated at each save station for the crest elevation considered. The jetty structure would require greater armor stone size on the leeside than the stone on the seaside if waves were transmitted to the leeside of the jetty structure by overtopping the jetty structure's crest. Generally, steeper jetty structure side slopes require larger/heavier stable armor stone size both on seaside and leeside of the

jetty structure. For example, results indicated the maximum design stone diameter would increase from 1.31 to 1.93 ft (0.4 to 0.6 m) for jetty structure side slopes changing from 1V:2.5H to 1V:1.5H, respectively, and in turn, the single stone weight would increase from 380 to 1,180 lb (0.19 to 0.59 ton). Consequently, large stones might be required at the seaward end of the jetties where larger storm waves could break over the steeper jetty structure slopes at deeper water depths.

It is noted that with a design storm water level elevation of 5 ft (1.52 m) MSL, the jetties and most of the island will be inundated. Under such conditions, there is no reason to increase the crest elevation of the jetties greater than the designed 3.84 ft (1.2 m) MSL. The effects of waves on jetties diminish as the depth of water above the structure increases. Because the low-crested jetty structure becomes submerged, waves are less affected by the structure. The estimates for low-crested jetties were also provided (Tables 3-5, 3-6, and 3-7). Results indicated maximum stone sizes and weights calculated for the submerged jetties were smaller than those for the exposed jetty structures. For a 1V:2.5H jetty side slope, maximum seaside and leeside armor weights were 140 and 380 lb (0.07 and 0.19 ton) (Table 3-5), respectively. Maximum seaside and leeside armor weights were 180 and 420 lb (0.09 and 0.21 ton) for 1V:2H slope (Table 3-6) and 280 and 460 lb (0.14 and 0.23 ton) for 1V:1.5H slopes (Table 3-7), respectively. Results indicated stone size increasing with increasing side slopes. Although a low-crested jetty structure would obviously have greater transmission, it would be less expensive to build and still provide a high level of energy reduction for typical wave conditions.

A range of 600 to 1,000 lb (0.3 to 0.5 ton) for armor stone weight for the south shoreline revetment was recommended in Chapter 3, with 1,250 lb (0.625 ton) as upper bound design estimate by applying a safety factor of 1.25 to minimize potential movement of stones. This was based on the recommendation made for a recent study for nearby Tangier Island south shoreline revetment structures. There was not much information available about the size and weight of submerged revetments during storms at different water depths under the combined effects of different water levels, waves, and currents.

The effects of SLR on the performance and stability of the Rhodes Point jetties were investigated, and results are provided in Chapter 3 in

Tables 3-8, 3-9, and 3-10 for three jetty side slopes. Results for the cross-section design estimates are provided in Table 3-11 and 3-12 for one jetty side slope (1V:2H), assumed to be the most likely slope used in construction. Transmitted wave heights were also calculated for the expected freeboard after 50 years of the most likely SLR (NRC-I) and also for a larger SLR to provide an upper limit (NRC-II). The effects of SLR with subsidence were factored into the calculations as depth increase and tables provide results for adjusted depths for both scenarios. In both cases, a constant rate of subsidence for Chesapeake Bay was included. Adjustment to wave heights at these increased depths and local settling caused by the weight of the jetty structure on the in situ material were not considered in these calculations. The emphasis for SLR calculations was on the expected effects of the SLR on leeside armor size and weight and transmitted wave heights.

Results for the 50-year SLR projection with the land subsidence for NRC-I curve (e.g., depth increase of 1.37 ft [0.4 m]) and jetty slope of 1V:2.5 indicated maximum leeside armor stone diameter, weight, and transmitted wave height were 1.5 ft (0.5 m), 560 lb (0.28 ton) and 2.34 ft (0.7 m), respectively. Using the NRC-II projected SLR (depth increase= 2.04 ft [0.6 m]), these values increased to 1.6 ft m (0.5 m), 680 lb (0.34 ton), and 2.61 ft (0.8 m).

For jetty side slope of 1V:2H, the NRC-I based estimates for maximum leeside armor stone diameter, weight, and transmitted wave height were 1.77 ft (0.5 m), 920 lb (0.46 ton), 2.52 ft (0.8 m), respectively. Using the NRC-II projected SLR, these values increased to 1.87 ft (0.6 m), 1,080 lb (0.54 ton), and 2.78 ft (0.8 m), respectively. For jetty side slope of 1V:1.5H, the NRC-I based estimates for maximum leeside armor stone diameter, weight, and transmitted wave height were 2.16 ft (0.7 m), 1,660 lb (0.83 ton), and 2.73 ft (0.8 m), respectively. Using the NRC-II projected SLR, these values increased to 2.28 ft (0.7 m), 1,960 lb (0.98 ton), and 3.0 ft (0.9 m), respectively. The bayside maximum armor stone size and weight for the above jetty structure condition remain nearly the same as without the SLR scenarios (Tables 3-1, 3-2, and 3-3). At the design water level plus the SLR with subsidence, much of the island will be inundated, leaving the jetties exposed as the isolated structure.

A site inspection should guide NAB to determine the desired land anchor points both for north and south jetties. These land anchor points should be selected at high tide at some proper high land elevation available. Jetty

connection locations should be moved if necessary to avoid low-lying and erosional spots. The selection of locations for the jetty roots should consider the nearest points shown in the models grids that offer some elevation and areas which include more resistant to erosion.

The structural design estimates were based on a 50-year design storm and a 5 ft (1.5 m) storm surge for a 5 ft (1.5 m) jetty crest elevation (MLLW) and 8 ft (2.4 m) crest width. It is likely that a more severe storm can occur during the life of the structure. The empirical equations used in these structural design estimates were based on assuming a low level of damage during the design event. The formulas include uncertainties with several parameters used in various equations.

In addition, measured wave and current data were not available to calibrate the numerical model. Impacts of these on calculated estimates would require further research and more time and funding. Due to these uncertainties, either the design estimates could be adjusted by incorporating a safety factor, or alternatively a more extreme design storm (i.e., a 100-year event) could be used in future design estimates. For the latter option, a detailed sensitivity analysis of key parameters affecting the design estimates should be performed to determine wave runup, over-topping, transmission, and SLR effects associated with a 100-year storm event on the required stone size and weight for the seaside/leeside of jetties.

Because further research and design estimates for a 100-year storm are cost prohibitive, the stone sizes for a 50-year design storm with the NRC curve II plus the subsidence yielded 3.84 ft (1.2 m) MSL (which is approximately 4 ft [1.2 m] MSL or 5 ft [1.5 m] MLLW) crest elevation for the jetties. Hence, this estimate of 4 ft (1.2 m) MSL (5 ft [1.5 m] MLLW) is recommended for the jetty design crest height at Rhodes Point, MD.

References

Basco, D. R., and C. S. Shin. 1993. *Design wave information for Chesapeake Bay and major tributaries in Virginia*. Technical Report No. 93-1. Norfolk, VA: Old Dominion University, Department of Civil Engineering, Coastal Engineering Institute.

Boon, J. D., J. M. Brubaker, and D. R. Forrest. 2010. *Chesapeake Bay land subsidence and sea level change*. Special Report 425 in Applied Science and Ocean Engineering. Gloucester Point, VA: College of William and Mary, Virginia Institute of Marine Science.

Buttolph, A. M., C. W. Reed , N. C. Kraus, N. Ono, M. Larson, B. Camemen, H. Hanson, T. Wamsley, and A. K. Zundel. 2006. *Two-dimensional depth-averaged circulation model CMS-M2D: Version 3.0, Report 2, sediment transport and morphology change*. ERDC/CHL TR-06-9. Vicksburg, MS: U.S. Army Engineer Research and Development Center.

Church, J. A., and N. J. White. 2011. Sea-level rise from the late 19th to the early 21st century. *Surveys in Geophysics* 32: 585–602.

Cialone M. A, T. C. Massey, M. E. Anderson, A. S. Grezgorzewski, R. E. Jensen, A. Cialone, D. J. Mark, K. C. Pevey, B. L. Gunkel, T. O. McAlpin, N. C. Nadal-Caraballo, J. A. Melby, and J. J. Ratcliff. 2015. *North Atlantic Coast Comprehensive Study (NACCS) coastal storm model simulations: Waves and water levels*. ERDC/CHL TR-15-14. Vicksburg, MS: U.S. Army Corps of Engineers Research and Development Center.

CIRIA. 2007. *The rock manual: The use of rock in hydraulic engineering*. 2nd Edition. London, England.

d'Angremond, K., J. W. van der Meer, and R. J. de Jong. 1996. Wave transmission at low-crested structures. In *Proceedings, 25th International Conference on Coastal Engineering, ASCE,* 3,305–3,318.

Demirbilek, Z., L. Lin, and G. P. Bass. 2005. Prediction of storm-induced high water in Chesapeake Bay. In *Proceedings, Solutions to Coastal Disasters 2005,* 187–201. Charleston, SC: American Society of Civil Engineers.

Demirbilek, Z., L. Lin, and A. Zundel. 2007. *WABED model in the SMS: Part 2; Graphical interface*. ERDC/CHL CHETN-I-74. Vicksburg, MS: U.S. Army Engineer Research and Development Center. http://acwc.sdp.sirsi.net/client/search/asset/1000352

Demirbilek, Z., and J. Rosati. 2011. *Verification and validation of the Coastal Modeling System: Report 1; Summary report*. ERDC/CHL TR-11-10. Vicksburg, MS: U.S. Army Engineer Research and Development Center. http://acwc.sdp.sirsi.net/client/search/asset/1005704

Demirbilek, Z., L. Lihwa, D. Ward, and D. King. 2015. *Modeling study for Tangier Island jetties, Tangier Island, VA*. ERDC/CHL TR-14-08. Vicksburg, MS: U.S. Army Engineer Research and Development Center. http://acwc.sdp.sirsi.net/client/search/asset/1042086

Department of the Army. 1984. *Shore protection manual*. 4th Edition. 2 Volumes. Vicksburg, MS: U.S. Army Engineer Waterways Experiment Station.

Houston, J. R. 2012. Global sea level projections to 2100 using methodology of the intergovernmental panel on climate change. *Journal of Waterway, Port, Coastal, and Ocean Engineering*. New York, NY: American Society of Civil Engineers.

Hudson, R. Y. 1959. Laboratory investigation of rubble-mound breakwaters. *Journal of the Waterways and Harbors Division*. 85(WW3)93-121. New York, NY: American Society of Civil Engineers.

Kraus, N. C. 2009. *Channel and shoreline stabilization, Rhodes Point navigation project, Smith Island, Maryland*. ERDC/CHL Memorandum for Record, prepared for U.S. Army Engineer District, Baltimore, 1 Feb 2009.

Lin, L., and Z. Demirbilek. 2005. Evaluation of two numerical wave models with inlet physical model. *Journal of Waterway, Port, Coastal, and Ocean Engineering* 131(4): 149–161. New York, NY: American Society of Civil Engineers.

Lin, L., Z. Demirbilek, H. Mase, and F. Yamada. 2008. *CMS-Wave: A nearshore spectral wave processes model for coastal inlets and navigation projects*. ERDC/CHL TR-08-13. Vicksburg, MS: U.S. Army Engineer Research and Development Center. http://acwc.sdp.sirsi.net/client/search/asset/1000803

Lin, L., Z. Demirbilek, R. Thomas, and J. Rosati. 2011a. *Verification and validation of the Coastal Modeling System: Report 2; CMS-Wave*. ERDC/CHL TR-11-10. Vicksburg, MS: U.S. Army Engineer Research and Development Center. http://acwc.sdp.sirsi.net/client/search/asset/1005705

Lin, L., Z. Demirbilek, and H. Mase. 2011b. Recent capabilities of CMS-Wave: A coastal wave model for inlets and navigation projects. In *Proceedings, Symposium to Honor Dr. Nicholas Kraus. Journal of Coastal Research* Special Issue 59: 7–14. Coconut Creek, FL: Coastal Education and Research Foundation, Inc.

Melby, J. A., and S. A. Hughes. 2004. Armor stability based on wave momentum flux. In *Proceedings, Coastal Structures 2003,* 53–65. New York, NY: American Society of Civil Engineers.

Melby, J. A. 2010. Time-dependent life-cycle analysis of breakwaters. In *IAHR Congress Proceedings, 4th International Short Conference/Course on Applied Coastal Research, IAHR*, 46–64.

Melby, J. A., and N. Kobayashi. 2011. Stone armor damage initiation and progression based on the maximum wave momentum flux. *Journal of Coastal Research* 27(1): 110–119. Coconut Creek, FL: Coastal Education and Research Foundation, Inc.

Melby, J. A., N. C. Nadal-Caraballo, and J. Winkelman. 2015. *Point Judith, Rhode Island, breakwater risk assessment*. ERDC/CHL TR-15-13. Vicksburg, MS: U.S. Army Engineer Research and Development Center.

Sanchez, A., W. Wu, T. Beck, H. Li, J. Rosati, R. Thomas, J. D. Rosati, Z. Demirbilek, M. Brown, and C. Reed. 2011a. *Verification and validation of the Coastal Modeling System: Report 3; CMS-Flow hydrodynamics*. ERDC/CHL TR-11-10. Vicksburg, MS: U.S. Army Engineer Research and Development Center. http://acwc.sdp.sirsi.net/client/search/asset/1005706

Sanchez, A., W. Wu, T. Beck, H. Li, J. Rosati, R. Thomas, J. D. Rosati, Z. Demirbilek, M. Brown, and C. Reed. 2011b. *Verification and validation of the Coastal Modeling System: Report 4; CMS-Flow sediment transport and morphology change*. ERDC/CHL TR-11-10. Vicksburg, MS: U.S. Army Engineer Research and Development Center. http://acwc.sdp.sirsi.net/client/search/asset/1005707

USACE. 2011. *Sea-level change considerations for civil works programs*. Engineering Circular EC 1165-2-212. Washington, DC: U.S. Army Corps of Engineers.

USACE. 2015. *Coastal engineering manual*. Engineer Manual EM 1110-2-1100. Washington, DC: U.S. Army Corps of Engineers.

Van Gent, M. R. A., and B. Pozueta. 2004. Rear-side stability of rubble mound structures. In *Proceedings, 29th International Conference on Coastal Engineering* (4)3,481–3,493. New York, NY: American Society of Civil Engineering.

Vidal, C. M., A. Losada, and E. P. D. Mansard. 1995. Stability of low-crested rubble-mound breakwater heads. *Journal of Waterway, Port, Coastal, and Ocean Engineering* 121(2): 114–122. New York, NY: American Society of Civil Engineers.

Zundel, A. K. 2006. *Surface-water Modeling System (SMS): Reference manual*. Version 9.2. Provo, UT: Brigham Young University, Environmental Modeling Research Laboratory.

Appendix A: Description of the Coastal Modeling System (CMS)

The CMS was used for the numerical modeling estimates of waves, currents, and sediment transport at Rhodes Point, Smith Island, MD. A brief description of the CMS is provided here for completeness.

As shown in Figure A-1, the CMS is an integrated suite of numerical models for waves, flows, and sediment transport and morphology change in coastal areas. This modeling system includes representation of relevant nearshore processes for practical applications of navigation channel performance and sediment management at coastal inlets and adjacent beaches. The development and enhancement of CMS capabilities continues to evolve as a research and engineering tool for desk-top computers. CMS uses the Surface-water Modeling System (SMS) (Zundel 2006) interface for grid generation and model setup, as well as plotting and post-processing. The Verification and Validation (V&V) Report 1 (Demirbilek and Rosati 2011) and Report 2 (Lin et al. 2011) have detailed information about the CMS-Wave features, and evaluation of the model's performance skills in a variety of applications. Report 3 and Report 4 by Sanchez et al. (2011a,b) describe coupling of wave-flow models and hydrodynamic and sediment transport and morphology change aspects of CMS-Flow. The performance of CMS for a number of applications is summarized in Report 1, and details are described in the three companion V&V Reports 2, 3, and 4.

The CMS-Wave, a spectral wave model, was used in this study because of the large extent of modeling domain over which wave estimates were required. It solves the steady-state wave-action balance equation on a nonuniform Cartesian grid to simulate steady-state spectral transformation of directional random waves. Wind-wave generation and growth, diffraction, reflection, dissipation due to bottom friction, white-capping and breaking, wave-current interaction, wave runup, wave setup, and wave transmission through structures are the main wave processes included in the CMS-Wave.

Figure A- 1. The CMS framework and its components.

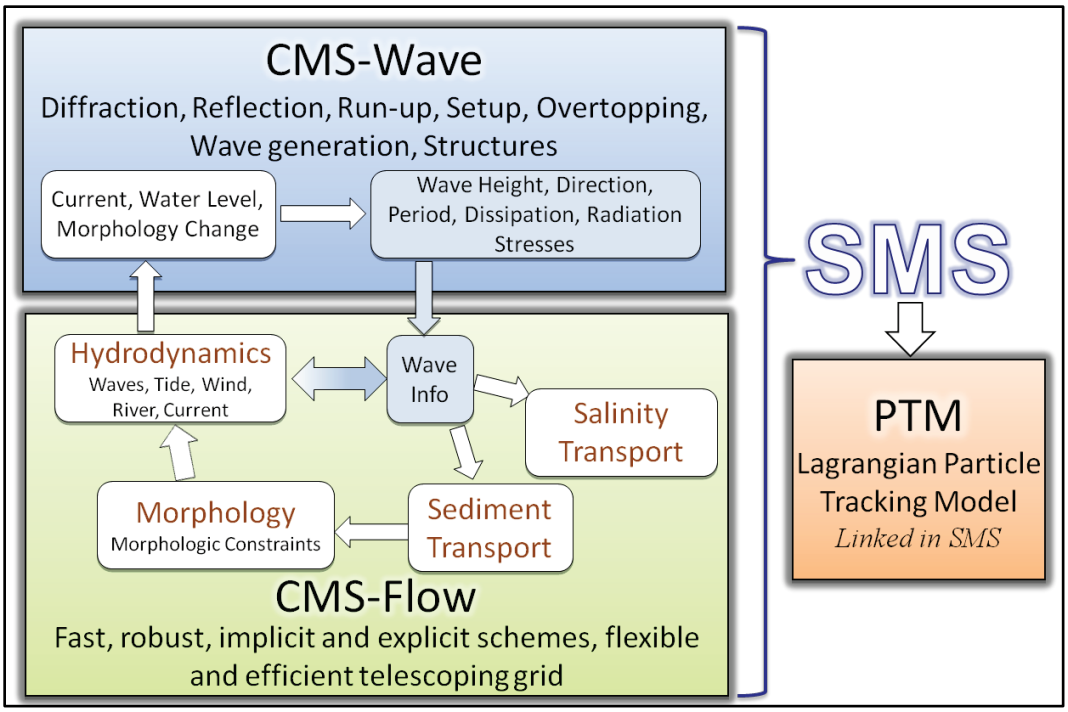

CMS-Wave is designed to simulate wave processes with ambient currents at coastal inlets and in navigation channels. The model can be used either in half-plane or full-plane mode for spectral wave transformation (Lin and Demirbilek 2005; Lin et al. 2008; Demirbilek et al. 2007). The half-plane mode is default because in this mode CMS-Wave can run more efficiently as waves are transformed primarily from the seaward boundary toward shore. Lin et al. (2008, 2011) provides features of the model and step-by-step instructions with examples for application of CMS-Wave to a variety of coastal inlets, ports, structures, and other navigation problems. Publications listed in the V&V reports and this report provide additional information about the CMS-Wave and its applications. Additional information about CMS-Wave is available from the CIRP website: http://cirp.usace.army.mil/wiki/CMS-Wave.

The CMS-Flow, a two-dimensional shallow-water wave model, was used for hydrodynamic modeling (calculation of water levels and currents) in this study. The implicit solver of the flow model was used in this study. This circulation model provides estimates of water level and current given the tides, winds, and river flows as boundary conditions. CMS-Flow calculates hydrodynamic (depth-averaged circulation), sediment transport, morphology change, and salinity due to tides, winds, and waves.

The hydrodynamic model solves the conservative form of the shallow-water equations that includes terms for the Coriolis force, wind stress, wave stress, bottom stress, vegetation-flow drag, bottom friction, wave roller, and turbulent diffusion. Governing equations are solved using the finite volume method on a nonuniform Cartesian grid. V&V Report 3 and Report 4 by Sanchez et al. (2011a,b) provides instruction for the preparation of the model at coastal inlet applications. Additional information about CMS-Flow is available from the CIRP website: http://cirp.usace.army.mil/wiki/CMS-Flow.

The CMS-Flow modeling tasks for this study included specification of surface winds, atmospheric pressures, and water levels for input to the model. The effects of waves on the circulation were input to the CMS-Flow and have been included in the simulations performed for this study.

There are three sediment transport models available in CMS-Flow: (a) a sediment mass balance model, (b) an equilibrium advection-diffusion model, and (c) a nonequilibrium advection-diffusion model. Depth-averaged salinity transport is simulated with the standard advection-diffusion model and includes evaporation and precipitation. The V&V Report 1, Report 3, and Report 4 describe the integrated wave-flow-sediment transport and morphology change aspects of CMS-Flow. The performance of CMS-Flow is described for a number of applications in the V&V reports.

Appendix B: Datums

B.1 Horizontal datums

The horizontal datum used for coordinate data input into the models was NAD83, State Plane Virginia, South (Federal Information Processing Standard state code: 4502) in meters.

B.2 Vertical datums

The vertical datum used in this study was MTL (mean tide level) in meters, based on NOAA benchmark at Bishops Head, Hoopers Strait, MD (Station 8571421). The station information is given as follows:

Station ID: 8571421 PUBLICATION DATE: 11/19/2012

Name: BISHOPS HEAD, HOOPERS STRAIT, MARYLAND

NOAA Chart: 12261 Latitude: 38° 13.2' N

USGS Quad: WINGATE Longitude: 76° 2.3' W

Tidal datums at BISHOPS HEAD, HOOPERS STRAIT based on:
LENGTH OF SERIES: 6 YEARS
TIME PERIOD: September 05 - August 09, and April 10 - March 12

TIDAL EPOCH: 1983-2001

CONTROL TIDE STATION: 8571892 CAMBRIDGE, CHOPTANK RIVER

Elevations of tidal datums referred to Mean Lower Low Water (MLLW), in meters:
HIGHEST OBSERVED WATER LEVEL (10/30/2012) = 1.309
MEAN HIGHER HIGH WATER MHHW = 0.624

MEAN HIGH WATER MHW = 0.575

North American Vertical Datum NAVD88 = 0.380

MEAN SEA LEVEL MSL = 0.307

MEAN TIDE LEVEL MTL = 0.307

MEAN LOW WATER MLW = 0.039

MEAN LOWER LOW WATER MLLW = 0.000

LOWEST OBSERVED WATER LEVEL (01/03/2008) = -0.559

The data above were obtained from the website http://tidesandcurrents.noaa.gov/data_menu.shtml?stn=8571421%20Bishops%20Head,%20MD&type=Bench%20Mark%20Data%20Sheets.

REPORT DOCUMENTATION PAGE

Form Approved
OMB No. 0704-0188

1. REPORT DATE	2. REPORT TYPE	3. DATES COVERED *(From - To)*
November 2016	**Final**	

4. TITLE AND SUBTITLE
Hydrodynamic Modeling for Channel and Shoreline Stabilization at Rhodes Point, Smith Island, MD

5a. CONTRACT NUMBER

5b. GRANT NUMBER

5c. PROGRAM ELEMENT NUMBER
060000

6. AUTHOR(S)
Zeki Demirbilek, Lihwa Lin, Thomas D. Laczo and Anthony A. Clark

5d. PROJECT NUMBER
113464

5e. TASK NUMBER
A1100

5f. WORK UNIT NUMBER
58F268

7. PERFORMING ORGANIZATION NAME(S) AND ADDRESS(ES)
Coastal and Hydraulics Laboratory
U.S. Army Engineer Research and Development Center
3909 Halls Ferry Road
Vicksburg, MS 39180

8. PERFORMING ORGANIZATION REPORT NUMBER
ERDC/CHL TR-16-17

9. SPONSORING/MONITORING AGENCY NAME(S) AND ADDRESS(ES)
U.S. Army Engineer District, Baltimore
10 South Howard St.
Baltimore, MD 21201
Headquarters. U.S. Army Corps of Engineers
Washington, DC 20314-1000

10. SPONSOR/MONITOR'S ACRONYM(S)
NAB

11. SPONSOR/MONITOR'S REPORT NUMBER(S)

12. DISTRIBUTION/AVAILABILITY STATEMENT
Approved for public release; distribution is unlimited.

13. SUPPLEMENTARY NOTES

14. ABSTRACT

This report documents numerical wave and flow modeling for stabilizing a shallow draft navigation channel and adjacent shorelines at Rhodes Point, located on Smith Island, Maryland, in Chesapeake Bay. The U.S. Army Engineer District, Baltimore (CENAB), maintains the channel and is considering structures to protect the western entrance of the channel on Chesapeake Bay side to reduce erosion of shorelines by armoring and stabilizing the channel. The U.S. Army Engineer Research and Development Center (ERDC), Coastal and Hydraulics Laboratory (CHL), performed a numerical modeling study to develop preliminary structure design estimates by investigating the optimal location for the structures, and by determining how structures in the impacted areas would be affected by waves and hydrodynamics. Estimates of water levels, waves, currents, and morphology change in and around the channel and adjacent beaches were calculated for a relative comparison of no-project (Alternative-0) and two alternatives investigated, and for the preliminary structural design calculations. The Alternative-1with a shore-normal north jetty provided a significant reduction in waves and currents in the channel and along the shorelines, offering a cost-effective solution. Alternative-2 with two parallel jetties provided similar wave energy reduction in the channel and along the shorelines, but showed higher currents and erosional pockets developing in the channel which could undermine the stability of the jetties.

15. SUBJECT TERMS
Channels (Hydraulic engineering), Chesapeake Bay (Md. And Va.), Coastal Engineering, Hydrodynamics—Computer Simulation, Jetties, Numerical Analysis, Rhodes Point (Md.), Shorelines, Waves—Computer simulation

16. SECURITY CLASSIFICATION OF:			17. LIMITATION OF ABSTRACT	18. NUMBER OF PAGES	19a. NAME OF RESPONSIBLE PERSON
a. REPORT	b. ABSTRACT	c. THIS PAGE			**Zeki Demirbilek**
Unlimited	Unlimited	**Unlimited**	**SAR**	110	**19b. TELEPHONE NUMBER** *(Include area code)* **601-634-2834**